NUMERICAL SIMULATION OF THERMO-MECHANICAL BEHAVIOR OF GYPSUM BOARD WALL ASSEMBLY

by

Zhili Quan

A Dissertation Submitted in Partial Fulfillment of the Requirements

for the Degree of

Doctor of Philosophy

in

Engineering

University of Alaska Fairbanks

May 2019

Approved:

Dr. J. Leroy Hulsey, Advisory Committee Chair

Dr. Il Sang Ahn, Committee Member

Dr. Cheng-fu Chen, Committee Member

Dr. Yujiang Xiang, Committee Member

Dr. J. Leroy Hulsey, Chair
Department of Civil Engineering

Dr. William E. Schnabel, Dean
College of Engineering and mines

Dr. Michael Castellini, Dean
Graduate School

Abstract

Fire safety has become a significant concern to public safety; especially in the aftermath of 9/11 attack where, according to official reports, three World Trade Center buildings collapsed because of fire. Therefore, the level of thermal insulation required from building material and structural elements has increased. In recent years, gypsum board wall assemblies have been increasingly used as compartmentation for high-rise residential and commercial buildings. The increasing popularity of gypsum board wall assemblies is due to their relatively high strength-to-weight ratio, ease of prefabrication, fast erection and good thermal insulation. Before implementation of any building material or structural element, its Fire Resistance Rating must be determined by subjecting the material or element to a standard furnace fire test. Over the years, a large database has been collected for the Fire Resistance Rating of building materials and structural elements. However, due to the expensive and time-consuming nature of the standard fire tests, determining an accurate Fire Resistance Rating can be a difficult task.

In this study, the author numerically evaluated the Fire Resistance Rating of a new gypsum board wall assembly. Composite steel-EPS (Expanded Polystyrene) insulation is added to a traditional gypsum board wall assembly. The author first did numerical simulation of an experiment on the thermal response of a non-load-bearing gypsum board wall assembly to verify the thermal modeling methodology. The author then did numerical simulation of an experiment on the mechanical response of a load-bearing gypsum board wall assembly to verify the mechanical modeling methodology. Finally, the author used the verified thermal and structural modeling methodology to simulate the new composite steel-EPS gypsum board wall assembly and obtained its numerical Fire Resistance Rating. This Fire Resistance Rating should be compared with future experimental results of the new wall assembly. All modeling was done with ABAQUS V6.14.

Table of Contents

List of Figures

List of Tables

List of Appendices

Acknowledgments

The completion of my PhD research could not have been done without the endless support of my dear advisor, Dr. Leroy Hulsey. He is a knowledgeable and experienced advisor, a dear friend, and a guiding father figure. I would also like to thank Dr. Il Sang Ahn for providing the crucial technical guidance to my study. Dr. Cheng-fu Chen and Dr. Yujiang Xiang also gave valuable advice throughout the course of my research, and I couldn't say thank you enough to both of them. Dr. Horacio Toniolo and Dean. Bill Schnabel both worked with and helped me since I started working on my PhD, and I feel very indebted to them as well.

I would like to show my gratitude to all the hardworking staff members that have helped and supported me, including: Suzette Brosky, Kenna Metivier, Diane Wallace, Megan Blanchard, Shelly Baumann, Reija Shnoro and Carol Holz. I couldn't have done it without their help and support.

I would like to thank University of Alaska Fairbanks for providing this opportunity for me to obtain my advanced education, and I will always remember the joyful time I spent there.

Last but not least, I want to say thank you to my parents, all my family and friends and everybody that has helped and supported me in my life.

Chapter 1   Introduction

1.1 Background

Due to the ever rising loss of properties and lives as a result of structural damage or failure caused by fire, fire safety design has become a significant engineering topic [1]. Several milestone incidents, including 9/11 attack, in which three World Trade Center buildings collapsed after catching fire, have attracted global attention to the topic [2].

There are generally two ways to approach fire safety design [3]. The first is the active approach where the main design methodology is to extinguish the fire before it starts causing major damage. Sprinklers or deluges can be installed in buildings for this approach. The second is the passive approach where the main goal is to prevent the fire from spreading out or to minimize damage as much as possible. In this approach, materials with good thermal insulation properties can be used as compartmentation to stop fire from spreading across a building. At the same time, materials must also provide good thermal insulation capability so the temperature of the structural elements of a building does not rise above the critical value that could cause structural failure, as most structural materials, e.g. steel, degrade mechanically when temperature rises [3].

Therefore, it is for the purpose of the passive approach to fire safety design to discover and study materials with good thermal insulation properties so they can be confidently used as compartmentation in buildings. Among those materials, gypsum boards are now widely used as compartmentation in commercial, industrial and residential buildings. The ever increasing popularity of gypsum boards is due to their good thermal insulation capability, high strength-to-weight ratio, fast erection and easy installation and their relatively inexpensive cost. All the above traits also make gypsum boards valuable structural elements in modern high-rise steel framed buildings [3].

As mentioned above, gypsum boards are extensively used as compartmentation materials and are usually framed by steel studs to form gypsum board wall assemblies. Figure 1.1 gives a typical gypsum board wall assembly without any insulation material in the cavity.
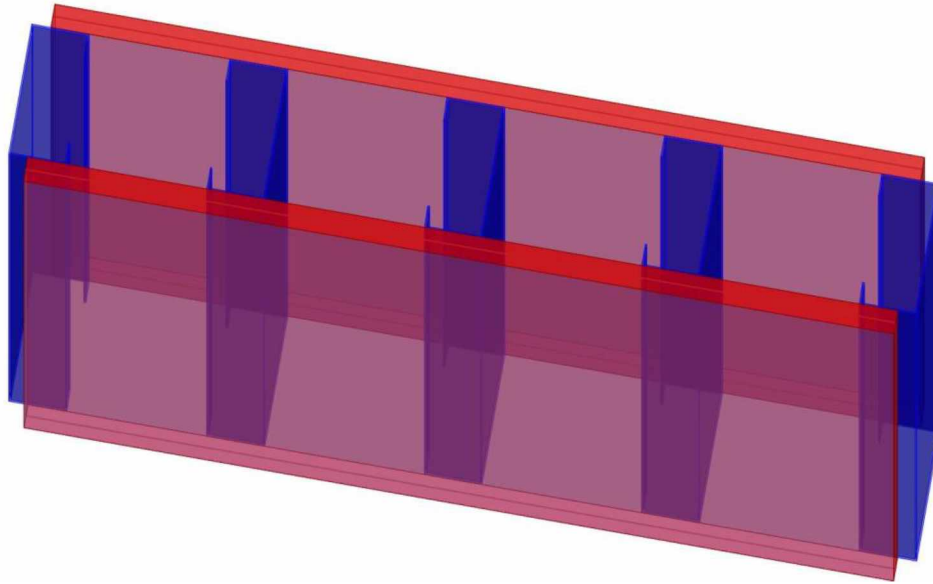
Figure 1.1: A typical gypsum board wall assembly without insulation material

It is also common practice to fill the cavity in the gypsum board wall assembly with insulation materials such as glass fiber, rockwool or EPS [3].

There are several advantages of using a gypsum board wall assembly with steel studs as compartmentation. As stated above, most construction materials, including steel, tend to degrade mechanically when their temperature rises. Certain gypsum boards such as Type X gypsum boards have very good thermal insulation so they can offer certain thermal protection to the steel studs inside the wall assembly to maintain their strength during an event of fire. In addition, gypsum boards can also function as a bracing device to steel studs as they are connected via fasteners such as nails or screws. Besides the above two advantages, low cost, easy installation and high strength-to weight-ratio are also positive traits that gypsum board wall assemblies possess. Gypsum board wall assemblies can be either load-bearing or non-load-bearing [4].

It is imperative to assess the Fire Resistance Rating (FRR) of any building material or structural element before it can be used in construction. Most codes and practices around the world require standard fire tests of individual building materials or structural elements to determine their FRR. Standard fire tests are usually done according to standard documents such as ASTM E119 or CAN/ULC-S101-M89. ASTM E119 serves as the standard document for fire tests in the US and CAN/ULC-S101-M89 in Canada. Some researchers such as Manzello [4] have pointed out there has been a large database built for lots of the experiments done on different building materials and

structural elements, including a variety of gypsum board wall assemblies with varying factors, such as thickness, types or number of layers of gypsum boards, types and sizes of steel and steel studs inside, and types and thickness of insulation inside.

ASTM E119 [5] provides the standard test methods in the US for fire tests of building materials and structural elements. The test methods apply to a variety of building materials or structural elements such as walls, columns and floors. The document prescribes a standard exposing fire of controlled extent and severity. Performance of building materials or structural elements is defined as the length of the period of resistance to standard exposure of fire before any of the failure criteria is observed. Performance or exposure of materials or elements shall be expressed as "2-h," "6-h," "1⁄2-h," etc., which is the elapsed period they can withstand in the prescribed fire test.

The fire tests shall be done with a furnace that follows a temperature vs time curve given in E119. Part of the temperature vs time curve is given in Table 1.1.

Table 1.1: Part of the standard temperature vs time curve in E119

Temperature (F)	Temperature (C)	Time (min)
1000	538	5
1300	704	10
1550	843	30
1700	927	60
1850	1010	120
2000	1093	240
2300	1260	480

The building materials or structural elements to be tested should be representative of the condition of real life construction in terms of size, workmanship, detailing, moisture content and load carrying capability. One side (exposed surface) of the materials or structural elements will be subjected to the furnace fire following the temperature vs time curve in E119. The other side (unexposed surface) is exposed to the ambient temperature. During the test, temperature as a function of time at different locations will be recorded via thermal gauges as stipulated in E119. Other information such as deformation, cracking, spalling can also be recorded depending on the specific goals the test.

According to E119, there are three critical criteria functioning as the judgement of the FRR of building materials or structural elements. These are:

a) The average temperature rise of any set of thermal gauges for the material or element being protected is more than 250°F (139°C) above the initial temperature, or the temperature rise of any one thermal gauge of the set for the material or element being protected is more than 325°F (181°C) above the initial temperature. (thermal insulation)

b) The test specimen failed the purpose of prevention of spread of fire because the passage of flame or gases through a crack or breach has become hot enough to ignite cotton waste (thermal integrity)

c) The structural member fails under the specified loading condition in the fire test due to the degradation of the mechanical properties of the building material or structural element (structural integrity)

However, due to the time-consuming nature of those fire tests and the high expenses for the conduction of these tests, the FRR of any new building materials or structural elements can be hard to assess. Therefore, numerical simulation of fire tests of new building materials or structural elements can be potentially very promising, due to their low cost and time saving characteristics [1, 6].

1.2 Objective

The objective of this study is to assess the FRR of a newly proposed gypsum board assembly. The new wall assembly is a composite steel-EPS wall assembly that consists of a varying number of layers of gypsum boards framed and insulated by composite steel-EPS material. The author presents existing standard fire tests of a load-bearing and a non-load-bearing gypsum board wall assembly, and then numerically simulates both fire tests to verify the modeling methodology. Subsequently, the verified modeling methodology is used to simulate the new composite steel-EPS gypsum board wall assembly, and the numerically simulated thermal and mechanical behaviors of the new wall assembly under the standard fire test according to E119 are calculated and studied. Finally, the FRR of the new wall assembly is deduced based on the numerical results.

1.3 Outline

The outline of this dissertation is given in the below content.

Chapter 1.   This chapter gives the general information of the dissertation, including: background information, objective of this research and outline of the dissertation.

Chapter 2.	This chapter introduces an existing fire test of a non-load-bearing gypsum board wall assembly. A numerical simulation is done to simulate the fire test of the non-load-bearing wall assembly. The numerical results are compared with the experimental results and a high degree of accuracy is achieved. Therefore, the thermal modeling methodology is verified.
Chapter 3.	This chapter introduces an existing fie test of a load-bearing gypsum board wall assembly. A numerical simulation is again done to simulate the fire test of the load-bearing wall assembly. The numerical results agree well with the experimental results. Subsequently, the agreement between the numerical and experimental results verifies the mechanical methodology.
Chapter 4.	The new composite steel-EPS gypsum board wall assembly is introduced, and the verified numerical modeling methodology is implemented to simulate an E119 standard fire test of this new wall assembly. The numerical results are thoroughly studied and the FRR of the new wall assembly is deduced.
Chapter 5.	The last chapter gives the summary, conclusion and future work of this dissertation.

1.4 References

[1]. Kolarkar, Prakash, Structural and Thermal Performance of Cold-formed Steel Stud Wall Systems under Fire Conditions, 2010

[2]. Hamilton, R. Scott, Performance-based Fire Engineering for Steel Framed Structures: a Probabilistic Methodology, 2011

[3]. Rahmanian, Ima, Thermal and Mechanical Properties of Gypsum Boards and Their Influences on Fire Resistance of Gypsum Board Based Systems, 2011

[4]. Manzello, Samuel, et al., Analysis of Inter-laboratory Testing of Non-load-bearing Gypsum/Steel-Stud Wall Assemblies, 2007

[5]. ASTM E 119-16: "Standard Test Methods for Fire Tests of Building Construction Materials," ASTM International, West Conshohocken, PA, 2016

[6]. Nassif, Ayman Y., et at., Full-scale fire testing and numerical modelling of the transient thermo-mechanical behavior of steel-stud gypsum board partition walls, 2014

Chapter 2   Numerical Evaluation of Fire Ratings: Non-load-bearing wall[1]

2.1 Abstract

Both non-load-bearing and load-bearing walls are used in commercial and residential buildings to function as partitioning walls. As modern buildings get progressively taller over time, fire safety related issues become more significant. Therefore, non-load-bearing and load-bearing walls must possess certain fire resistance capabilities to assure public safety from potential fire hazards. Standard fire tests of bearing walls have been conducted over the years and a large database has been established. Those fire tests were expensive, labor-intensive and required the expertise of technicians, not to mention the time-consuming nature of the preparation and conduction of the tests. However, it is shown in this paper that numerical models can accurately predict the behavior and response of a wall assembly that is subjected to a fire test. In this study, existing experimental results from fire tests of a series of non-load-bearing gypsum board wall assemblies were reviewed, and a numerical model was developed in ABAQUS to simulate the fire test. Subsequently, the numerical results were compared with the experimental results.

2.2 Introduction

In the aftermath of the World Trade Center attack, fire protection has become increasingly important in modern building design, especially in high-rise building design. Modern buildings have been steadily getting taller over the last several decades [1]. The evacuation of occupants from a high-rise building during a fire can be difficult and time-consuming. Wall assemblies are usually constructed with fire protective exteriors and steel studs to maintain structural integrity. The fire protective exterior can be made of one of a variety of materials such as gypsum board, plasterboard, or glass. The assembly can be hollow so that air will function as the insulation. However, convection and radiation in the cavity between the exterior walls will take place, and the heat transfer via either means could be significant. Besides leaving a cavity inside the wall assembly, insulation material such as rockwool or glass fiber can be installed to fill the cavity, and only thermal conduction through the insulation material will take place [2]. However, putting insulation material inside of the wall assembly is expensive and its effectiveness is still unknown.

---

[1] This chapter will be submitted for publication as Quan, Zhili, Hulsey, Leroy, Journal of Structural Fire Engineering.

In order to precisely assess the fire resistance rating of a specific non-load-bearing or load-bearing wall, standard fire tests can be done on the wall based on standard documents such as ASTM E119 [3] or CAN/ULC-S101-M89 [4]. ASTM E119 is the standard document for fire resistance tests of building materials and structural elements in the US and CAN/ULC-S101-M89 is the standard document in Canada. There have been many tests conducted to evaluate the fire resistance of individual construction materials but few of them were tests for actual wall assemblies. Wall assemblies are structural elements that consist of multiple materials and are constructed in a specific way. Moreover, any variation of the setup of the wall assemblies, such as types of material, thickness of the material, and dimensions (height or width) of the assembly, can create uncertainty. It is economically impractical to conduct tests that are only slightly different from tests that have been already conducted, but a slight difference might contribute to a significant difference in results [5].

Therefore, numerical simulation of fire tests of non-load-bearing and load-bearing wall assemblies can potentially be very useful. Numerical simulation before a fire test of a wall assembly can often reasonably predict results which can provide great insight [5]. After the test, numerically generated results can give a level of confidence on the accuracy of the test depending on whether the experimental results and the simulated results match well. In addition, when funding is not adequately provided, numerical simulation of wall assemblies under study can at least give some insight into whether the wall assemblies will meet the requirements of the construction industry. There is literature available on fire tests done on both non-load-bearing and loading-bearing wall assemblies and numerical simulations of these tests. ASTM C1396/C1396M [6] gives the standard properties of different kinds of gypsum boards, such as the manufacturers of different gypsum boards, fire resistance (burning period before failure) based on the thickness of different gypsum boards, flexural strength, and deformation under humidity. However, ASTM C1396/C1396M does not give any information regarding the thermal properties of gypsum boards, such as thermal conductivity or specific heat.

Therefore, researchers have begun individual experiments to test the thermal properties of different types of gypsum boards before conducting fire tests of gypsum board wall assemblies. Manzello, et al. [7] conducted a series of fire tests in the US on gypsum board wall assemblies and recorded the temperature on the unexposed surface of the gypsum boards as a function of time. Manzello, et al. [7] also measured the thermal properties of the gypsum boards used in the tests according to ASTM E 1269 [8] for the future possibility of numerically modelling the fire tests. Manzello, et al. [9] later conducted another series of tests in Japan and recorded the experimental results. The

North American fire tests were compared with the Japanese fire tests. Manzello, et al. [10] also conducted a test which subjected a gypsum board wall assembly to a real fire scenario. The experimental temperatures and deflection of the wall assembly were recorded during the test. Sultan, et al. [11, 12] conducted a series of tests to study the factors that could influence the performance of a gypsum board wall assembly. The test included variables such as the type of the gypsum boards used, the thickness of the gypsum boards, and the influence of cross bracing on the wall assembly. Mahendran, et al. [13, 14, 15] also conducted several studies on the fire resistance of gypsum board wall assemblies.

Other researchers have done numerical simulation in addition to their physical experiments in order to compare the results. Wang and Rahmanian [16] did a numerical simulation of a single gypsum board fire test with varying thicknesses. Nassif, et al., [17] conducted a fire test on a single gypsum board wall assembly with insulation material (rockwool) between the gypsum boards, and subsequently they did a numerical simulation of the test to verify their modeling methodology by comparing the experimental results with the numerical results. Liu, et al. [18] conducted a series of fire tests on gypsum board wall assemblies with different factors, such as the type of the gypsum board, the thickness and the number of layers in the assembly. Subsequently, a series of numerical simulations were conducted in order to verify the numerical results with the experiment results.

The study presented here involves a numerical simulation procedure done with ABAQUS and gives a detailed description of the procedure along with the numerical results. The numerical simulation modeled a series of fire tests on a non-load-bearing wall assembly presented by Manzello, et al [9]. In this study, the experimental results of Manzello, et al. [9] are compared to the numerically simulated results.

One thing that is worth mentioning is Manzello, et al. [9] only provided thermal experimental results (temperature) for the unexposed side of the wall assemblies. The temperature results at other locations such as the cavities of the wall, the middle section of the steel studs and the exposed side of the wall assembly were not included in their study. Furthermore, the deflection of the wall assemblies was never recorded.

The objective of this study is to verify the numerical modeling methodology. The main reason behind this objective is the amount of time and cost associated with these standard furnace fire tests. If the numerical results and the experimental results are comparable with a high degree of accuracy, then it is plausible to use the same modelling technique on other non-load-bearing walls that need to be tested. Of course, numerical results should be studied with exhaustive parametric analysis.

2.3 Experimental Description

2.3.1 Wall Assembly

The non-load-bearing wall used in tests by Manzello, et al [9] consisted of two layers of gypsum boards on both sides of the wall. The wall was framed using steel studs, which were attached to the gypsum boards as shown in Figure 2.1.
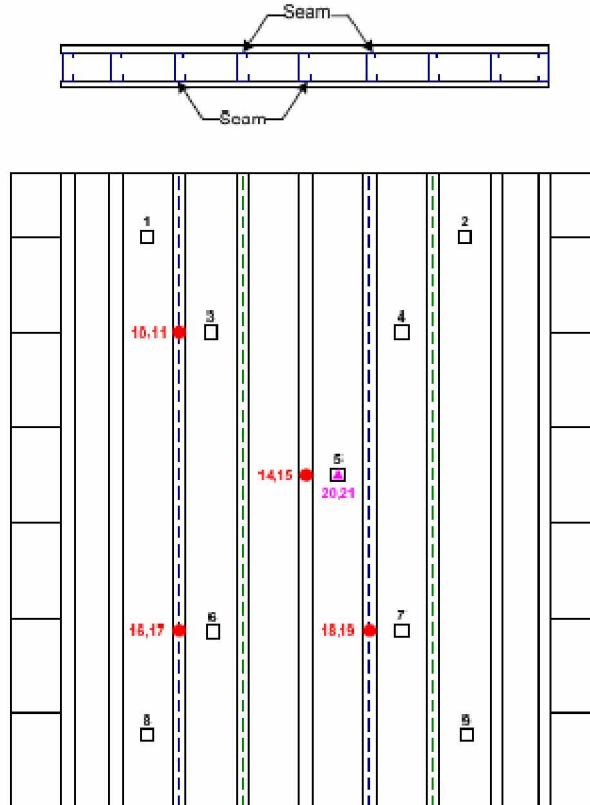
Figure 2.1: Wall assembly used in fire tests by Manzello, et al. [9]

The wall tested with a dimension of 3050 mm by 3050 mm had steel studs (width: 92mm, thickness: 25 gauge) spaced at 406 mm and type X gypsum boards with a thickness of 15.9 mm. The studs were spaced at 406mm on center except the two studs on the outside which were 305mm apart from the ones next to them.

2.3.2 Properties of Material

2.3.2.1 Type X gypsum board

Thermal properties of the gypsum boards provided for this series of fire tests were measured and compared to those of off-the-shelf Type X gypsum boards [5]. Thermal conductivity, specific heat, contraction and mass loss were all measured and recorded as functions of temperature. Figure 2.2 gives the thermal conductivity as a function of temperature for both the Type X gypsum boards used in the tests and off-the-shelf Type X gypsum boards. In Figure 2.2, NAFTL-Type X (North American Fire Testing Laboratories Consortium) is the type of gypsum boards used in the tests and Type X is the off-the-shelf gypsum boards. The specific heat of the gypsum boards was also measured as a function of temperature, as shown in Figure 2.3. Mass loss and volume contraction will take place when Type X gypsum boards burn. Therefore, those two properties were measured against temperature, as shown in Figure 2.4 and Figure 2.5.
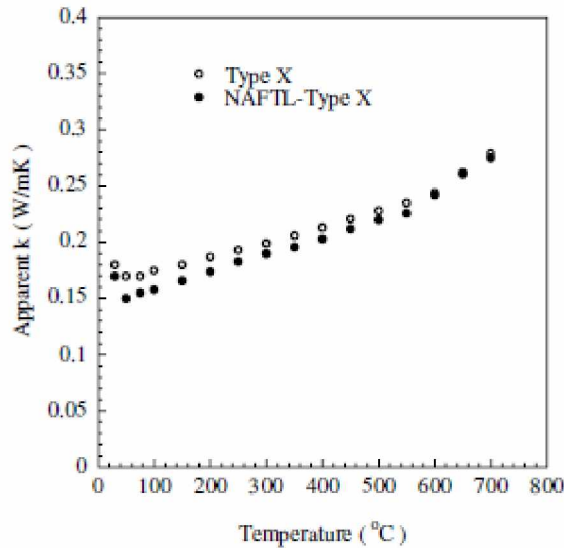
Figure 2.2: Thermal conductivity of gypsum boards vs temperature [9]

11
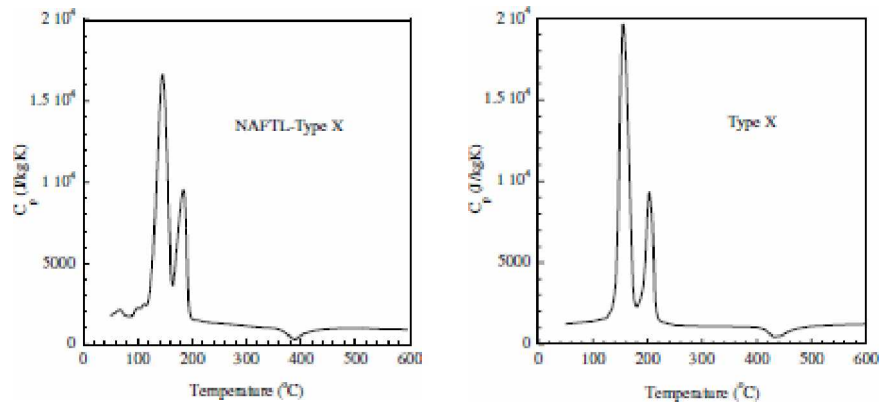
Figure 2.3: Specific heat of gypsum boards vs temperature [9]
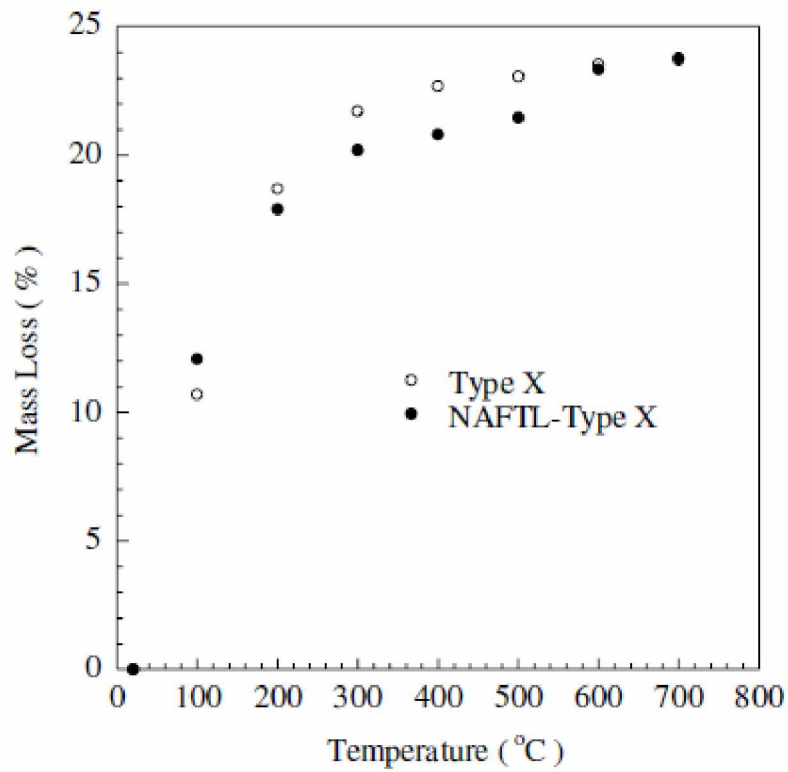
Figure 2.4: Mass loss vs temperature [9]
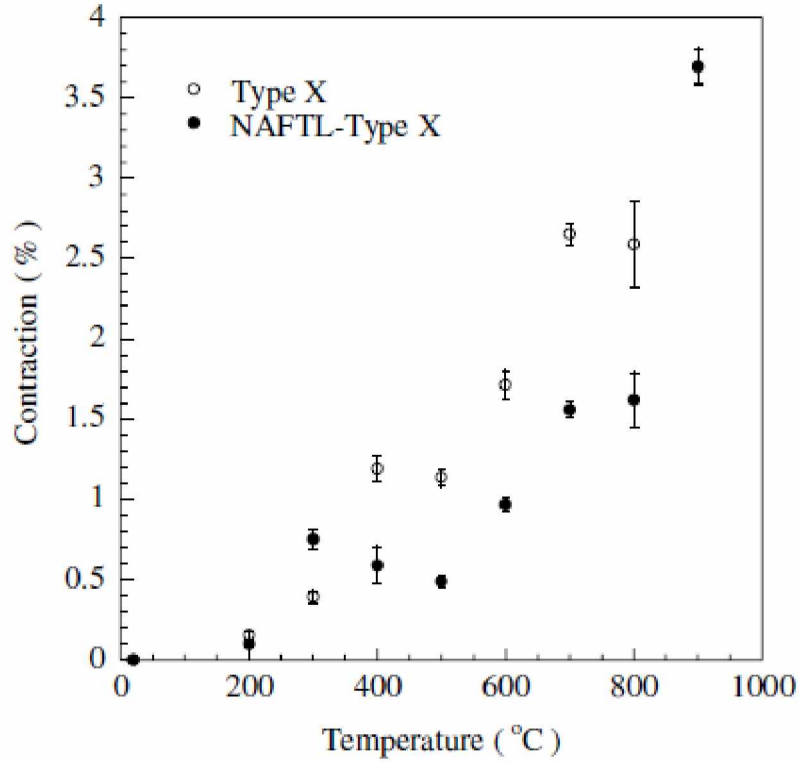
Figure 2.5: Contraction percentage vs temperature [9]

The thermal conductivity of the gypsum boards was only measured after the gypsum boards were dehydrated and cooled back down. Moreover, the thermal conductivity of the gypsum boards was only measured at fixed temperatures; see Figure 2.2 [9]. Gypsum boards used in the tests were not pre-dehydrated and the temperatures of the gypsum boards were constantly changing. Therefore, using the thermal conductivity given by Manzello, et al. [9] in numerical modeling could lead to inaccurate results.

2.3.2.2 Steel Studs

The type of steel for the studs was not given explicitly in the study done by Manzello, et al [9]. However, general properties of steel are given in the section of Numerical Modeling.

2.3.3 Fire Test Procedure

The wall assembly was used as a lid for a box-shaped furnace. Figure 2.6 shows technicians mounting a wall assembly on the furnace. The temperature inside of the furnace was following the standard temperature-time curve in ASTM E119. Manzello, et al. [9] reported the temperature of the wall assembly as a function of time at various locations during the test.

Temperature to be measured on the unexposed surface of the wall assembly
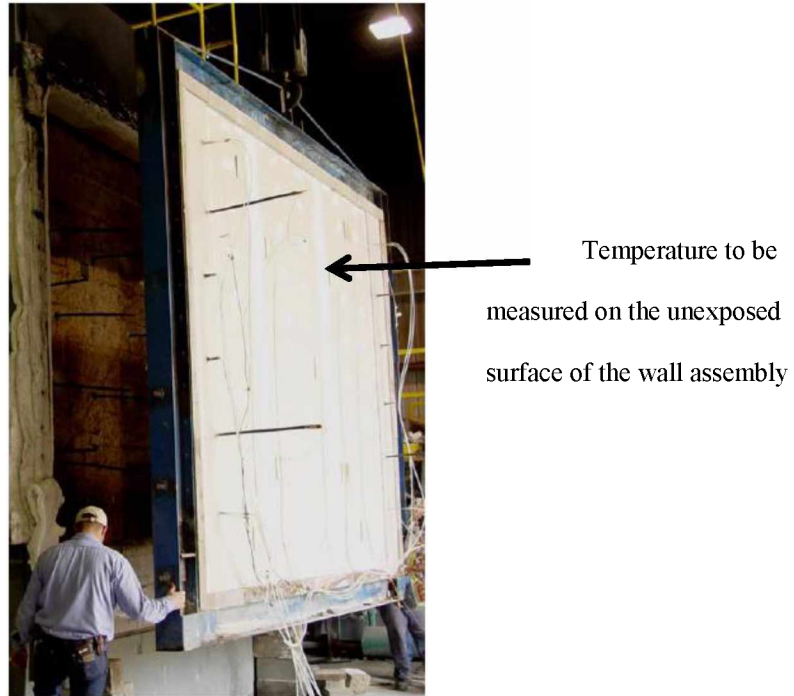
Figure 2.6: Wall assembly being mounted on the test furnace [7]

2.4 Experimental Results

2.4.1 Failure Description

According to Manzello, et al. [7], the failure of the wall assembly was defined as when any of the three failure criteria was met: a) when average temperature recorded on the unexposed side of the wall reached 139 C above its initial average temperature; b) when the maximum temperature recorded on the unexposed side of the wall reached 181 C above its initial average temperature; c) a crack opened up in the wall large enough to allow hot air to ignite cotton waste.

2.4.2 Temperature Results of the Furnace Tests

The temperature results of the furnace tests conducted in North America are plotted in Figure 2.7 and designated as NA-1 to NA-10. The temperature results of the furnace tests conducted in Japan are plotted in Figure 2.8 and designated as J-1 to J-6. In both Figures, the dashed line represents the standard temperature curve from the ASTM E119 specification. The temperature results given by Manzello, et al. [9] were all measured on the unexposed surface of the gypsum board wall assemblies, as shown in Figure 2.6. The average temperature increases on the surface of the unexposed gypsum board for the North American and the Japanese furnace tests are displayed in Figure 2.9 and Figure 2.10, respectively.
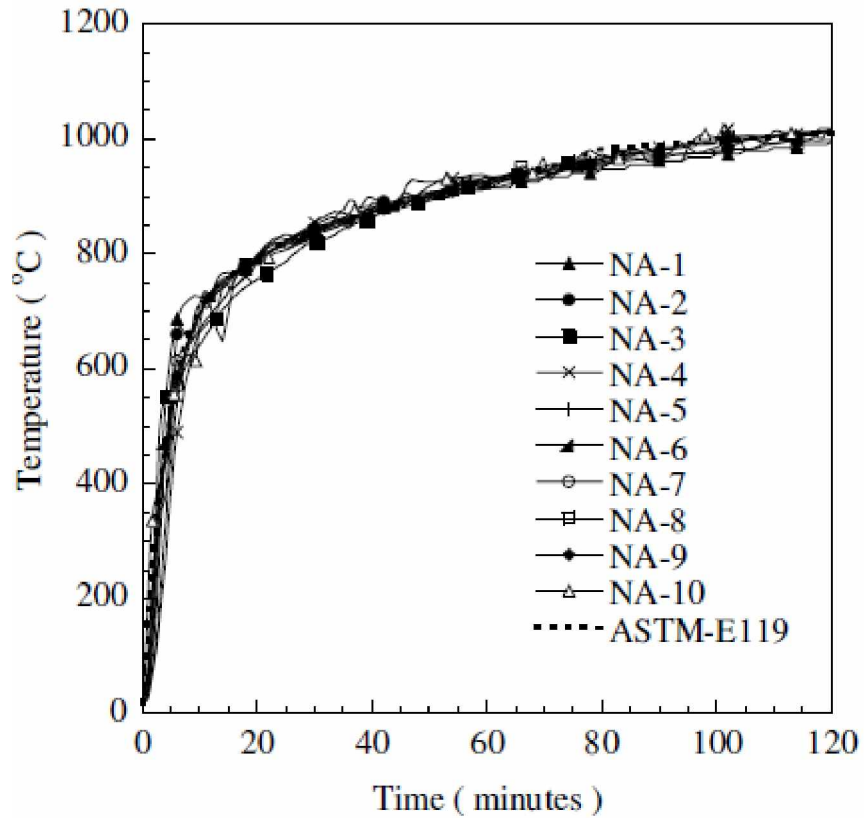
Figure 2.7: Temperature results from North American furnace tests [9]
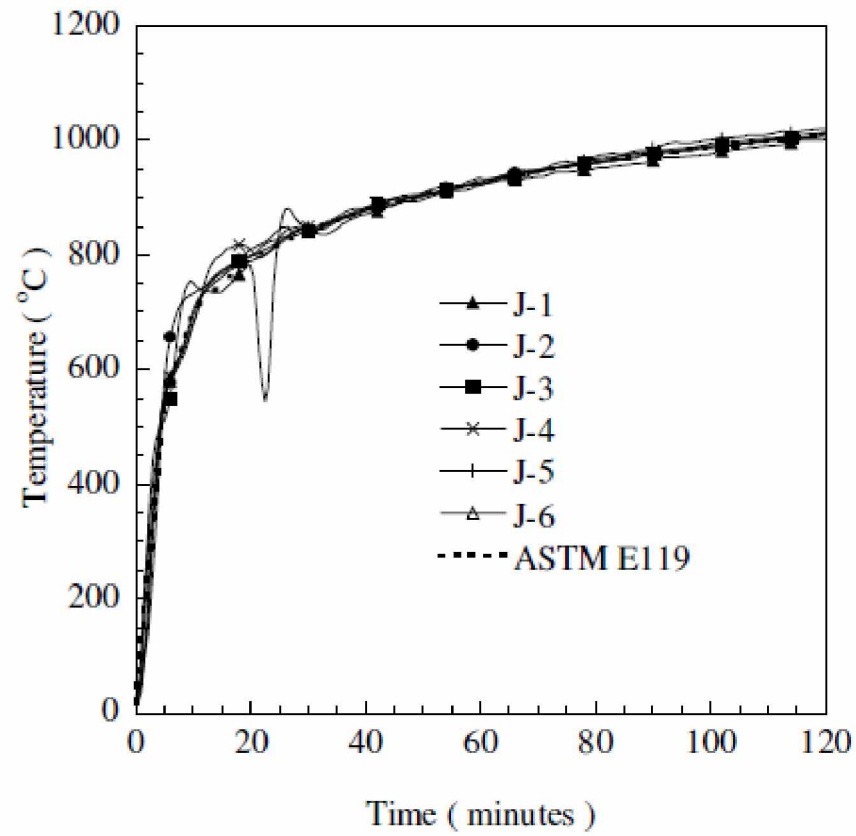
Figure 2.8: Temperature results from Japanese Furnace tests [9]
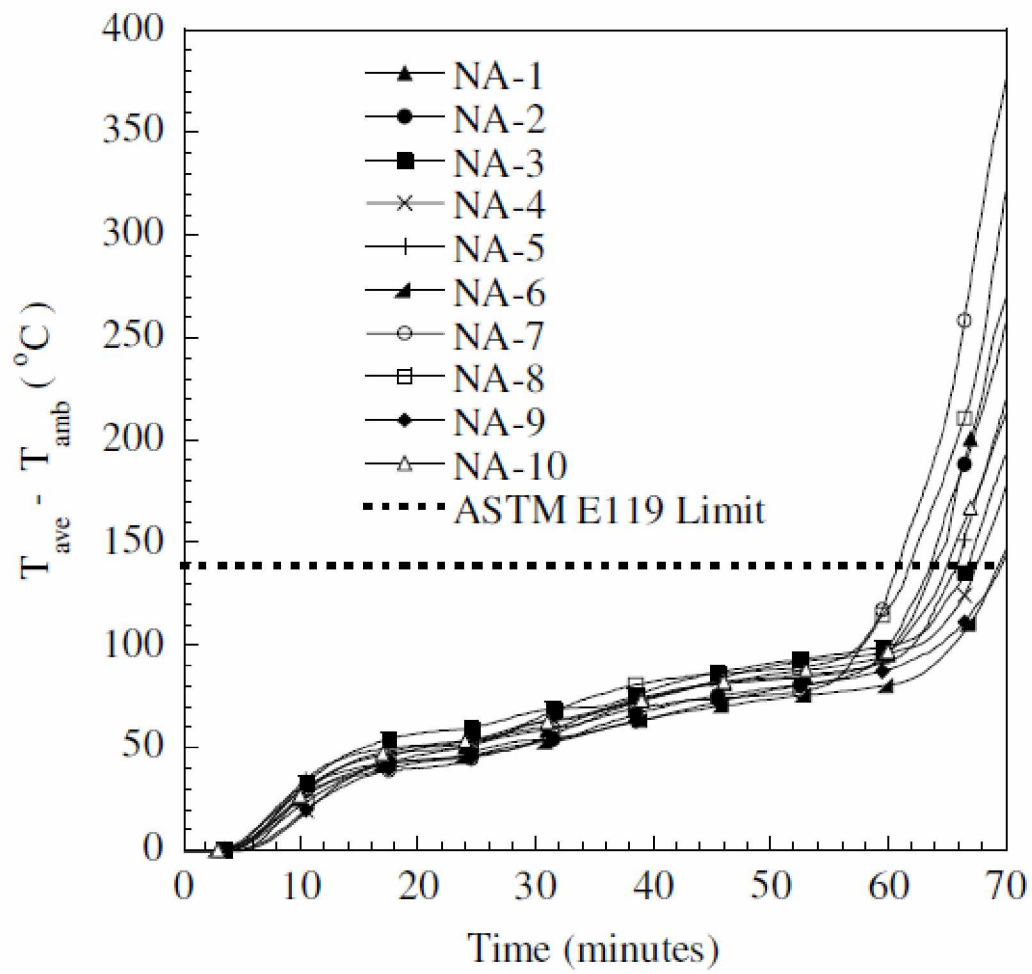
Figure 2.9: North American furnace tests temperature results on the unexposed surface [8]
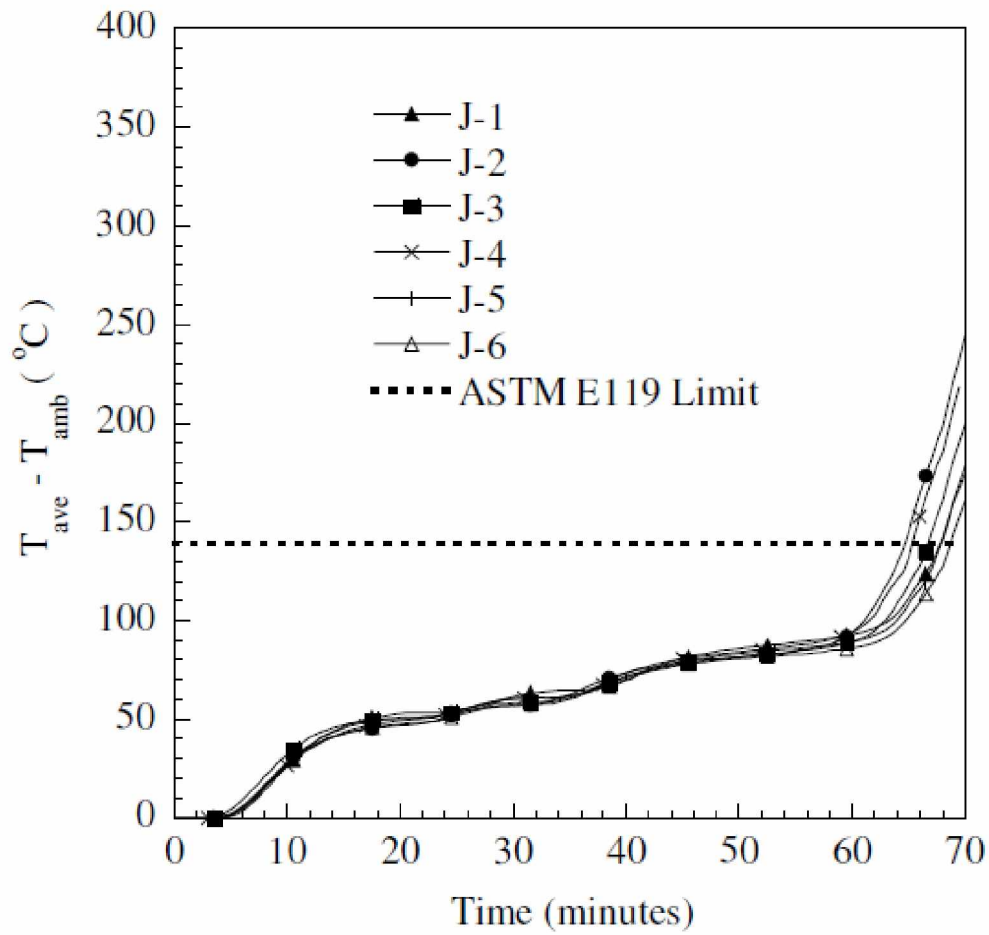
Figure 2.10: Japanese furnace tests temperature results on the unexposed surface [9]

2.4.3 Discussion of the Experimental Results

Figure 2.7 and Figure 2.8 show how close the furnace temperature was to the standard temperature curve, given in ASTM E119. In Figure 2.8, the temperature recorded by J-1 had a sharp decline around 25 minutes into the test, and this was due to a temporary failure of the furnace. It was corrected around 30 minutes into the test, at which point the temperature started following more closely the standard temperature curve once again.

Figure 2.9 and Figure 2.10 show the increase on the unexposed side of the assembly wall for both the North American and Japanese laboratories. As mentioned earlier, one of the failure criteria for the wall assembly in a furnace test was when the average temperature increase on the unexposed side of the wall assembly reached 139 C above its initial average temperature. The failure at 139 C is marked with a dashed line for both the North American

18

and Japanese tests. The temperature increases in the North American furnace tests were not as clustered as the Japanese furnace tests, but the overall pattern between temperature and time was consistent across all tests. As seen in the two figures, all the average temperature increases exceeded 139 C between 60 and 70 minutes into the test. Therefore, all the gypsum boards passed the 1 hour fire test. It can also be observed that after about 60 minutes there was a sharp increase in the temperature. It can be assumed that around that time the gypsum board on the furnace side essentially fell off, or big fissures appeared on that board.

2.5 Numerical Modeling

ABAQUS [19] is a finite element analysis software that can simulate different physical or engineering problems such as structural analysis, heat transfer simulation, and fluid dynamics. Moreover, it also has the feature to do coupled analysis which can combine different forms of analysis together. The experimental fire tests reported by Manzello, et al. [9] were numerically simulated using ABAQUS V6.14.

2.5.1 Material Properties

The type of steel for the steel studs in the wall assembly was not given explicitly in the study published by Manzello, et al. [9]. However, general thermal properties of carbon steel are well known and given in Table 2.1 [16]. The thermal properties of air are given in Table 2.2.

The thermal properties of the Type X gypsum board measured by Manzello, et al. [9] were plotted in Figures 2.2, 2.3, 2.4 and 2.5. However, the specific heat of the Type X gypsum boards used in the model was modified from the original specific heat of the gypsum board wall assemblies measured by Manzello, et al. [9], in order to accurately simulate the temperature results. The modified thermal properties of the Type X gypsum boards were calculated based on conservation of energy, existing theories regarding the thermal behavior of Type X gypsum boards, and the experimental temperature results. The thermal conductivity of the gypsum boards originally reported by Manzello, et al. [9] was used in the model, however, in combination with the modified specific heat. Table 2.3 gives the modified specific heat of the Type X gypsum boards. A detailed discussion on the necessity of using the modified specific heat of the Type X gypsum boards is given below.

Table 2.1: Properties of steel [20]

Thermal Conductivity	45 W/m*C
Specific Heat	600 J/kg*C
Density	7850 kg/m3

Table 2.2: Properties of air vs temperature [21]

Temperature (K)	Specific Heat C_p (kJ/kg*K)	Thermal Conductivity (10-5 kW/m*K)	Prandtl Number	Kinematic Viscosity (10^{-5} m²/s)	Density (kg/m³)
225	1.0027	2.02	0.728	0.935	1.569
250	1.0031	2.227	0.72	1.132	1.412
275	1.0038	2.428	0.713	1.343	1.284
300	1.0049	2.624	0.707	1.568	1.177
325	1.0063	2.816	0.701	1.807	1.086
350	1.0082	3.003	0.697	2.056	1.009
375	1.0106	3.186	0.692	2.317	0.9413
400	1.0135	3.365	0.688	2.591	0.8824
450	1.0206	3.71	0.684	3.168	0.7844
500	1.0295	4.041	0.68	3.782	0.706
550	1.0398	4.357	0.68	4.439	0.6418
600	1.0511	4.661	0.68	5.128	0.5883
650	1.0629	4.954	0.682	5.853	0.543
700	1.075	5.236	0.684	6.607	0.5043
750	1.087	5.509	0.687	7.399	0.4706
800	1.0987	5.774	0.69	8.214	0.4412
850	1.1101	6.03	0.693	9.061	0.4153
900	1.1209	3.897	6.276	0.696	9.936
950	1.1313	6.52	0.699	10.83	
1000	1.1411	6.754	0.702	11.76	0.3922
1050	1.1502	6.985	0.704	12.72	0.3716
1100	1.1589	7.209	0.707	13.7	0.353
1150	1.167	7.427	0.709	14.7	0.3362
1200	1.1746	7.64	0.711	15.73	0.3209
1250	1.1817	7.849	0.713	16.77	0.3069
1300	1.1884	8.054	0.715	17.85	0.2941
1350	1.1946	8.253	0.717	18.94	0.2824
1400	1.2005	8.45	0.719	20.06	0.2715
1500	1.2112	8.831	0.722	22.36	0.2615
1600	1.2207	9.199	0.724	24.74	0.2521
1700	1.2293	9.554	0.726	27.2	0.2353
1800	1.237	9.899	0.728	29.72	0.2206
1900	1.244	10.233	0.73	32.34	0.2076

Table 2.3: Modified thermal properties of Type X gypsum board

Temperature (C)	Specific Heat (J/kg*C)
60	1000
70	10000
140	10000
150	1000

2.5.2 Wall Assembly

The model of the wall assembly built in ABAQUS is given in Figure 2.11. Detailed dimensions of the wall assembly are given in Figure 2.12 with the temperatures at Locations 1, 2, 3 and 4 to be recorded in the analysis. Note that Location 4 is the unexposed surface of the gypsum board and is also where Manzello et al. [9] recorded the experimental temperature results. Each gypsum board had the dimension of 3000mm X 3000mm X 15.9mm, and each steel stud had the dimension of 92mm X 41mm X 12.7mm X 0.48mm (3.625 in X 1.625 in X 0.5 in X 0.0188 in).

2.5.3 Boundary Conditions

The fire side of the type X Gypsum board was subjected to heat transfer from the oven, which takes place in three forms: thermal conduction, thermal convection and thermal radiation. The temperature of the furnace followed the ASTM E119 temperature curve, which is given in Figure 2.13. The convective heat transfer coefficient used was 25 W/m^2*K for the furnace side of the Type X Gypsum board [21]. The emissivity of the Type X Gypsum boards used was 0.9 under all conditions [21]. The convective heat transfer coefficient used was 10 W/m^2*K for the unexposed side of the Type X Gypsum board [21]. The ambient temperature chosen was 20 C. The demonstration of the boundary conditions is given in Figure 2.12.
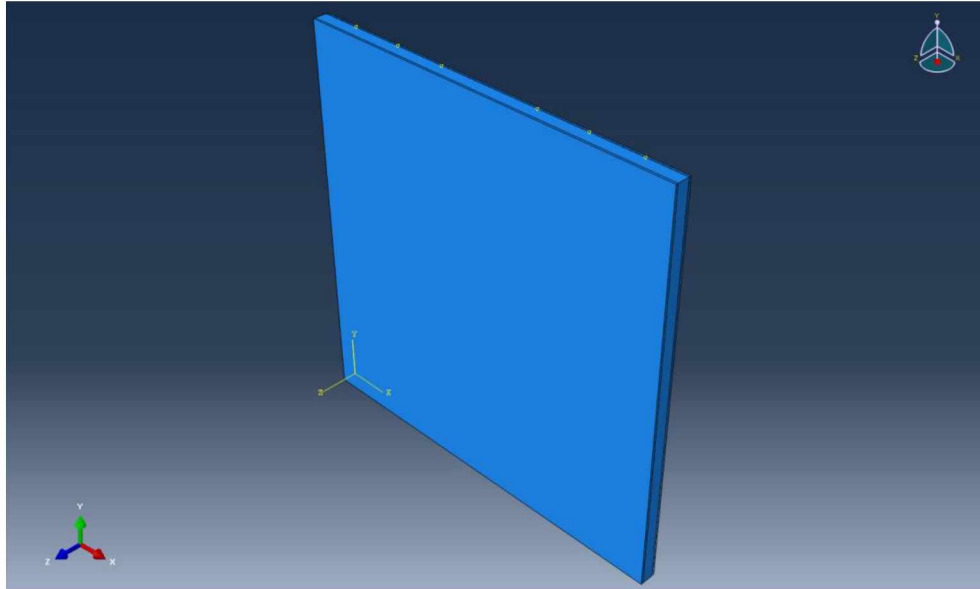
Figure 2.11: 3D model of wall assembly in ABAQUS
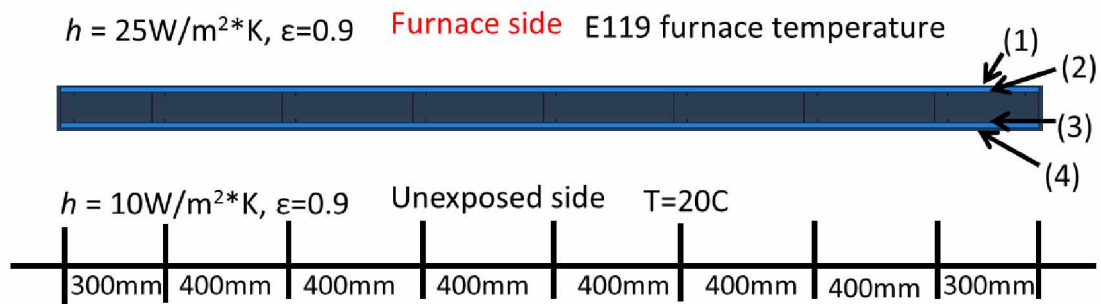
Figure 2.12: Detailed dimension of the wall assembly model and temperatures to be recorded at Locations 1, 2, 3 and 4
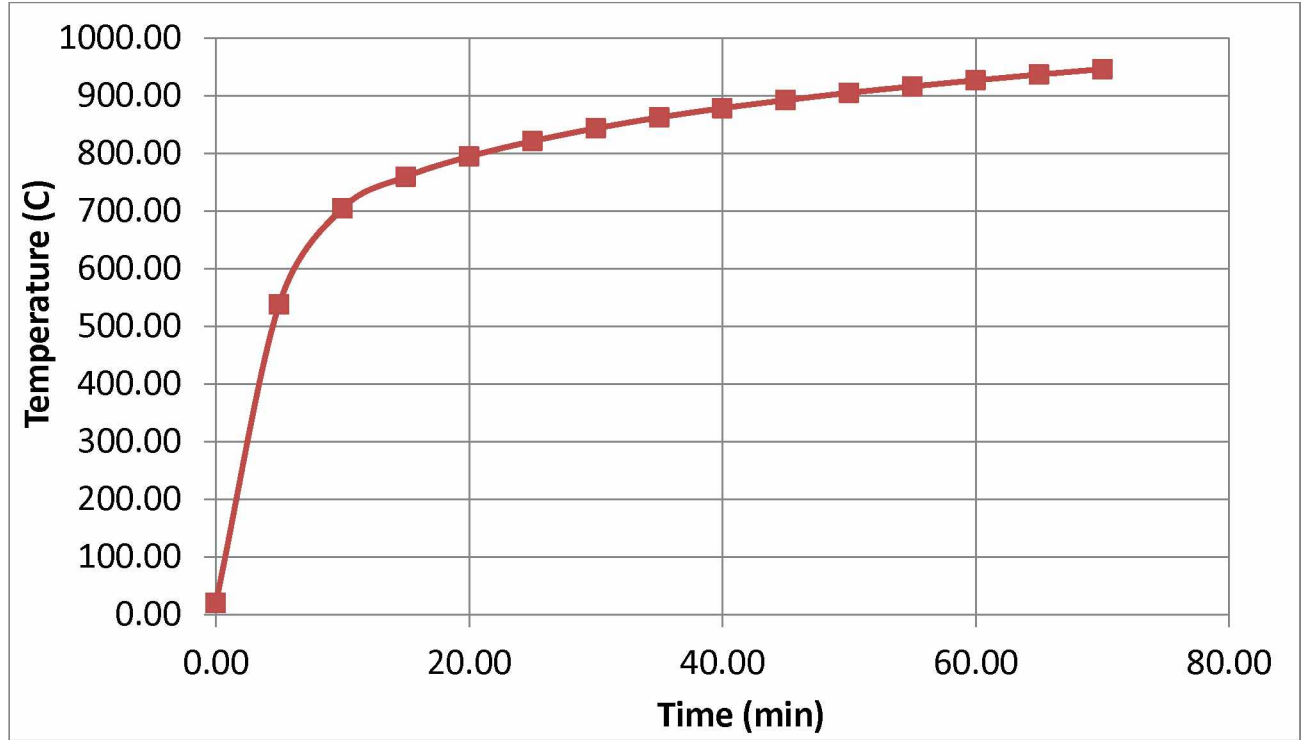
Figure 2.13: ASTM E119 temperature curve

In the experiment, the wall assembly was heavily insulated on all sides. After about 60 minutes into each test, there was an apparent breach was on the fire side of the wall assembly, at which point the flames and hot steam would touch the ambient gypsum board directly [9]. In the model, it was assumed that after 60 minutes into the analysis a breach would appear on the furnace side of the gypsum board, at which point 1/10 of the heat flux from the furnace fire would go directly into the interior surface of the ambient gypsum board. It was assumed that after 65 minutes into the analysis the entire gypsum board on the furnace side would fall off, and the entire furnace heat flux would go directly into the interior surface of the gypsum board on the ambient side.

2.5.4 Heat Transfer in Cavity

The heat transfer in the cavity of the wall assembly takes places in two forms: thermal convection and thermal radiation. The total heat transfer is given in Equation 2.1, and convective heat transfer and radiative heat transfer are given in Equations 2.2 and 2.3 [22].

$$\dot{Q}_{total} = \dot{Q}_{conv} + \dot{Q}_{rad} \qquad (2.1)$$

$$\dot{Q}_{conv=}(T_1 - T_2)\frac{K_{eff}}{L}A \tag{2.2}$$

$$\dot{Q}_{rad} = (T_1^4 - T_2^4)\varepsilon\sigma FA \tag{2.3}$$

Where:

$\dot{Q}_{total}$ is the total heat transfer in the cavity of the gypsum board wall assembly;

$\dot{Q}_{conv}$ is the convective heat transfer in the cavity of the gypsum board wall assembly;

$\dot{Q}_{rad}$ is the radiative heat transfer in the cavity of the gypsum board wall assembly.

The following symbols were used in modeling:

T_1 is the temperature of the surface of cavity on the fire side;

T_2 is the temperature of the surface of cavity on the ambient side;

L is the distance of the cavity in the gypsum board wall assembly, 92 mm in this case;

K_{eff} is the effective thermal conductivity of air in the cavity of the wall assembly;

ε is the thermal emissivity of gypsum board, 0.9; and

σ is the Stefan Boltzmann constant, $5.67*10^{-8}$ W/m^2*K^4 or $1.714\times10-9$ BTU/hr*ft^2*R^4.

Although the radiative heat transfer can be analyzed handily, the convective heat transfer cannot be analyzed directly. Instead, the convective heat transfer in the cavity of the wall assembly was analyzed by introducing the concept of the Nusselt number, Nu, which greatly simplifies the convective heat transfer analysis by equating convective heat transfer to a modified conductive heat transfer. The modified conductive heat transfer is assumed to take place in the cavity of the wall assembly with an effective thermal conductivity K_{eff} and is given in Equation 2.4.

Equation 2.4 gives the effective thermal conductivity. K_{air} is the thermal conductivity of air and Nu is the Nusselt number in the cavity of the wall assembly. The Nusselt number in the cavity of two rectangular plates can be calculated with Equations 2.5 and 2.6.

$$K_{eff} = K_{air}Nu \tag{2.4}$$

$$Nu = 0.46Ra_L^{1/3} \tag{2.5}$$

$$Ra_L = \frac{g\beta(T_1-T_2)L_c^3}{v^2}Pr \tag{2.6}$$

Where:

Ra_L is the Rayleigh number;

g is the gravitational acceleration, m/s^2 or ft/s^2;

β is the coefficient of volume expansion, $1/K$ ($\beta = 1/T$ for ideal gas);

L_c is the characteristic length, m or ft ($L_c = 92\ mm$ in this case);

υ is the kinematic viscosity of the fluid, m^2/s or ft^2/s; and

Pr is the Prandtl number.

The view factor between any two parallel plates is calculated according to Equation 2.7.

$$F = \frac{1}{\pi w^2}\left(ln\frac{x^4}{1+2w^2} + 4wy\right)$$ (2.7)

Where:

$$w = H/L$$ (2.8)

H is the height of the gypsum board, 3050 mm in this case

$$x = \sqrt{1 + w^2}$$ (2.9)

$$y = x \cdot arctan(\frac{w}{x}) - arctan(w)$$ (2.10)

The above equations were implemented in ABAQUS in a recursive manner. As can be seen in Equation 2.4, the effective thermal conductivity is the product of the air thermal conductivity and the Nusselt number. If the Nusselt number were to be equal to 1, that would mean that there would be no convection in the cavity of the wall assembly and the air would be acting like a solid medium. On the other hand, if the Nusselt number were to be infinity, the cavity in the wall assembly would have no thermal insulation effect, and the temperature at Location 2 and Location 3 would become the same. The author first assumed the Nusselt number to be equal to 1 at all times and then ran the analysis. Next, the author calculated the new Nusselt number based on the temperature result from the previous run and then repeated the iteration. The iteration ended when the difference between the new Nusselt number and the previous Nusselt number became negligent. Figure 2.14 shows the effective thermal conductivity of the air in the cavity as a function of temperature for 3 iterations. The effective thermal conductivity of the air in the cavity in the first iteration (K_eff_I1) was obtained from the temperature results from the model, in which the Nusselt number was 1 (K_eff = K_air). The effective thermal conductivity of the air in the second iteration

(K_eff_I2) was obtained from the temperature results from the model with K_eff_I1. It can be seen in Figure 2.13 that the effective thermal conductivity converged after only 3 iterations of analysis.
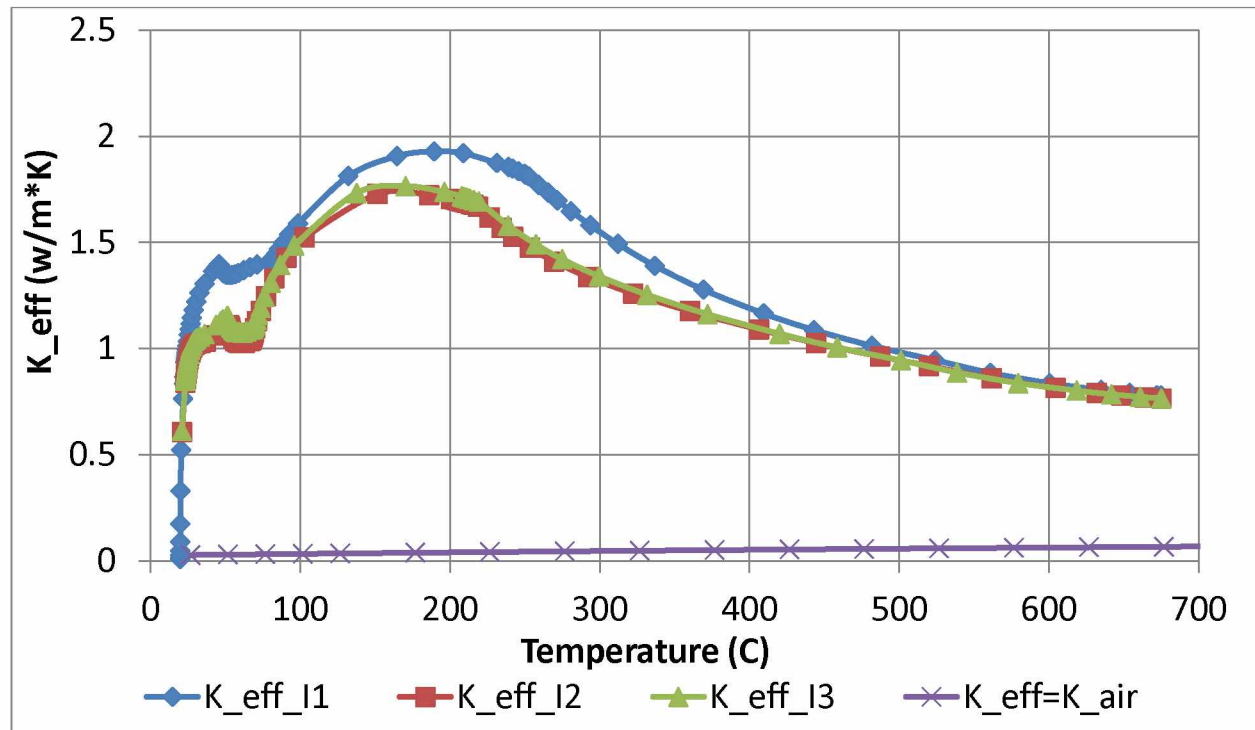
Figure 2.14: Convergence of effective thermal conductivity, K_eff

2.5.5 Meshing of the Model

The meshing of a single steel stud (left) and the meshing of the wall assembly (right) are given in Figure 2.15. The entire model was made of DC3D8 elements with 24,366 nodes and 12,120 elements. All the simulations were conducted on Windows 10 installed on a Dell, Optiplex 9010, with an Intel ® Core ™ i&-3770, CPU@3.40GHz processor and 32GB RAM.

The verification of the heat transfer analysis in ABAQUS against theoretical analysis is given in Appendix A, which only gives the heat transfer analysis in a single direction because it was assumed in this study heat only transferred across in the direction of the thickness of the gypsum board wall assembly. Therefore, the temperature along the height of the wall assembly was constant at every cross section.
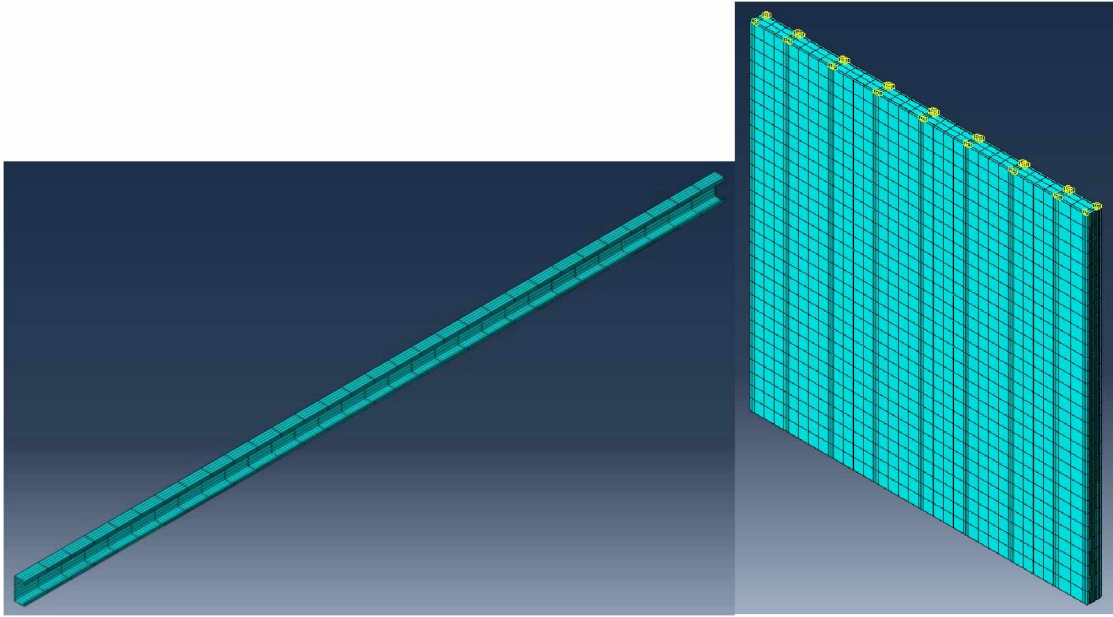
Figure 2.15: Meshing of a single stud (left) and meshing of the entire wall assembly (right)

2.6 Discussion of the Numerical Results

As stated in the section on numerical modeling, the specific heat of the gypsum boards in the model was modified to obtain the desired numerical temperature results. The explanation of this modification is given in the content below.

In the measurement given by Manzello, et al. [9], the thermal conductivity of the gypsum board was tested after the gypsum board was dehydrated [7, 9]. The dehydration of the gypsum board was achieved by heating up the gypsum board until all the chemically bound water was released and vaporized. The chemically bound water starts releasing from the gypsum board when the temperature reaches about 100 C and the dehydration stops at about 200 C [7, 9]. The thermal conductivity of the dehydrated gypsum board was measured at different temperatures, which were held constant throughout each test. On the other hand, the gypsum boards in the wall assembly fire tests were not dehydrated prior to the test because the chemically bound water in the gypsum boards was the primary element contributing to the fire resistance of the wall assembly. The thermal conductivity of a dehydrated gypsum board can be very different from that of a gypsum board prior to dehydration. In addition, in the tests of undehydrated gypsum boards, unlike in the tests of dehydrated gypsum boards, water vapor migration due to water vapor being released when heated can change the thermal conductivity during the tests. Besides the difference in thermal conductivity

28

between the measured values by Manzello and the in-situ values, a change can also occur in the specific heat for the gypsum boards. The specific heat of the gypsum boards was measured by Manzello and given in Figure 2.3. The measurement was taken by using a calorimeter at a temperature rise rate of 20 C/min [9]. The measurement was again taken in a different way than how the wall assembly fire tests were conducted. The temperature curve of the fire tests is given in Figure 2.13. It can be observed in Figure 2.13 that the temperature rise rate, especially in the first 10 minutes of the fire tests, was significantly faster than 20 C/min. Therefore, the specific heat as a function of temperature for the gypsum boards in the fire tests might not follow the one given by Manzello in Figure 2.3. However, the total enthalpy of a gypsum board, which equals the integrated area of the specific heat vs temperature, as seen in Figure 2.3, should always remain about the same due to the principle of conservation of energy.

Gypsum boards are also known to get damaged after a prolonged period of burning during fire tests [2]. In the tests by Manzello, failure was observed when a crack opened up on the gypsum board exposed to the fire and the temperature was high enough to ignite cotton waste [7, 9]. The cracking and damaging of the burning gypsum board over time can influence the thermal conductivity of the material, but it was assumed in this study that the specific heat of gypsum boards would not be affected by the cracking and damaging.

The thermal conductivity can also be affected by the temperature variation on the exposed side and the unexposed side of the gypsum boards. For example, the overall average temperature on the unexposed side of the gypsum board could be at only 70 C, but some local temperatures could be well over 100 C and the dehydration process could have already started.

Therefore, the modified specific heat was devised to fit the numerical temperature results with the experimental temperature results on the unexposed side of the gypsum board in ABAQUS modeling. The modified specific heat was based on the geometric configuration of the wall assembly, the principle of conservation of energy and the characteristics of the experimental results. As detailed in the section on numerical modeling, the modified specific heat was necessary for the simulation, especially because a dramatic increase in the measured specific heat, as shown in Figure 2.3, could cause ABAQUS to abort its numerical process due to numerical instability.

Figure 2.16 gives the modified specific heat in comparison with the reported values, and Figure 2.17 gives the numerically simulated results in comparison with the North American (NA) results and Japanese (J) results. It is worth noting that only the upper bound and lower bound temperature values of the experimental results are given, as shown in Figure 2.17 and the upper and lower bound temperature values were chosen from Figure 2.9 and Figure

29

2.10. In addition, the numerically simulated temperature results, both with steel studs and without steel studs in place, are given in Figure 2.17. It can be seen that the steel studs have very little impact on the overall simulated temperature results. It is believed that the thinness of the steel studs (25 gauge) and the high thermal conductivity of steel contributed to such behavior.
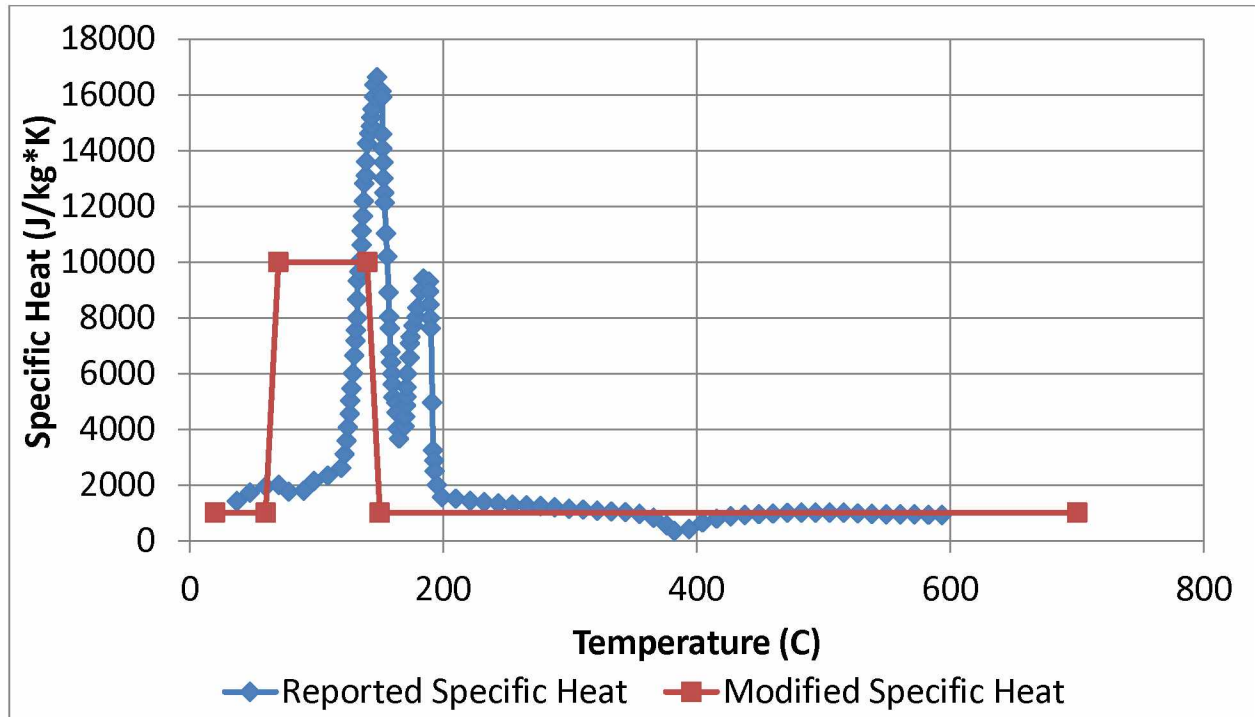
Figure 2.16: Modified specific heat of the gypsum board used in the model
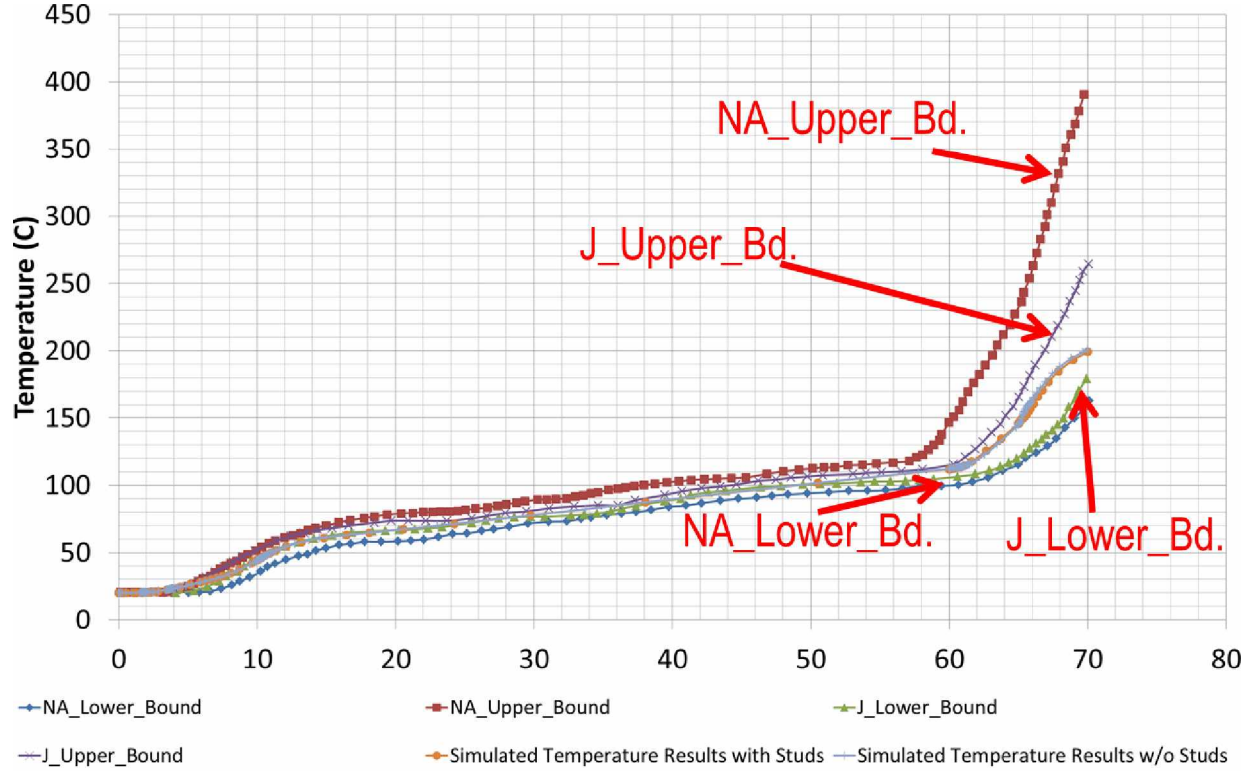
Figure 2.17: Temperature on the unexposed side (numerical results vs experimental results at Location 4)

Figure 2.18 gives the parametric analysis of the gypsum board wall assembly in furnace tests with different effective thermal conductivities, K_eff. Figure 2.18 gives the temperature results at Locations 1, 2, 3 and 4 with the Nusselt number equal to zero (Nu_0), one (Nu_1), infinity (Nu_Inf), the calculated Nusselt number given in Figure 2.14 (Nu_Cal) and the Nusselt number equal to zero but with double the radiation heat transfer (Nu_0 with double radiation). All the simulations were done without steel studs in the wall assembly. In the parametric analysis, it was assumed that the gypsum boards did not break so the heat transfer was allowed to continue for up to 180 minutes. It can be seen that the heat transfer in the cavity of the wall assembly had very little effect on the temperatures of the furnace side, Location 1, and the unexposed side, Location 4, of the gypsum boards. The heat transfer $\dot{Q}$ in the cavity relates as follows:

$$\dot{Q}_{Nu_{Inf}} > \dot{Q}_{Nu_0 \, with \, double \, radiation} > \dot{Q}_{Nu_{Cal}} > \dot{Q}_{Nu_1} > \dot{Q}_{Nu_0} \qquad (2.11)$$

It can be seen that the higher the heat transfer $\dot{Q}$ in the cavity, the closer the temperature results at Location 2 and 3 are. Table 2.4 gives the elapsed time of each simulation.

31
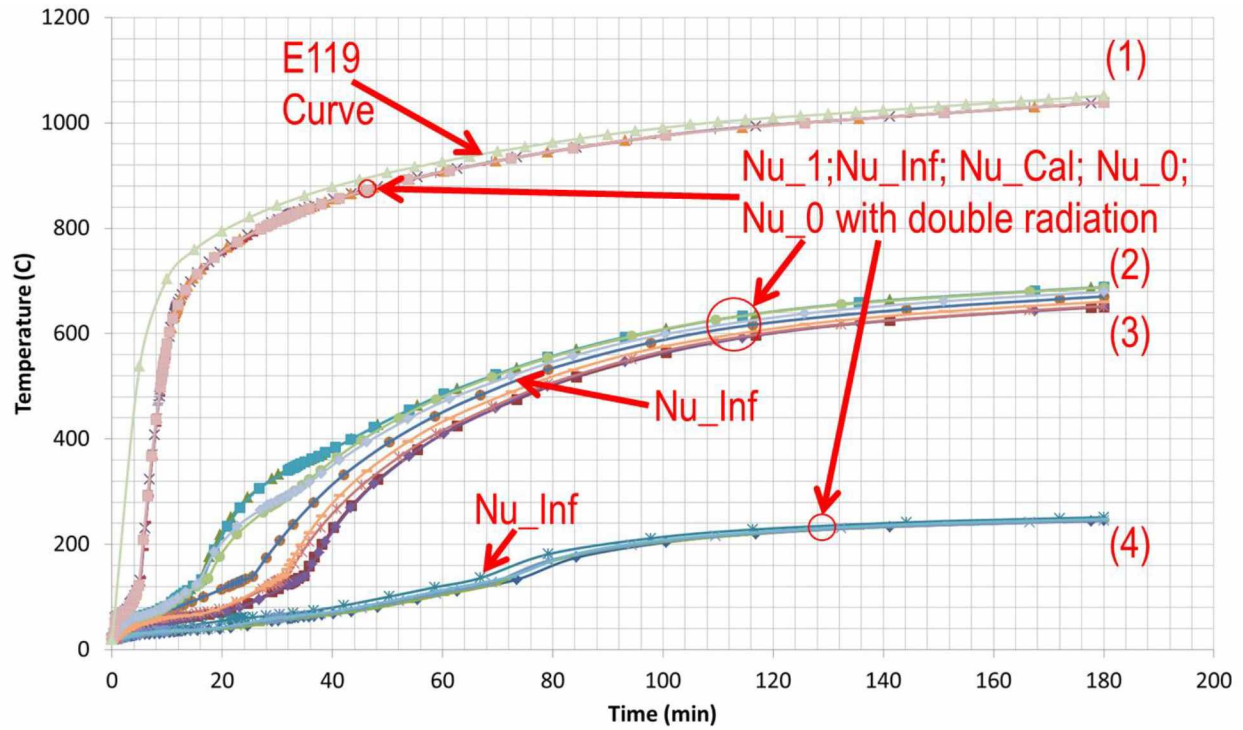
Figure 2.18: Temperature of the wall assembly with different effective thermal conductivity K_eff

Table 2.4: Elapsed time of each simulation

Steel studs	Nusselt Number	Elapsed time (s)
Yes	Nu_Cal	758.2
No	Nu_0	124.5
No	Nu_1	207
No	Nu_Cal	190.1
No	Nu_0 with double radiation	156.7
No	Nu_Inf	154.6

2.7 Conclusions

It was the purpose of the study to show that numerical modeling using ABAQUS can be an effective methodology to simulate furnace fire tests of non-load-bearing gypsum board wall assemblies. An ABAQUS numerical model was created to simulate the thermal response of the non-load-bearing gypsum board wall assembly

fire tests by Manzello, et al. [9]. Modified thermal properties were designed to fit the numerical results with the experimental results and were created based on two assumptions:

      1. The thermal conductivity was assumed to be unchanged but the specific heat was modified to achieve the desired results.

      2. The integrated area across the temperature range in the specific heat diagram was the same for both the reported specific heat and the modified specific heat. The integrated area across the temperature range equals the enthalpy of the gypsum boards, and the enthalpy should always be the same because of the principle of conservation of energy.

      It was found that the heat transfer rate in the cavity of the gypsum board wall assembly had very little effect on the overall temperature results on the furnace side, Location 1, and unexposed side, Location 4, of the gypsum boards.

      The simulated temperature results with the modified thermal properties fit right within the upper bound and low bound temperature values of the North American (NJ) and Japanese (J) tests.

2.8 Reference

[1]. Hamilton, R. Scott, Performance-based Fire Engineering for Steel Framed Structures: a Probabilistic Methodology, 2011

[2]. Kolarkar, Prakash, Structural and Thermal Performance of Cold-formed Steel Stud Wall Systems under Fire Conditions, 2010

[3]. ASTM E 119-16: "Standard Test Methods for Fire Tests of Building Construction Materials," ASTM International, West Conshohocken, PA, 2016

[4]. CAN/ULC-S101-14: "Standard Methods of Fire Endurance Tests of Building Construction and Materials, 5th Edition", Underwriters Laboratories of Canada, 2014

[5]. Rahmanian, Ima, Thermal and Mechanical Properties of Gypsum Boards and Their Influences on Fire Resistance of Gypsum Board Based Systems, 2011

[6]. ASTM C1396-04: "Standard Specification for Gypsum Wallboard," ASTM International, West Conshohocken, PA, 2014

[7]. Manzello, Samuel, et al., Analysis of Inter-laboratory Testing of Non-load-bearing Gypsum/Steel-Stud Wall Assemblies, 2007

[8]. ASTM E 1269-01: "Standard Method for Determining Specific Heat Capacity by Differential Scanning Calorimetry," ASTM International, West Conshohoken, PA, 2001

[9]. Manzello, Samuel, et al., Furnace Testing of Full-Scale Gypsum Steel Stud Non-Load-bearing Wall Assemblies: Results of Multi-Laboratory Testing in Canada, Japan, and USA, 2009

[10]. Manzello, Samuel, et al., Experimental study on the performance of a load-bearing steel stud gypsum board wall assembly exposed to a real fire, 2011

[11]. Sultan, Mohamed A. and Alfawakhiri, Farid, FIRE RESISTANCE OF LOADBEARING LSF ASSEMBLIES, 2000

[12]. Sultan, M. A. and Kodur, V. K. R, Factors Influencing Fire Resistance of Load-bearing Steel Stud Walls, 2005

[13]. Ariyanayagam, A. & Mahendran, M., Fire performance of cold-formed steel stud walls lined with calcium silicate boards, 2017

[14]. Ariyanayagam, A. & Mahendran, M., Fire Resistance of Light Gauge Steel Frame Wall Systems Lined With Gypsum Plasterboards, 2015

[15]. Kesawan, Sivakumar & Mahendran, Mahen, Fire tests of load-bearing LSF walls made of hollow flange channel sections, 2015

[16]. Rahmanian, I and Wang Y. C., A combined experimental and numerical method for extracting temperature-dependent thermal conductivity of gypsum boards, 2011

[17]. Nassif, Ayman Y., et al., Full-scale fire testing and numerical modelling of the transient thermo-mechanical behaviour of steel-stud gypsum board partition walls, 2014

[18]. Liu, Faqi, et al., Fire performance of non-load-bearing light-gauge slotted steel stud walls, 2017

[19]. ABAQUS, Dassault Systèmes, 2014

[20]. Eurocode 4 - Design of composite steel and concrete structures - Part 1-2: General rules - Structural fire design, 2005

[21]. Keerthan, P. and Mahendran, M., Numerical Studies of Gypsum Plasterboard Panels Under Standard Fire Conditions, Fire Safety Journal 53: 105-119, 2012

[22]. Cengel, Y and Ghajar, A, *Heat and Mass Transfer, Fundamentals & Applications*, 2011

Chapter 3   Numerical Evaluation of Fire Ratings: Load-bearing Wall[2]

3.1 Abstract

Gypsum board wall assemblies are used in modern structures as non-load-bearing and load-bearing walls. Due to potential fire hazards existing in commercial or residential buildings nowadays, the loading capacity of the studded gypsum board wall assemblies under fire has become an important subject. Traditionally, the loading capacity of gypsum board wall assemblies under fire has been determined by standard fire tests. However, due to the high expense and lengthy time period associated with the fire tests, people have been trying to use other means to analyze the loading capacity of studded gypsum board wall assemblies when exposed to fire.

In this study, the experimental result of a studded gypsum board wall assembly subjected to a standard fire test was studied and a Finite Element Model (FEM) analysis was done to simulate the experiment. The numerical results obtained from the FEM simulation compared closely to the experimental results. The FEM analysis can potentially be used to simulate and predict the thermal and structural behavior of the gypsum wall assemblies without the need for future fire tests.

3.2 Introduction

Non-load-bearing and load-bearing gypsum wall assemblies have become increasingly popular in modern day construction due to their characteristically high ratio of loading capacity to weight [1]. In modern day construction, as skyscrapers become more and more common, fire safety is also becoming a significant issue, especially in the aftermath of 9/11 attack where multiple high-rise, steel-framed buildings caught fire and eventually collapsed [2]. Therefore, the inherent fire-resistant nature of wall assemblies composed of gypsum boards framed by steel studs makes them some of the best choices available for modern structural compartmentation purposes [3]. The Fire Resistance Rating (FRR) of a gypsum board wall assembly can be determined by subjecting the wall assembly to standard fire tests. Fire tests usually consist of a furnace burning while a gypsum board wall assembly is used as the lid of the furnace. The furnace must be well insulated. The temperature of the inside of the furnace has to be controlled to follow a standard temperature vs time curve, such as the one given by the document ASTM E119 [4] in

the US. According to E119, the failure criteria to test the FRR of a specific structural member can be categorized as such:

a) If the average temperature rise or the maximum temperature rise of the ambient side gypsum board exceeds certain values (thermal insulation);

b) If a breach occurs on the tested structural member so that flames can escape and spread (thermal integrity);

c) If the structural member experiences any structural failure under the specified loading condition in the fire test due to the degradation of the mechanical properties of the structural member (structural integrity).

There has been research done on the thermal and structural behaviors of gypsum board wall assemblies when exposed to fire. Manzello, et al. [5] did a series of tests in North America to study the effects on the thermal behavior of several gypsum board wall assemblies. The wall assemblies consisted of 10 samples of the same configuration: 10 ft (3.05 m) X 10 ft (3.05 m) wall assembly covered by single layer of gypsum boards on both sides with 9 20 gauge steel studs inside; the gypsum boards were 5/8 in (16 mm) thick; the studs were 16 in (40.64 cm) O.C., except for the two studs on the outside which were 12 in (30.5 cm) from the ones next to them. They recorded the temperatures on unexposed side of the gypsum boards of the wall assemblies from the beginning of the tests until the wall assemblies failed according to the failure criteria given in ASTM E119 [4]. In 2007, they did another set of tests in Japan [6] with the exact same configuration for the wall assemblies so they could compare the results from the North American Laboratory with the ones obtained from the Japanese Laboratory. Their research captured the thermal behavior of the gypsum board wall assemblies by recording the temperature rise on the gypsum boards but not the structural behavior of the wall assemblies, such as the vertical and lateral deflections of the wall assemblies.

On the other hand, some researchers did experiments to study both the thermal behavior and the structural behavior of gypsum board wall assemblies. Nassif, et al. [7] did a fire test on a 3 m X 3 m gypsum board wall assembly. The wall assembly was stuffed with rockwool as insulation material and there were two layers of 12.5 mm gypsum boards on both sides. The gypsum board wall assembly had 6 studs inside which were held together by two tracks, one on the top and one on the bottom of the wall assembly. Kolarkar [1] did a series of tests covering a variety of gypsum board wall assemblies of different configurations according to the Australian Standard [8]. Kolarkar gave very detailed descriptions of his tests and recorded both the temperatures and the deflections of the

gypsum board wall assemblies at various locations. The tests shed light on how gypsum board wall assemblies would behave at ambient temperatures and in fire tests both structurally and thermally. Kesawan and Mahendran [9] also did a series of fire tests on different types of gypsum board wall assemblies with different configurations. However, they also varied the types of studs in the wall assemblies for different tests and compared the results of these tests, something most researchers did not consider. They concluded that different types of studs can influence the thermal and structural behavior of the wall assemblies quite significantly. Chen, et al. [10, 11] did a series of wall assemblies' fire tests. They kept the studs the same for all the tests. However, they varied the boards in different fire tests in order to observe and study the difference different boards would make. The types of boards used included gypsum boards, Bolivian magnesium board and oriented standard boards. They also varied the insulation materials stuffed in the wall assemblies. Their results gave insightful information on the insulating capability of different types of boards and insulation materials. Some researchers such as Vieira Jr. [12] only did thorough and detailed experiments on gypsum board wall assemblies at ambient temperature. In the tests done at ambient temperature, only structural behaviors, such as loading capacity and deflection, were recorded. However, regardless of the fact that only the structural behaviors were studied at ambient temperature in these tests, the results of these tests can still serve as a great resource for the study of gypsum board wall assemblies under fire.

Besides experiments done on actual gypsum board wall assemblies, numerical simulation studies have also been done. Some researchers only did numerical simulation on the loading of gypsum board wall assemblies at ambient temperature. Abedi [13] used ABAQUS to simulate a stud-framed shear wall sheathed with a layer of steel sheet. Lateral deflection of the shear wall under lateral load was simulated and the buckling behavior or the shear wall was modeled. Vieira Jr. [12] simulated numerous experiments done on a variety of gypsum board wall assemblies at ambient temperature with ABAQUS and he was able to obtain very similar numerical results compared with the experimental results. Moreover, Nassif, et al., [7] conducted a fire test on a gypsum board wall assembly and a numerical simulation for the very same test and were able to achieve similar results.

Experimental data is also available for the thermal and mechanical properties of gypsum boards and steel at elevated temperatures. Kolarkar [1] conducted a series of experiments on the thermal and structural behavior of the studded gypsum board wall assemblies under fire. The steel studs were all made of G500 steel. Therefore, Kolarkar conducted tests on G500 steel's mechanical properties at ambient to elevated temperatures (from 27 C to 800 C). The experiments were done according to Australian Standard AS 2291 [8]. The stress levels at 0.2%, 0.5%, 1.5%

and 2% strain and ultimate strength were recorded. The Young's modulus was determined as the linear proportionality of the stress and strain curve up until the yield point. The recorded stress and strain levels and Young's modulus values at different temperatures from 27 C to 800 C were all tabulated in Kolarkar's publication. It is common practice to assume 200 GPa as the Young's modulus value for all steel grades and 500 MPa as the minimum design yield stress for G500 steel at ambient temperature. However, the recorded yield stress was 569 MPa and the Young's modulus was 214 GPa in the in-situ tests by Kolarkar [1]. Vieira Jr. [12] did a series of in-situ coupon tests in North America according to ASTM standards [14] at ambient temperature. The tests were done on steel samples with a design yield stress of 50 ksi (345 MPa) and Young's modulus of 29,000 ksi (200 GPa). The coupon test results were again higher than the design values. Other researchers also did tensile tests on steel samples in various regions according to different standards and they all obtained higher values for yield stress and Young's modulus for the sampled steel [15, 16, 17, 18] than their design values. The coefficient of thermal expansion for cold-formed steel is conventionally chosen as 1.17 E-5/K.

The mechanical properties for gypsum boards have been studied by different researchers. Ima [3] conducted detailed tests to study the thermal and mechanical properties of gypsum boards at different temperatures. In Ima's study, the gypsum boards tested were British products. Some researchers such as Vieira Jr. [10] and Nassif, et al. [7] conducted an extensive literature review on the mechanical properties of gypsum boards so that they could use the existing values in their numerical simulations. Both Ima and Nassif concluded in their research that gypsum boards have very little strength at high temperatures. Unlike most materials, gypsum boards actually shrink during their dehydration process and no thermal expansion occurs after the dehydration process despite the increase of temperature [4, 17]. The dehydration process occurs when the temperature of gypsum boards reaches 100 C, the temperature where chemically bound water starts being released and vaporizing. Both the volume and mass of gypsum boards become smaller after dehydration. Nassif, et al. [7] neglected gypsum boards' stiffness in his numerical simulation. They argued that gypsum boards are only 0.2% (480 MPa) as strong as steel (200 GPa) at ambient temperature and the material loses its strength at above 150 C. However, Nassif, et al. [7] only did the simulation at high temperature so it was reasonable for them to neglect the strength of the gypsum boards. Vieira Jr. [10] used 993 MPa as the Young's modulus for the gypsum boards in his numerical simulation and he only did simulations at ambient temperature. Ima [3] did tests to find out the mechanical properties of British gypsum boards and he concluded that the Young's modulus of the gypsum boards tested at ambient temperature was 1573 MPa and

only 518 MPa at 180C. The tested gypsum boards' yield stress was 1.6 MPa at ambient temperature and 0.643 MPa at 180 C.

The objective of this dissertation is to provide the industry an inexpensive alternative to evaluate the FRR for wall assemblies. A lot of fire tests for a single set of gypsum board wall assembly are usually conducted to account for potential discrepancy and the mean values of these repetitive tests are to be used as reference values. Many tests are also usually conducted by varying different parameters, such as the thickness or the types of the gypsum boards in the wall assembly, for the same set of gypsum wall assembly so the results of these tests with varying parameters can be compared, in order to study the significance of these parameters. With a credible numerical modeling methodology to simulate these tests, lots of resources and energy can be saved due to the costly and time consuming nature of those fire tests.

In this study, one of the fire tests of a gypsum board wall assembly was chosen and then studied. Subsequently, an FEM analysis in ABAQUS V6.14 was conducted to simulate the test. The FEM analysis was done by varying parameters that can affect the gypsum board wall assembly's performance, such as the mechanical properties of the steel or the magnitude of the imperfection of the steel studs. The numerical results from the simulation were compared to the experimental results. With certain parameters, the numerical results obtained were closest to the experimental results. Those parameters could potentially be used for the modeling of gypsum board wall assemblies to be tested in the future.

3.3 Experimental Description

3.3.1 Gypsum Wall Assembly

As mentioned in the Introduction section, a series of gypsum board wall assembly tests were presented by Kolarkar [1] and one of the tests was chosen in this study for numerical simulation. The wall assembly is given in Figure 3.1 (left), and the framing inside the wall assembly is given in Figure 3.1 (right) with vertical studs in numerical sequence 1 to 4. It can be seen in Figure 3.1 (right) that stud 2 and stud 4 both had two pieces of gypsum board fastened together to form a joint. Two tracks were installed on both the top and bottom of the 4 studs to secure their positions. Each stud was a 90 mm X 40 mm X 14 mm X 1.15 mm lipped channel and was made of G500 grade steel.
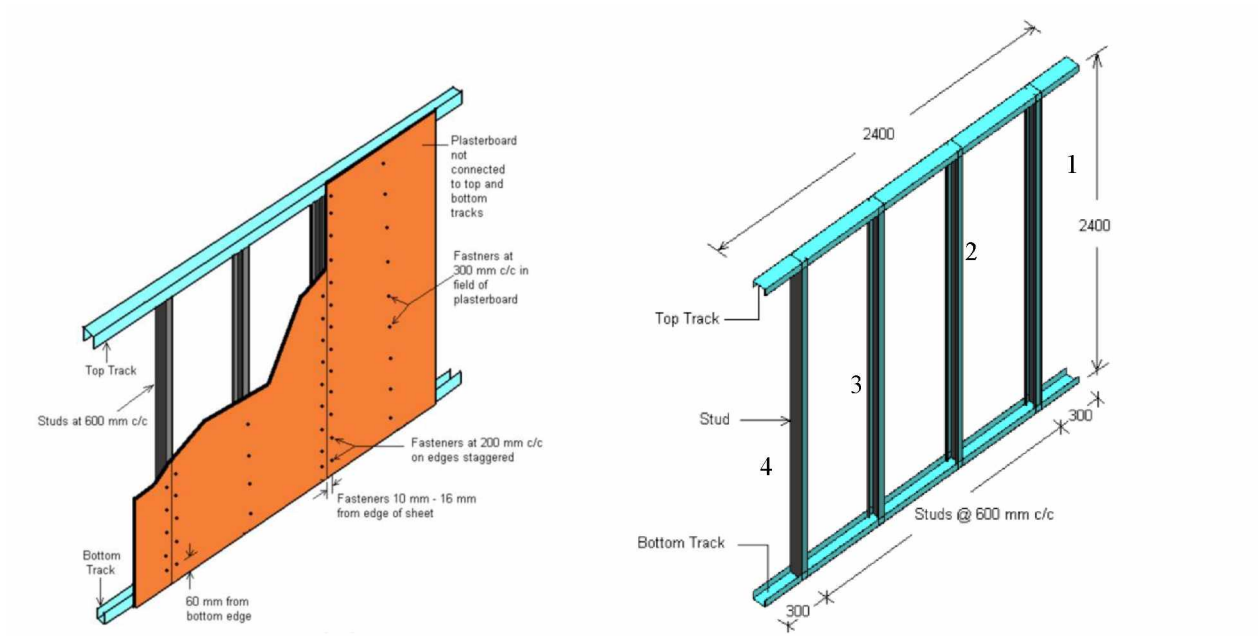
Figure 3.1: Gypsum board wall assembly (left) and steel studs (right) [1]

3.3.2 Properties of Materials

Kolarkar [1] did not give any information on the thermal properties of the materials (gypsum board and steel) used in the tests. The thermal properties include thermal conductivity and specific heat. The temperature of the steel studs in the gypsum board wall assembly was recorded as a function of time in the experiment via thermal gauges. The recorded temperatures were used for the modeled steel studs in the FEM analysis so the heat transfer analysis part of the wall assembly test was skipped in this study. However, the phenomenon of the thermal expansion of steel is one of the key features in this study because the uneven thermal expansion of the steel studs in the test caused thermal bowing and the fire side of the gypsum board was deforming towards the furnace.

3.3.2.1 Gypsum Board

The mechanical properties of gypsum boards include Young's modulus and yield strength. Kolarkar [1] did not give any information on the mechanical properties of the gypsum boards used in the tests. Studies by other researchers show that there is little variation in the mechanical properties of gypsum boards [3, 7, 12]. The

40

mechanical properties of the gypsum boards for the numerical simulation in this study were chosen from the literature studied.

3.3.2.2 Steel

Mechanical properties of steel include the Young's modulus, the yield strength and the coefficient of thermal expansion. The Young's modulus and yield strength of steel decrease as temperature increases. In fire tests done by Kolarkar [1], the steel studs were made of G500 steel and the mechanical properties of the steel were tested. The coefficient of thermal expansion plays a significant role in the structural behavior of the gypsum board wall assemblies because of the uneven thermal expansion of the steel studs between the fire and ambient sides of the wall assemblies.

3.3.3 Description of the Ambient Loading and Fire Loading Tests

The gypsum board wall assembly was mounted in a loading frame for both the ambient and fire loadings tests. The wall assembly together with the loading frame was mounted on the furnace to function as the lid for the furnace. Figure 3.2 shows the schematic diagram of the furnace-wall, assembly-loading frame setup. It can be seen that two universal beams are supporting the wall assembly, and four hydraulic jacks can load the wall assembly until it fails. Kolarkar tested the loading capacity of the wall assemblies at both ambient and elevated temperatures and the results of the tests were recorded [1].
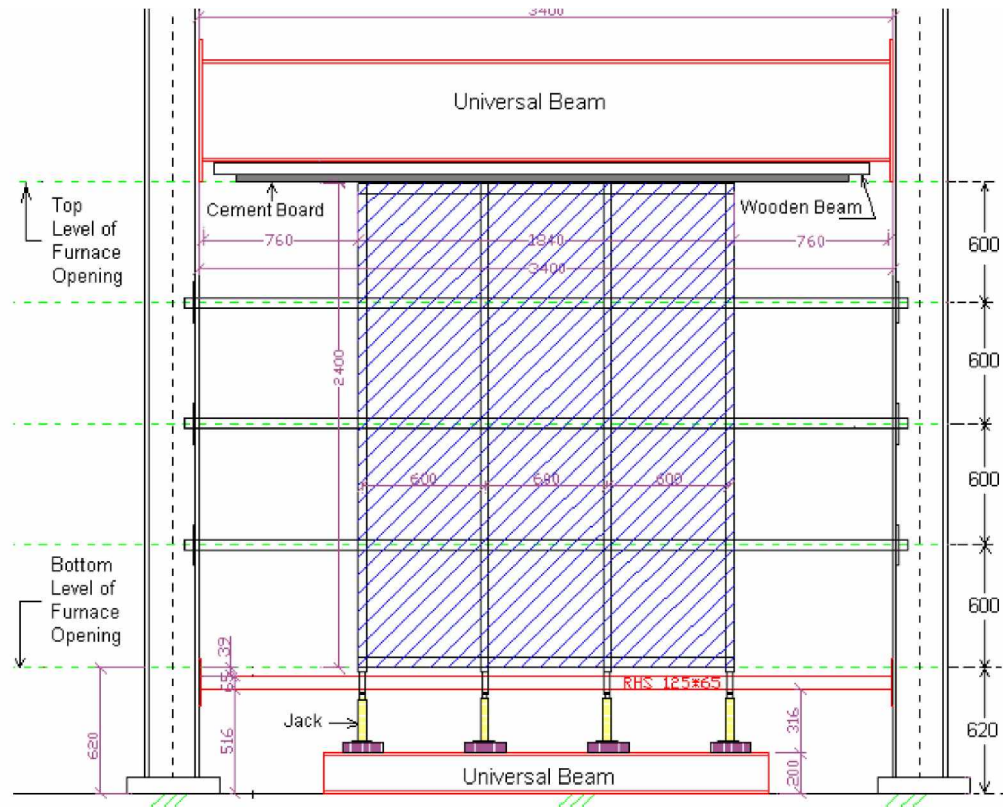
Figure 3.2: Schematic diagram of furnace-wall assembly-loading frame [1]

3.3.4 Experimental Results

In the ambient loading test, the wall assembly was loaded by the hydraulic jacks and the responses, including vertical load (kN) and vertical deflection (mm), were recorded. Buckling waves can be seen visibly when the load exceeded 52 kN/stud. The wall assembly failed to support the hydraulic jacks at 79 kN/stud and the test stopped. Figure 3.3 (a) shows the buckling shapes of stud 1 and stud 4. It can be observed that stud 1 and stud 4 both buckled at locations close to the end where the hydraulic jacks were loading the wall assembly.

The fire loading test was carried out once each hydraulic jack was loading each stud at a constant 15 kN at ambient temperature. The temperature, vertical deflection and lateral deflection at different locations were recorded as functions of time during the fire test. The recording went on until the wall assembly failed under loading. After the fire loading test, the wall assembly was unmounted from the loading frame and the deformed studs are shown in Figure 3.3 (b). Due to equipment malfunction from minute 8 to minute 17, the temperature and deflection during

that period were not recorded. However, it is reasonable to assume the responses during that time period were continuous with the responses before and after.

(a)

Stud 4

Stud 3

Stud 2

Stud 1

(b)

Figure 3.3: (a) Buckled shapes of stud 1 (left) and stud 4 (right); (b) Deformed studs after fire test

3.4 Numerical Modeling

In this section, a series of numerical modeling done with ABAQUS to simulate the tests by Kolarkar [1] is presented. The models were able to simulate the structural behavior of the gypsum board wall assembly in both the ambient and fire tests. In the modeling of the fire test, the stud temperature distribution was assigned on the stud model based on the temperature recorded during the fire test. In the model, only one stud was simulated where the recorded temperature was the highest. Since only one stud was modeled, only part of each gypsum board was modeled as well, and each chosen part of the gypsum boards was the tributary area to the steel stud. Figure 3.4 gives the schematic illustration of the stud with the tributary gypsum boards that was modeled in ABAQUS. Moreover, for simplicity, the tributary gypsum boards were modeled by linear springs to represent the stiffness provided by the gypsum boards.
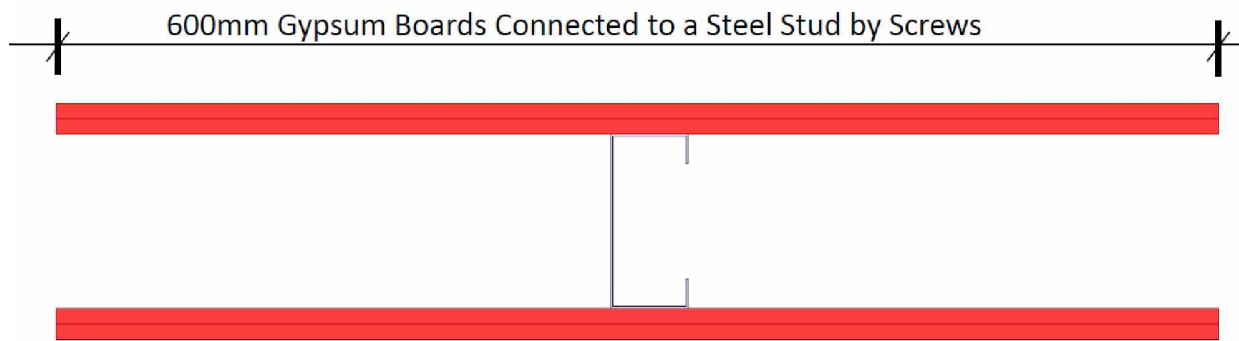
Figure 3.4: Schematic illustration of the stud fastened to the tributary gypsum boards

3.4.1 Properties of Materials

The mechanical properties of the steel and gypsum boards used in the test were introduced in the Experimental Description section above. In the model, two sets of mechanical properties of steel and one set of mechanical properties of gypsum boards were used. Kolarkar [1] did a series of in-situ tests to study the mechanical properties of G500 grade steel at different temperatures. As expected, the in-situ mechanical properties (Young's modulus and yield strength) of G500 grade steel were higher than the design values. The design value of Young's modulus of G500 steel is 200 GPa (29,000 ksi) and the design yield strength of G500 steel is 500 MPa (72.5 ksi) at ambient temperature (20 C/68 F). The in-situ mechanical properties of G500 at different temperatures were given in

Table 3.1. In the numerical modeling analysis, the in-situ mechanical properties of steel were designated as "Strong" and the design mechanical properties of the steel were designated as "Weak".

Table 3.1: In-situ mechanical properties of G500

Temperature (C)	Young's Modulus (GPa)		Yield Stress (MPa)		Poisson's ratio
	In-situ Values	Design Values	In-situ Values	Design Values	
27	214	200	569	500	0.3
100	210	196	565	497	0.3
200	194	181	560	492	0.3
300	167	156	539	474	0.3
400	154	144	400	352	0.3
500	85.3	80	219	192	0.3
600	63.2	59.1	69	60.6	0.3
700	43.2	40.4	39.5	34.7	0.3
800	11.9	11.2	23	20.2	0.3

The mechanical properties of the gypsum boards used were not tested in Kolarkar's [1] study. However, there is data available for the mechanical properties of different types of gypsum boards in different regions of the world and the mechanical properties in the existing literature vary in a relatively narrow range [3, 7, 12]. Also, it is almost a consensus among different researchers that gypsum boards lose most of their strength when the temperature exceeds 200 C [4, 17]. Moreover, the gypsum boards were not explicitly modeled in this study but modeled as linear spring elements installed on the stud instead. Therefore, at ambient temperature the Young's modulus of the gypsum boards was chosen to be 480 MPa for the simulation of the spring elements.

3.4.2 Wall Assembly

A model of the stud was built in ABAQUS and is given in Figure 3.5 (a). As stated before, the gypsum boards were not explicitly modeled in the analysis but modeled as springs instead. Springs were located at the locations of the fasteners (nails) along stud 2, as shown in Figure 3.1 (left). However, each spring was evenly distributed over 9 locations on the stud to avoid numerical instability, as demonstrated in Figure 3.5 (a) and Figure 3.5 (b). It is noted in Figure 3.5 (b) that spring elements only provide stiffness in the y and z directions and it was assumed that the gypsum boards provided enough lateral restraint to prevent studs from buckling in the x direction [1]. The springs represented the stiffness provided by the gypsum board. The calculation of spring stiffness is given in Appendix B.
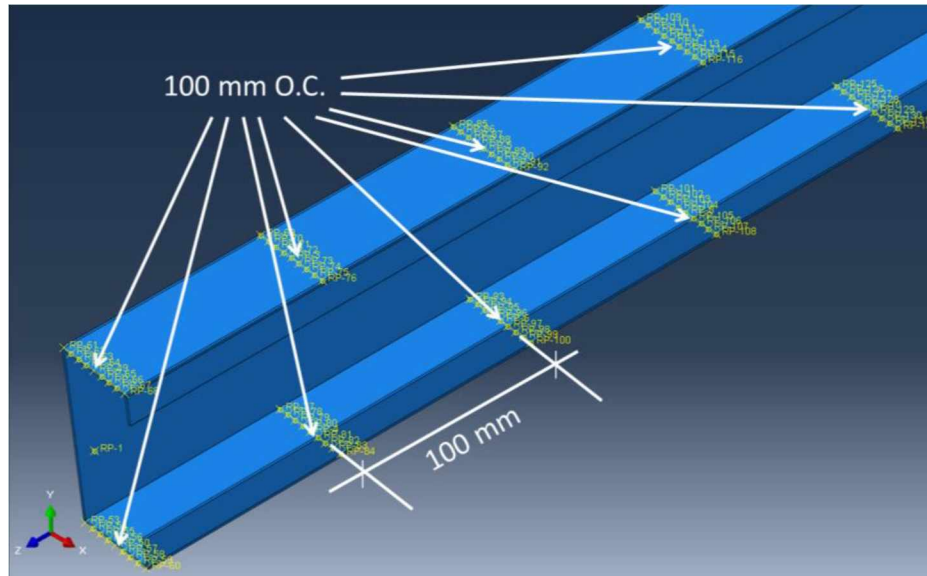
(a)
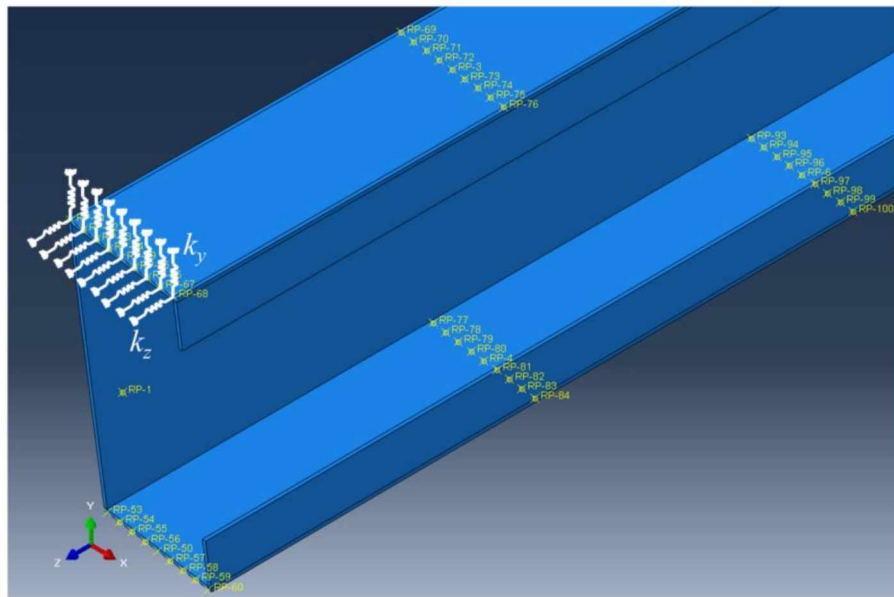
(b)

Figure 3.5: (a) Modeled steel stud in ABAQUS; (b) gypsum boards modeled as springs in ABAQUS

3.4.3 Loading and Boundary Conditions

Since the gypsum boards were modeled as linear spring elements installed on the stud, it is imperative to

know the spring stiffness in order to accurately represent the gypsum boards. Spring elements can be installed on a

beam element as shown in Figure 3.5 (b) where the stud is strengthened by translational springs in the y and z directions at each location of the fastener. The stiffness can be calculated based on the material properties of the gypsum boards and the geometric configuration of the gypsum board wall assembly in the fire test. Figure 3.1 (left) shows the locations of the screws. Studs 2 and 4 had two pieces of gypsum board fastened together by staggered nails (see Figure 3.1). The gypsum boards' joints were protected with 50 mm wide water paper and covered with two coats of joint compound [1].

The stiffness of the spring elements representing the gypsum boards in ABAQUS were calculated only in the y and z directions and it was assumed that the connection between the gypsum boards and the steel stud in the x direction was rigid. The stiffness in the y and z directions represented the flexural resistance and compressive resistance of the gypsum boards. Each line of spring elements is connected to the ground and is 100 mm O.C. as shown in Figure 3.5 (a). Each line of spring elements consisted of 9 sub-springs to avoid numerical instability. The stiffness of the spring elements in the y and z directions is given in the content below.

3.4.3.1 Stiffness of the Spring Elements in the y Direction:

The stiffness of the gypsum boards provides addition flexural strength to the studs in the y direction. Therefore, a beam model with a cross sectional area according to Figure 3.4 was designed. The beam model represented a stud being strengthened by part of the gypsum boards attributed to it. The beam model will deform under uniform loading in the y direction. The maximum beam model deflection (deflection at mid-point) should be the same as the maximum deflection of the stud model strengthened by spring elements as shown in Figure 3.5 (a). It was discovered that the stiffness of each sub-spring in the y direction was 350 N/m/spring. The derivation of the spring stiffness is given in Appendix B.

3.4.3.2 Stiffness of the Spring Elements in the z Direction:

The stiffness of the gypsum boards also provides additional strength in the z direction when the wall is compressed. The stiffness of each sub-spring was calculated to be 9000 N/m as demonstrated in Appendix B. It is assumed that the gypsum boards act like a column under compressive load.

The boundary condition can be seen in Figure 3.6. The two ends of the stud were pin-connected to the centroids of rigidity of both ends as given in Figure 3.6 (a) and Figure 3.6 (b). The centroid on one end was

restrained in the x, y and θ_Z directions, as given in Figure 3.6 (a), and the centroid on the other end was restrained in the x, y, z and θ_Z directions, as given in Figure 3.6 (b). A concentrated compressive load was imposed on the top centroid of the stud to simulate the loading in both the ambient and the fire tests. Two sets of boundary conditions were used to simulate the connection between the gypsum boards and the stud in the models. The "Partial" boundary condition signifies when only the nodes representing nails were restrained in the x direction, and the "All" boundary condition signifies when all the nodes along the middle line of the stud's web were restrained in the x direction.

Among the steel studs tested, stud 2 had the highest temperature. The average temperature across stud 2 along its height is given in Figure 3.7. The dashed vertical line signifies the time when the wall assembly failed in the fire test. It can be seen that there is a discontinuity in the recording of the stud's temperature due to the faulty equipment in the fire test. However, it can be safely assumed that the temperature before and after the discontinuity can be smoothly connected, due to the continuous nature of the temperature [1]. In the model, the recorded temperature of stud 2 was used to simulate the fire test and the temperature distribution of stud 2 was assumed to be linear. The temperature distribution is given in Figure 3.8 and the temperature is assumed to be constant across the thickness of the stud given the negligible thickness of the stud (1.15 mm/0.045 inch). To simulate the ambient test, the model was compressively loaded at the centroids of the ends and the load would increase until the numerical simulation failed to continue. For the fire test, the model was loaded at the same locations up to 15 kN, and then the fire simulation would start by assigning the recorded temperature on the stud as a function of time. The compressive load would stay at 15 kN and the simulation stopped when the numerical simulation failed to continue.
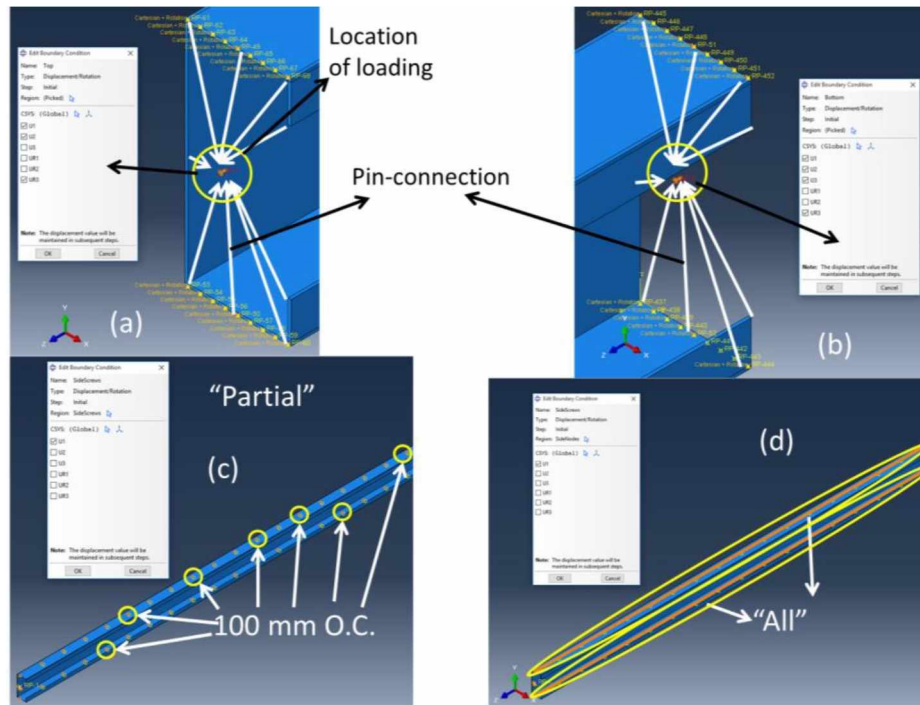
Figure 3.6: Boundary conditions of the steel stud in ABAQUS
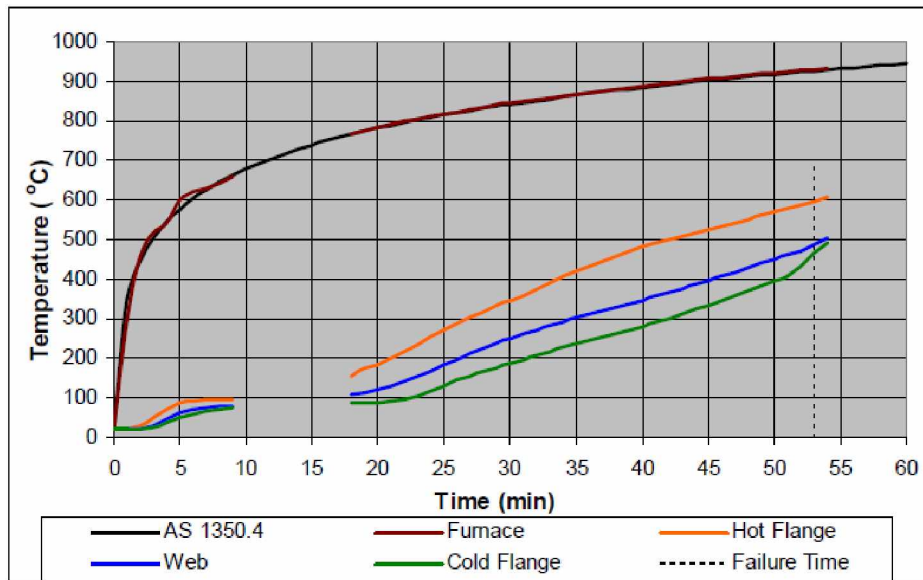
Figure 3.7: Average temperature across stud 2 [1]
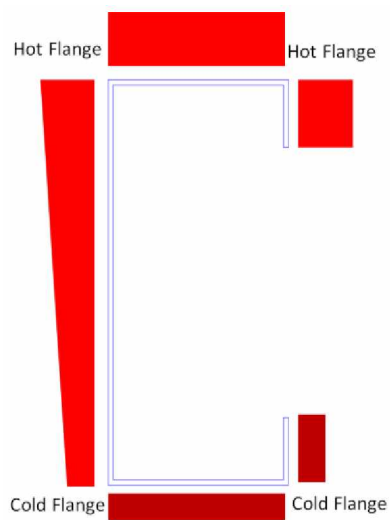
Figure 3.8: Temperature distribution across stud

3.4.4 Meshing of the Stud in ABAQUS

The meshing of the stud model is given in Figure 3.9. The model is made of C3D20R elements with 150,463 nodes and 21,120 elements. All the simulations were conducted in Windows 10 installed on a Dell, Optiplex 9010, with an Intel ® Core ™ i&-3770, CPU@3.40GHz processor and 32GB RAM.
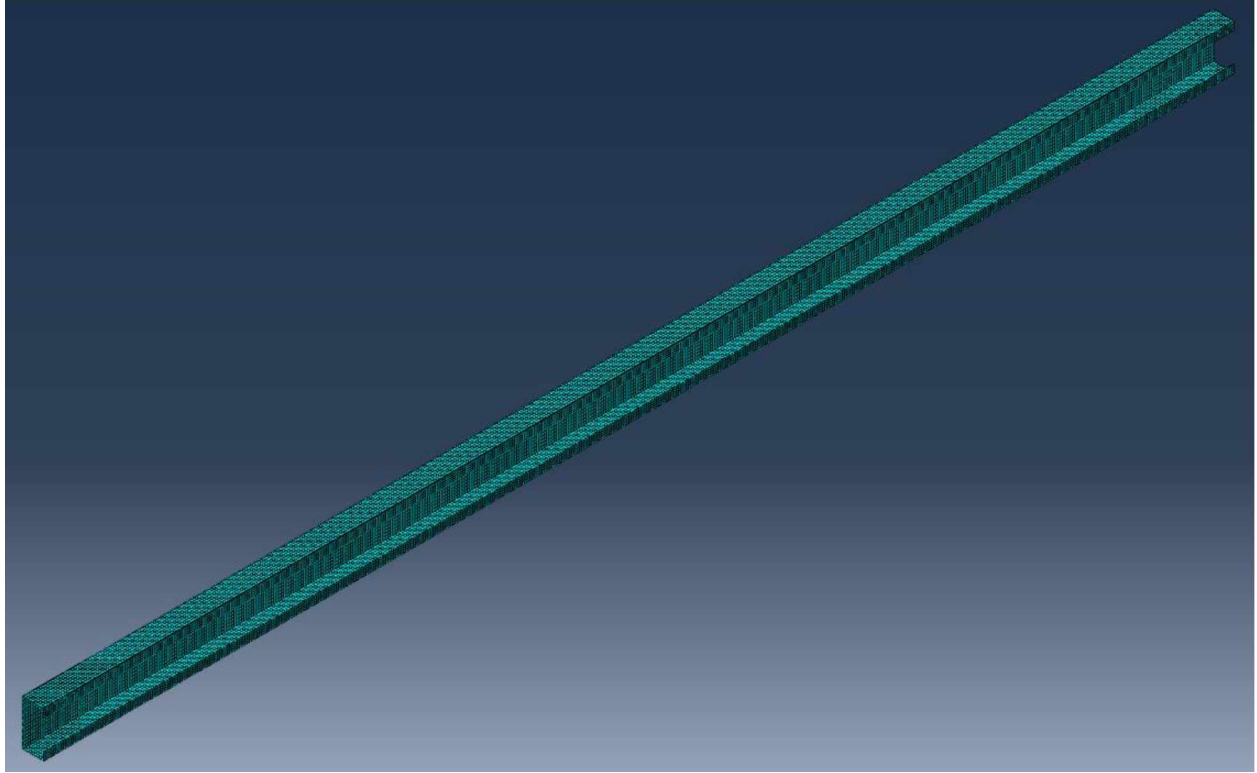
Figure 3.9: Meshing of the stud in ABAQUS

3.4.5 Numerical Results

The final meshing of the model was chosen based on a convergence test. The objective of the convergence test was to make sure that the numerical results would always converge regardless if the meshing was made any finer. The detailed convergence test analysis is given in Appendix C.

After the appropriate mesh size was chosen (5.625 mm X 5 mm X 1.15 mm), a series of simulations was conducted. Figure 3.10 (a) gives a typical first buckling mode of the stud model, Figure 3.10 (b) gives a typical structural failure of the steel stud model under compressive load in the ambient test and Figure 3.10 (c) gives a typical final deformation of the stud model in the fire test according to the temperature input recorded by Kolarkar [1]. The vertical load was imposed and the vertical deflection was measured at the location given in Figure 3.10 (b) in the ambient loading test simulation and the vertical and lateral deflections were measured at the locations given in Figure 3.10 (c). The numerically simulated buckling shape, given in Figure 3.10 (a), was verified by the numerical studies done by other researchers [19, 20] as they obtained very similar buckling shapes.

(a)

Centroid; location where compressive load imposed and vertical deflection to be recorded

(b)
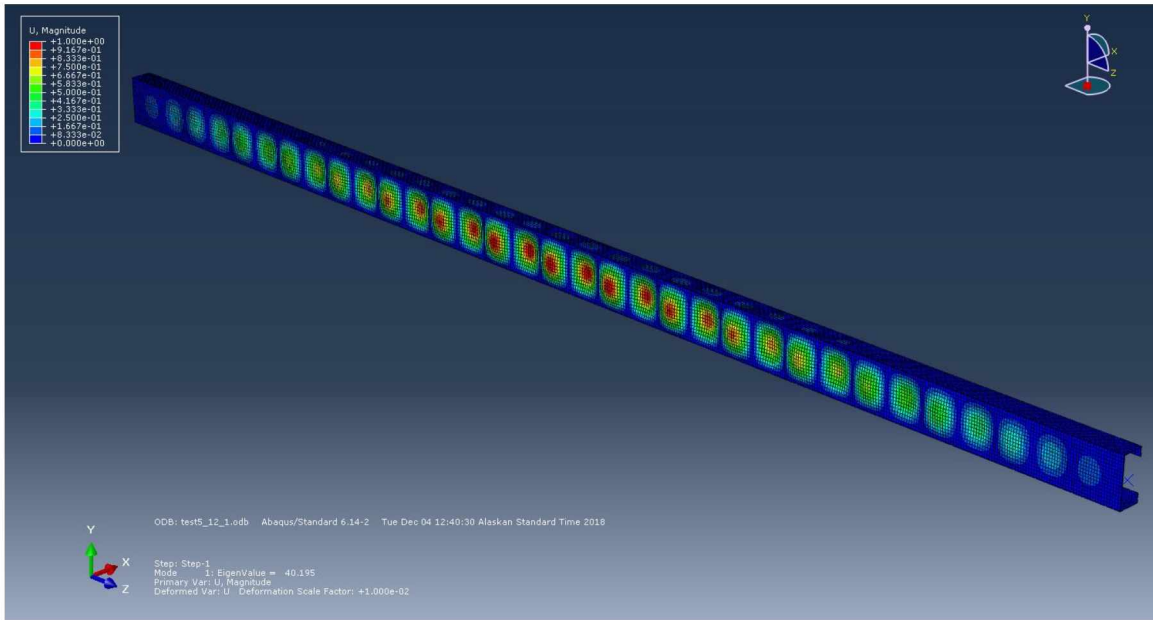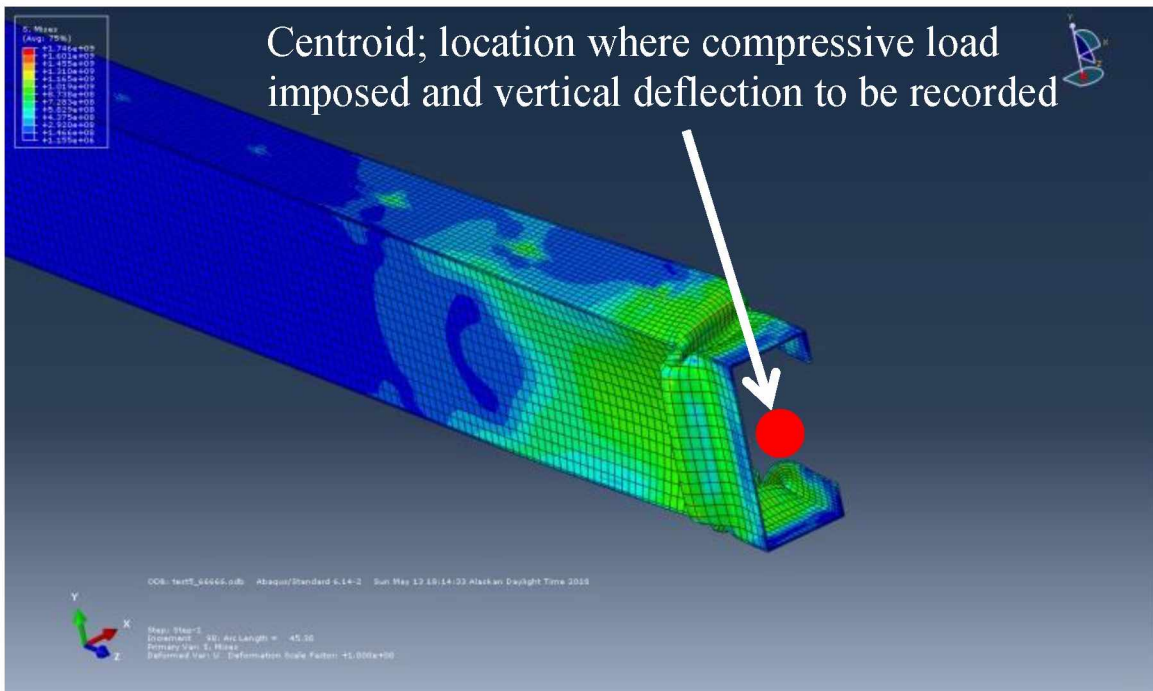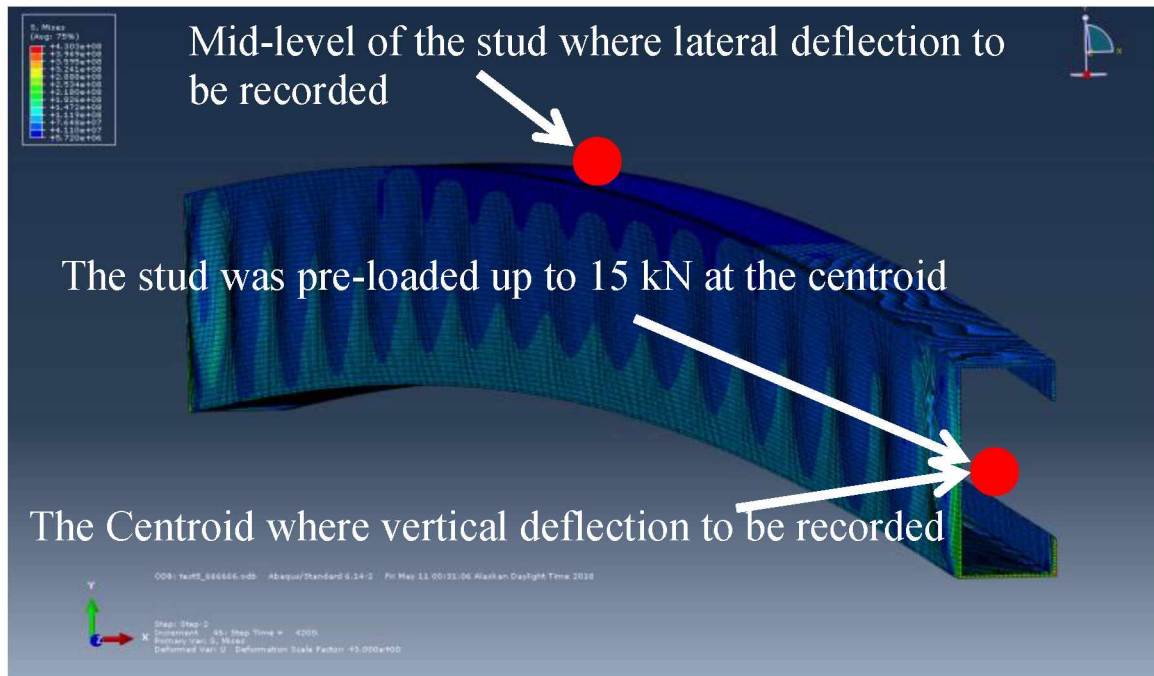
Figure 3.10: (a) First buckling mode of the stud model; (b) structural failure of the stud model in the ambient test; (c) final deformation of the stud model in the fire test

Each simulation was done on the stud model with a specific set of parameters such as the mechanical properties of the steel stud or the magnitude of imperfection of the stud. The numerical result of each simulation was calculated by ABAQUS and the result was given in this section. The parameters considered in this study included: the effect of the stiffness provided by the gypsum boards at ambient temperature (gypsum board loses almost all its strength at temperatures exceeding 200 C); the different magnitudes of imperfection of the steel stud; the connection pattern between the stud and the gypsum boards ("All" or "Partial"); the difference between in-situ mechanical properties of steel ("Strong" steel); and recommended design mechanical properties of steel ("Weak" steel) [5]. The numerical results obtained from each stud model were compared against each other and with the experimental results.

The magnitude of imperfection of the stud can potentially make a sizeable difference to the response of the stud in both ambient and fire tests. The magnitudes of imperfection in this study were chosen as "0/1000" (no imperfection), "1/1000" (L/1000 imperfection) and "2/1000" (L/500 imperfection). Magnitude of imperfection was defined as the ratio of the largest lateral initial deflection to the height of the stud (2.4 m). The shape of the

imperfection was imported from the first buckling shape of the stud model and the largest lateral deflection to be the product of the height of the stud (2.4 m) and the magnitude of imperfection (0/1000, 1/1000 or 2/1000). The typical first buckling shape for the steel stud was given previously in Figure 3.10 (a), and the typical failure shapes of the stud in the ambient and fire tests were given in Figure 3.10 (b) and Figure 3.10 (c), respectively.

Figure 3.11 (a), (b) and (c) show the simulated results of the stud model assigned with both in-situ ("Strong") and design ("Weak") mechanical properties of steel and three different magnitudes of imperfection in both the ambient and fire tests. The failure load (kips) of the stud in each simulation of the ambient test is defined as the largest compressive load of the model before the compressive load bifurcated and started decreasing and is circled in Figure 3.11 (a). The failure time of the stud in each simulation of the fire test is defined as the time (min) when the simulation stopped converging and led ABAQUS to abort the job due to large, nonlinear deflections, as shown in Figure 3.11 (b) and (c). All the studs failed in the simulation of fire tests except the one assigned with "Strong" steel and "0/1000" magnitude of imperfection where the responses stayed constant until the end of the simulation, as shown in Figure 3.11 (b) and (c). The failure times were circled in the figure. All the results were obtained with the stud assigned with the "All" boundary condition, as given in Figure 3.6 (d).

(a)

(b)

56
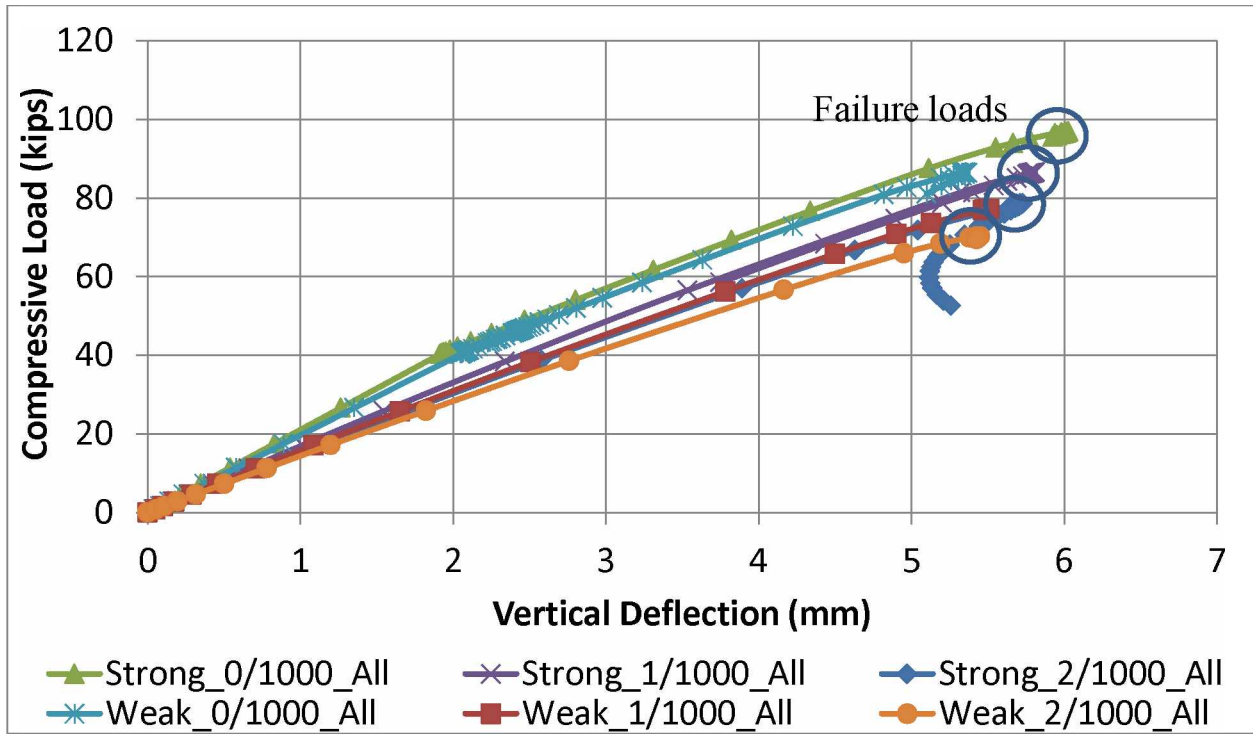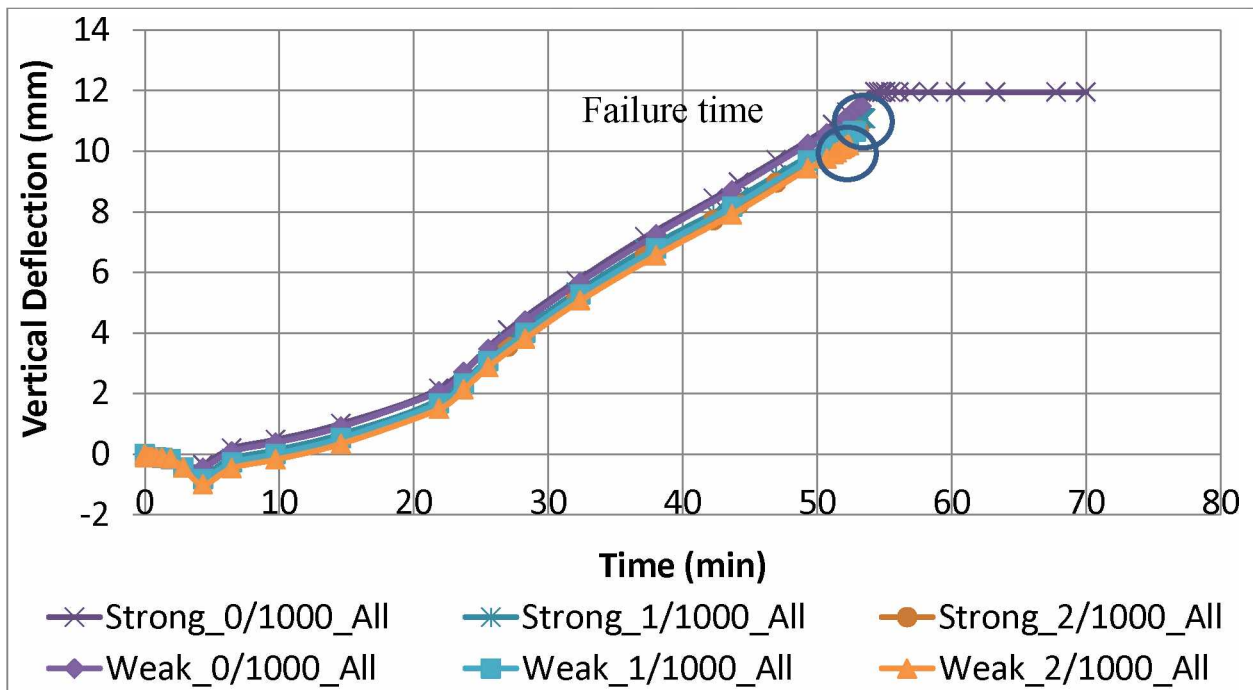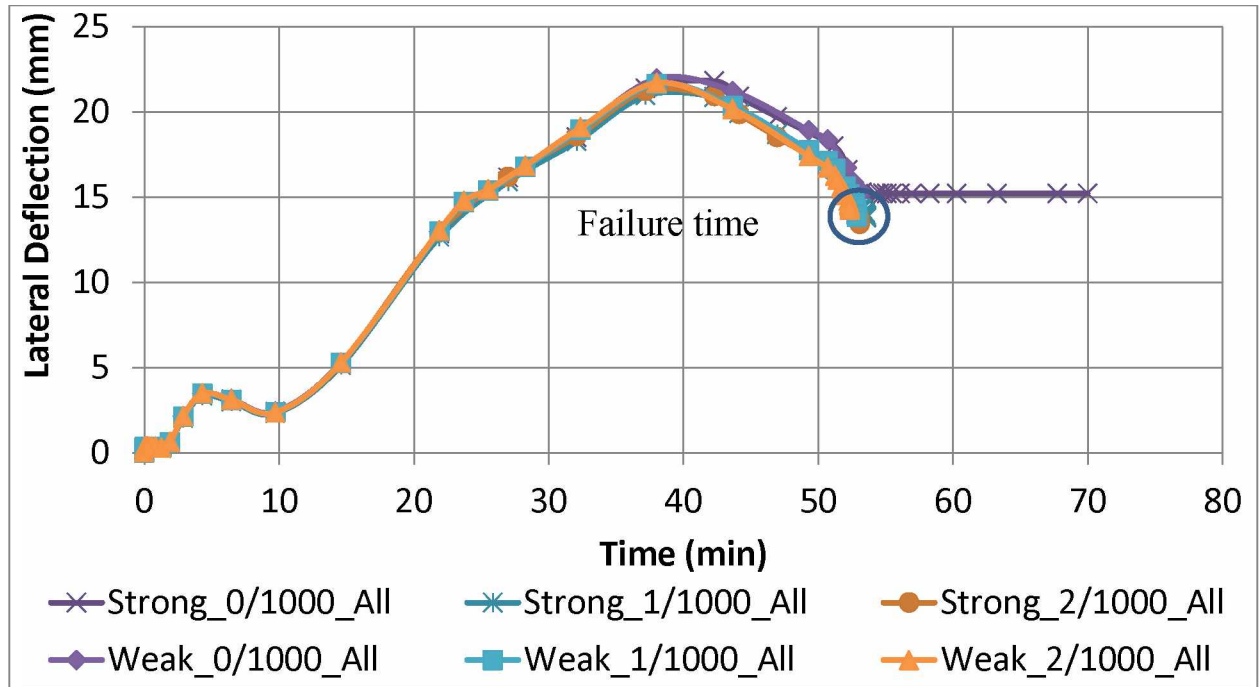
(c)

Figure 3.11: (a) Simulated compressive load vs vertical deflection of the stud in the ambient test; (b) simulated vertical deflection of the stud in the fire test; (c) simulated lateral deflection of the stud in the fire test

Figure 3.12 (a) and (b) give the simulated results of the stud with both "All" and "Partial" boundary conditions in the ambient test and the failure loads were again circled in the figure. Figure 3.13 (a) and (b) give the simulated results of the stud with both "All" and "Partial" boundary conditions in the fire test with the failure times circled. It can be seen that the stud assigned with "Strong" steel did not fail with either "All" or "Partial" boundary condition.

(a)

Failure loads
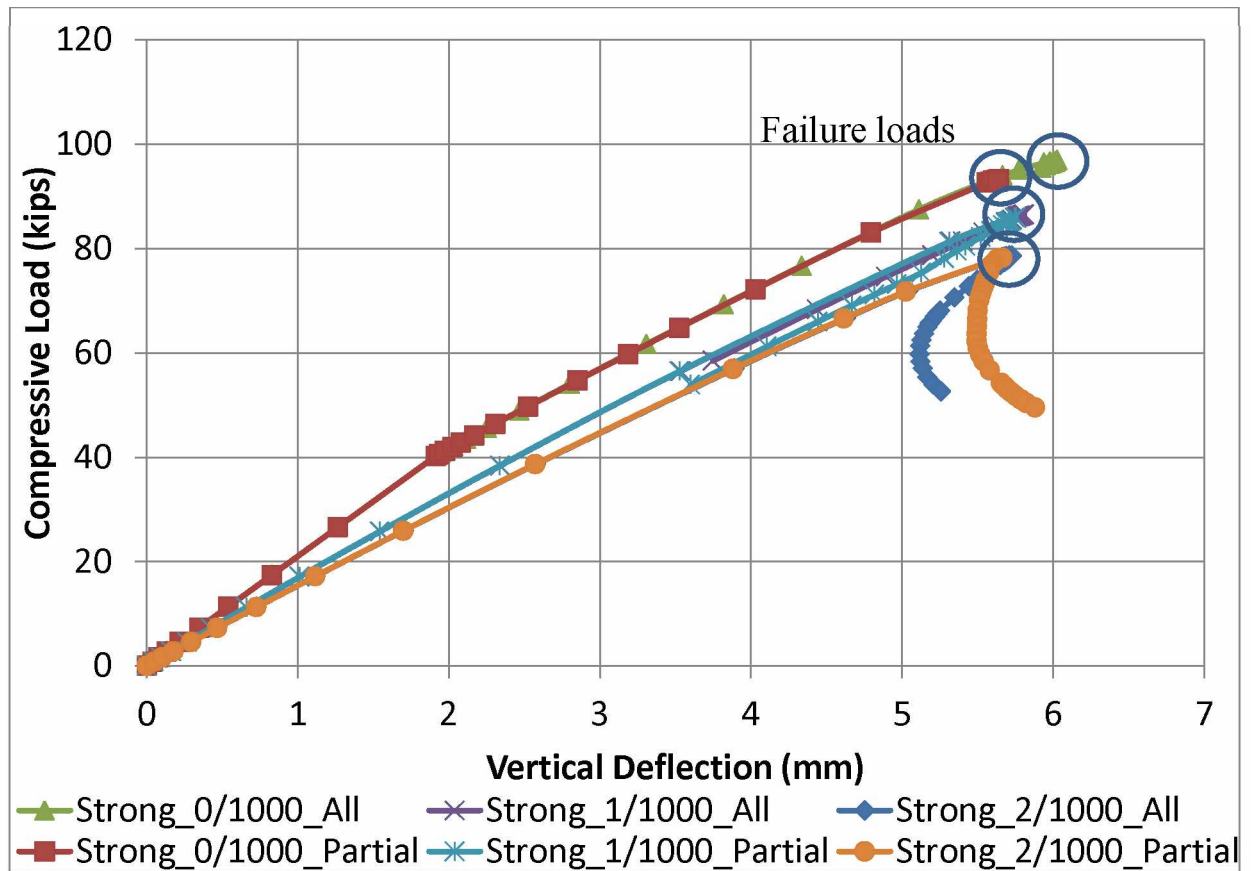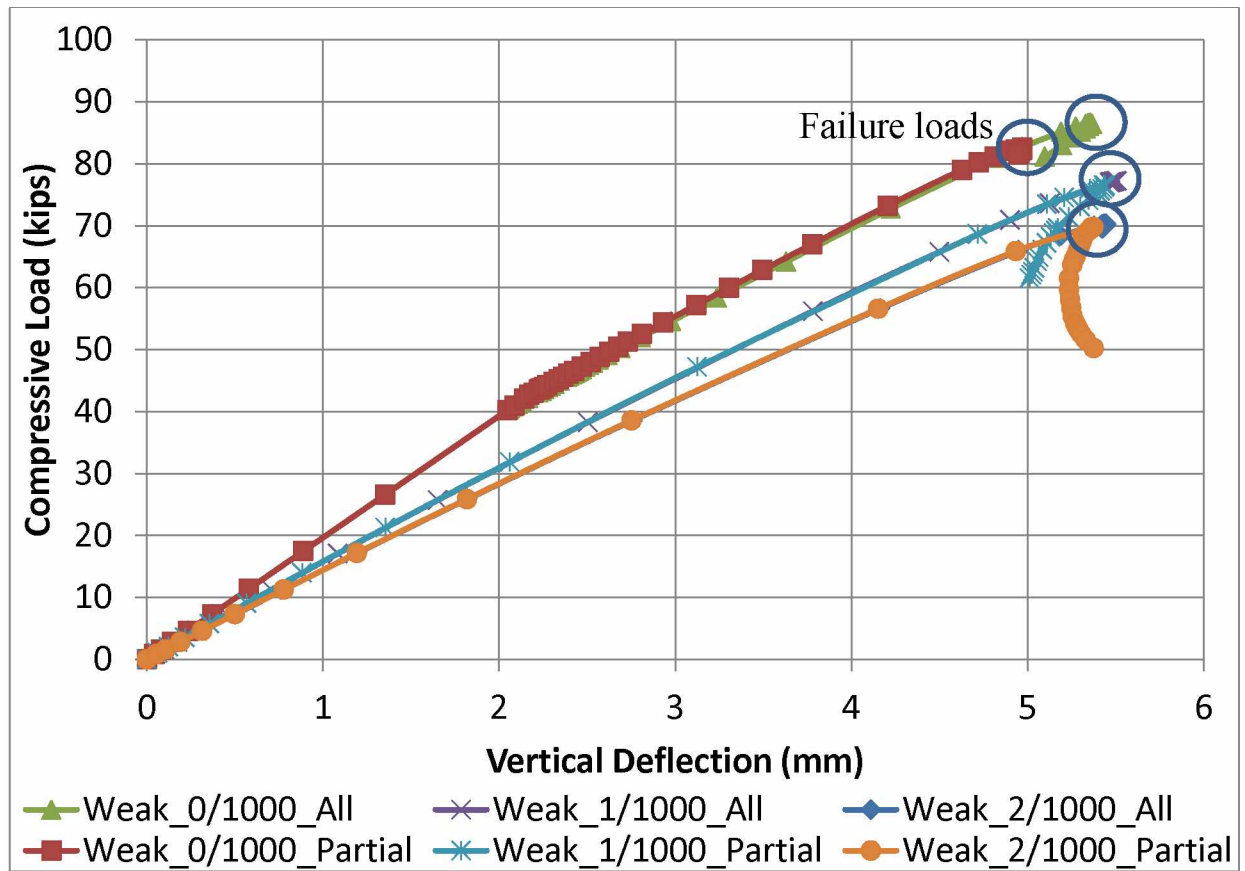
(b)

Figure 3.12: (a) Simulated results of the "Strong" stud with both boundary conditions in the ambient test; (b) simulated results of the "Weak" stud with both boundary conditions in the ambient test
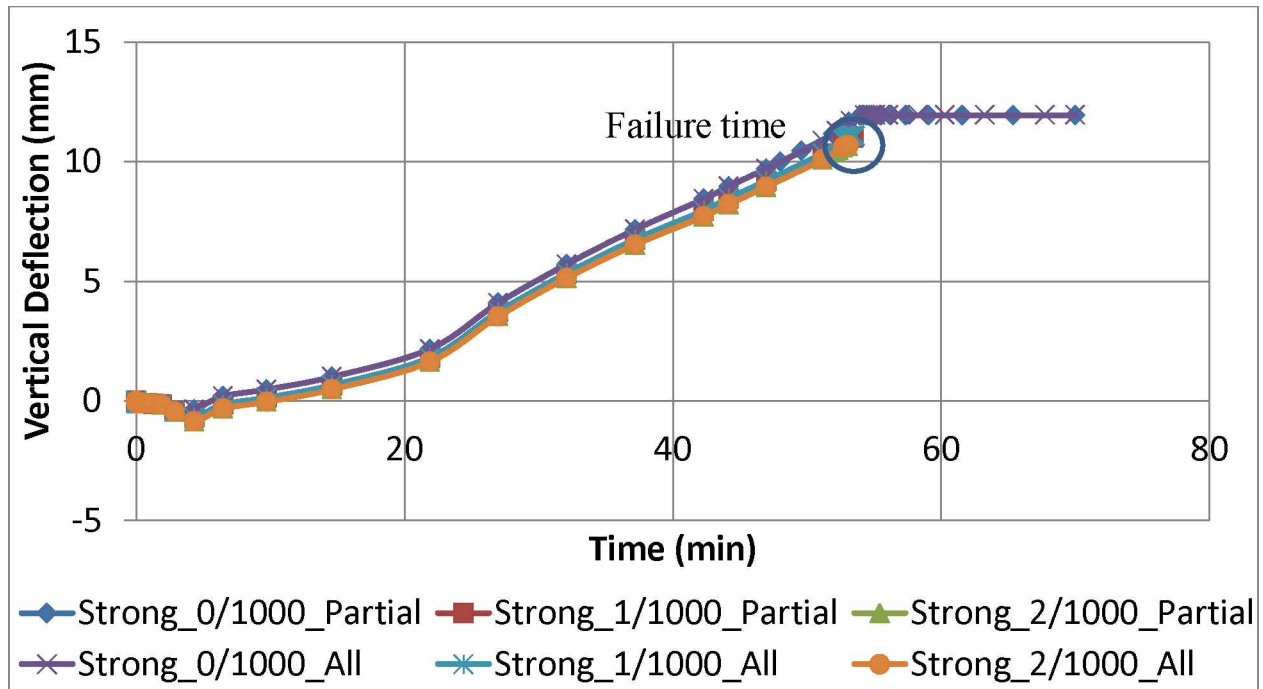
(a)
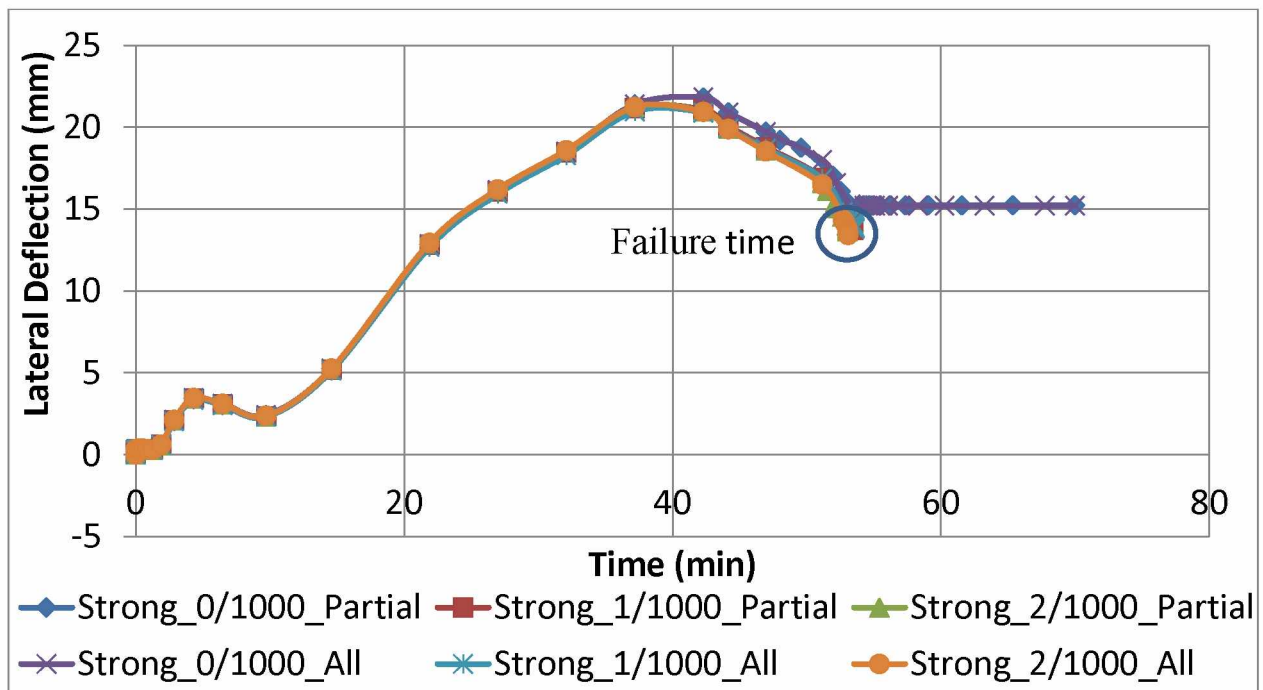
(b)

Figure 3.13: (a) Simulated vertical deflection of the stud with both boundary conditions in the fire test; (b) simulated lateral deflection of the stud with both boundary conditions in the fire test

Gypsum boards provide additional stiffness to the studs in both the y and z directions. However, gypsum boards are considered a weak material compared to steel (only 0.2% as strong) [4]. It can be very beneficial to study the significance of additional stiffness from the gypsum boards to the stud, and see how much difference the additional stiffness from the gypsum boards can make. The gypsum boards were modeled as spring elements in the analysis, as given in Figure 3.5. The stud models assigned with spring elements were designated as "Spring". Figure 3.14 shows the comparison between responses of the studs with and without the support of the gypsum boards. The stud was assigned with in-situ ("Strong") steel mechanical properties. Gypsum boards lose almost all their strength at elevated temperatures [3], so the studs assigned with spring elements were not simulated in the fire test.
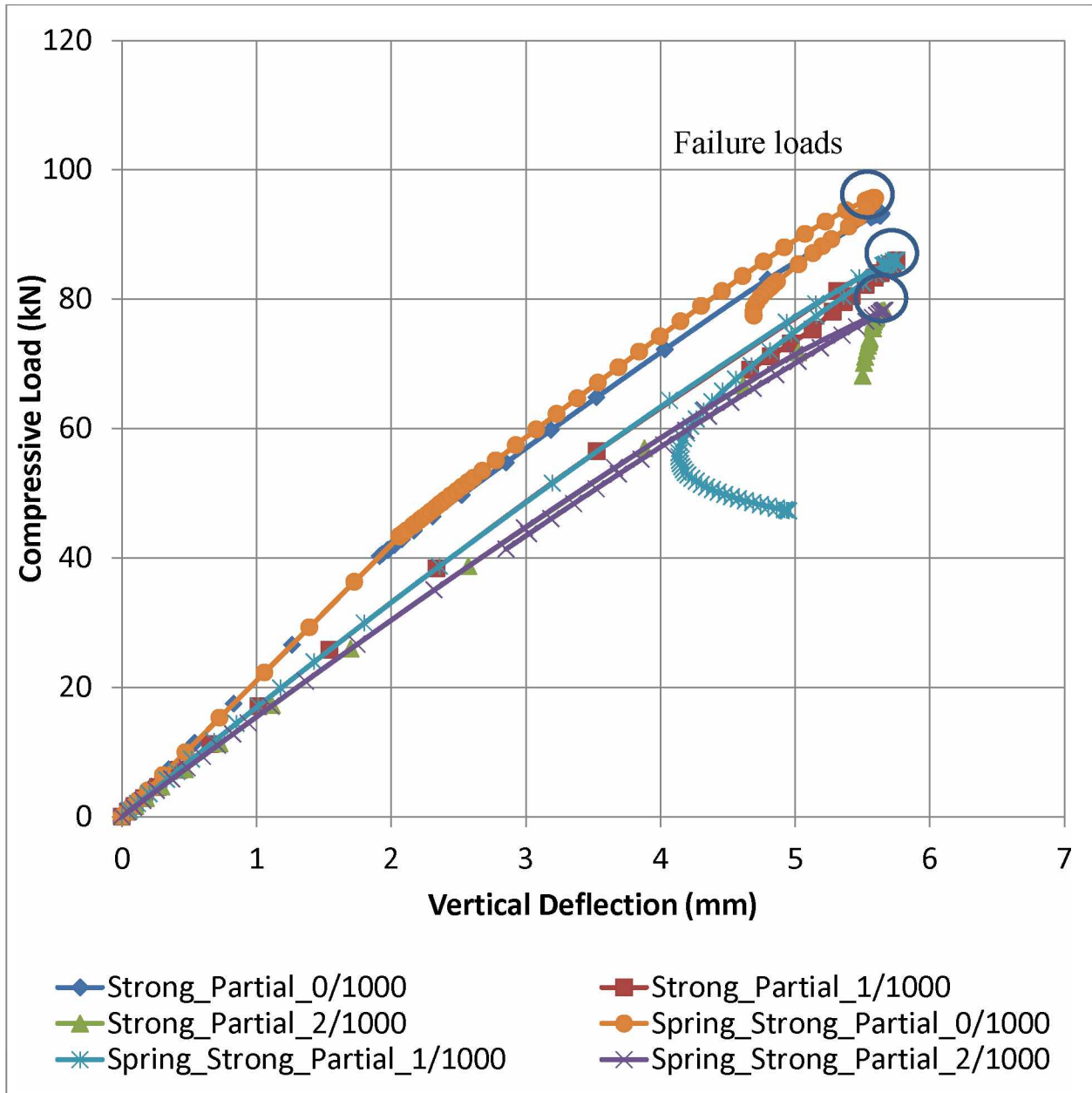
Figure 3.14: Comparison of the numerical results for studs at ambient temperature with and without spring elements representing gypsum boards

Finally, the experimental results were plotted against the closest numerical results, as seen for the ambient test in Figure 3.15 and the fire test in Figure 3.16. The corrected experimental vertical deflection in the ambient test accounts for the "slack" at the beginning of the loading process where the deflection increased much faster than the rest of the test and the discrepancy is marked on the graph, as shown in Figure 3.15. Figure 3.16 gives the

comparison between the experimental results and the selected numerical results of the stud that are the closest to the experimental results in the fire test.

The original fast increase of vertical deflection due to "slack" in the wall assembly

Weak_1/1000_Ambient
Strong_2/1000_Ambient
Ambient_Experimental
Ambient_Experimental (Corrected)
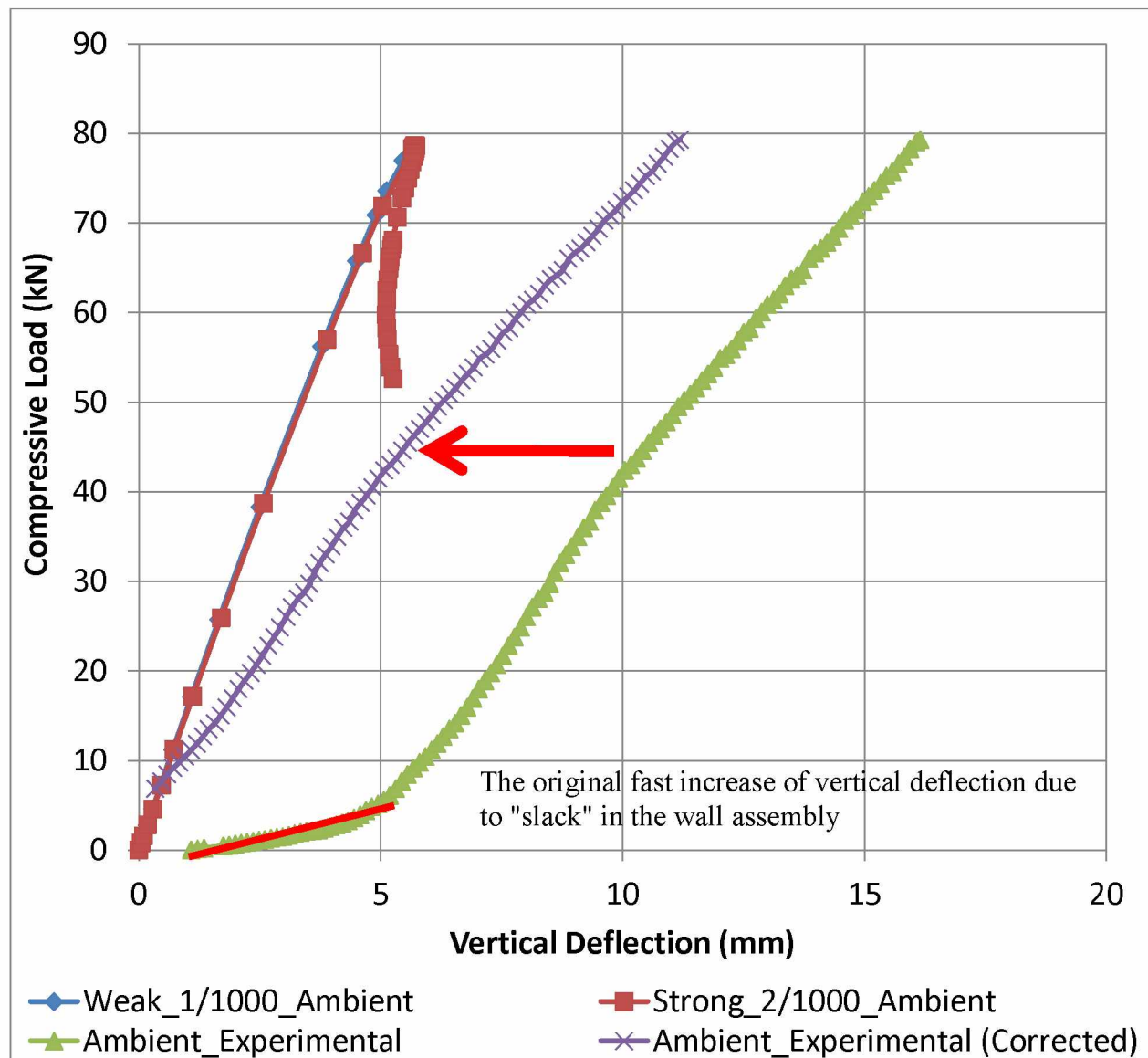
Figure 3.15: Comparison between the experimental results and selected numerical results for the ambient test
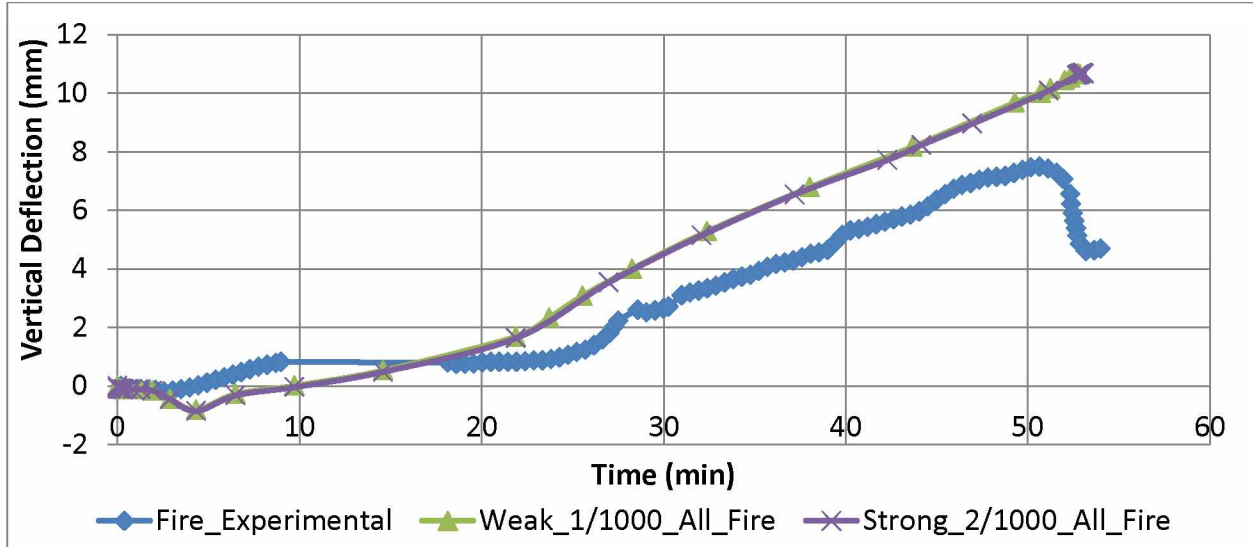
(a)
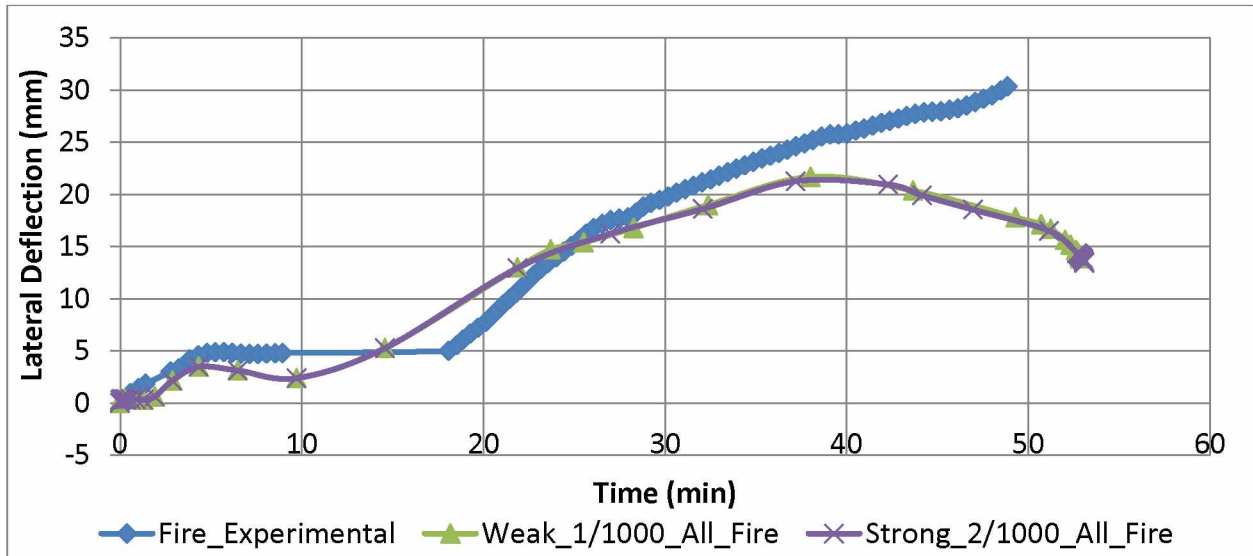
(b)

Figure 3.16: (a) Comparison of vertical deflection between the experimental results and selected numerical results for the fire test; (b) comparison of lateral deflection between the experimental results and selected numerical results for the fire test

3.4.6 Elapsed Time for Each Simulation

The elapsed time for each simulation is given in the following table.

Table 3.2: Elapsed time for each simulation

Elapsed Time (s)	B. C.	Steel	Spring	Imperfection	Test
5370.2	All	Strong	NA	0/1000	Ambient
4059.7	All	Strong	NA	1/1000	Ambient
3741.9	All	Strong	NA	2/1000	Ambient
6149.1	All	Weak	NA	0/1000	Ambient
3421.1	All	Weak	NA	1/1000	Ambient
1949.2	All	Weak	NA	2/1000	Ambient
3010.8	Partial	Strong	NA	0/1000	Ambient
1660.3	Partial	Strong	NA	1/1000	Ambient
1841.2	Partial	Strong	NA	2/1000	Ambient
4984.8	Partial	Weak	NA	0/1000	Ambient
4020	Partial	Weak	NA	1/1000	Ambient
2727.2	Partial	Weak	NA	2/1000	Ambient
7411.6	Partial	Strong	Y	0/1000	Ambient
7447.2	Partial	Strong	Y	1/1000	Ambient
5250	Partial	Strong	Y	2/1000	Ambient
5654.5	All	Strong	NA	0/1000	Fire
9953	All	Strong	NA	1/1000	Fire
6265	All	Strong	NA	2/1000	Fire
5310	Partial	Strong	NA	0/1000	Fire
6438	Partial	Strong	NA	1/1000	Fire
6275	Partial	Strong	NA	2/1000	Fire
5816.5	All	Weak	NA	0/1000	Fire
6133.8	All	Weak	NA	1/1000	Fire
6359.7	All	Weak	NA	2/1000	Fire
6217.5	Partial	Weak	NA	0/1000	Fire
6070.7	Partial	Weak	NA	1/1000	Fire
6380.8	Partial	Weak	NA	2/1000	Fire

3.5 Discussion of the Numerical Results

Figure 3.11 (a) shows how different magnitudes of imperfection and different mechanical properties of steel can change the response of the stud rather significantly in the ambient test. The response follows the presumed pattern that the greater the degree of imperfection and the weaker the steel is, the lower the failure load will be. Figure 3.11 (b) and (c) show that a stud with zero imperfection and with in-situ mechanical properties of steel ("Strong") can potentially lengthen the failure time in a fire test as the stud in the model did not fail at the experimental failure time. The response plateaued after reaching the experimental failure temperature. The stud failed at almost the same time for the rest of the simulations. Overall, Figure 3.11 (b) and (c) show that the imperfection value and the mechanical properties of steel do not contribute significantly to the response of the stud in the fire test, except when it was zero imperfection and in-situ ("Strong") steel mechanical properties where the stud did not fail.

Figure 3.12 (a) and (b) demonstrate that "All" or "Partial" boundary conditions result in negligible differences in the response of the steel studs in the ambient test, especially if non-zero imperfection was assigned to the stud. Therefore, it can be postulated that the nail spacing makes very little difference if the spacing is 100 mm or lower, as shown in Figure 3.6.

The gypsum boards can add additional stiffness to the stud and Figure 3.14 gives the response of the stud with extra stiffness provided by the gypsum boards. The gypsum boards' stiffness was modeled by spring elements installed at the locations of the stud as shown in Figure 3.5. It can be observed that for the stud with zero imperfection, the stud with spring elements representing the gypsum boards was slightly stiffer than the one without spring elements. For the studs with magnitudes of imperfection being either "1/1000" or "2/1000", spring elements barely made any difference, as the responses for both studs with or without spring elements were almost identical. It can be concluded that the stiffness of the gypsum boards contributes little additional resistance to the stud overall other than acting as a bracing devise, especially if non-zero imperfection values are assigned to the stud.

Finally, some selected responses of stud models listed above were compared with the experimental response, and the comparison is given in Figure 3.15 and Figure 3.16. Figure 3.15 shows that the numerical model is slightly stiffer than the wall assembly stud and with very close failure loads in the ambient test. However, Figure 3.16 (a) shows that the stiffness of the numerical model was less than the wall assembly stud for the vertical deflection in the fire test. A potential explanation could be that the difference is due to the uneven temperature

distribution of the stud in the fire test. Figure 3.16 shows that the numerical model has a very similar response to the experimental wall assembly stud. However, the numerical response did not capture the exact behavior of the dehydration process, where the temperature and the deflections remained almost constant. During the dehydration process, the gypsum board releases chemically bound water and then the water evaporates in heat and the temperature remains relatively constant for a meaningful period of time during the fire test. Thus the dehydration process functions as a fire-proofing mechanism. Also, the numerical responses of the stud peaked at around 38 min into the fire test and reversed afterwards until the stud failed. The experimental response of stud 2 did not have the reverse effect. In the study done by Kolarkar [1], a series of tests with different gypsum board wall assemblies was done and the reverse effect of the stud in the fire tests was observed during most of the tests.

Overall, the responses of the numerical model are reasonably close to the experimental responses, regardless it was found that there were some differences between the numerical responses and the experimental responses. In addition, the numerical model only modeled one stud of the entire gypsum board wall assembly that consisted of 4 studs in the tests. The nonlinear interaction among the studs in the experimental tests can further complicate the response of the gypsum board wall assembly. Table 3.3 gives a summary of the numerical results of different models with varying parameters for comparison.

Table 3.3: Compiled responses of numerical models with different parameters

Failure Load (kips)	BC	Steel	Spring	Imperfection	Test
96.88	All	Strong	NA	0/1000	Ambient
86.5323	All	Strong	NA	1/1000	Ambient
78.61	All	Strong	NA	2/1000	Ambient
86.55	All	Weak	NA	0/1000	Ambient
77.2	All	Weak	NA	1/1000	Ambient
70.3	All	Weak	NA	2/1000	Ambient
93.3	Partial	Strong	NA	0/1000	Ambient
86	Partial	Strong	NA	1/1000	Ambient
78.23	Partial	Strong	NA	2/1000	Ambient
83.1	Partial	Weak	NA	0/1000	Ambient
76.52	Partial	Weak	NA	1/1000	Ambient
70	Partial	Weak	NA	2/1000	Ambient
95.7	Partial	Strong	Y	0/1000	Ambient
86	Partial	Strong	Y	1/1000	Ambient
78.3	Partial	Strong	Y	2/1000	Ambient
Failure Time (min)	**BC**	**Steel**	**Spring**	**Imperfection**	**Test**
NA	All	Strong	NA	0/1000	Fire
53.6	All	Strong	NA	1/1000	Fire
53.1	All	Strong	NA	2/1000	Fire
NA	Partial	Strong	NA	0/1000	Fire
53.5	Partial	Strong	NA	1/1000	Fire
53.06	Partial	Strong	NA	2/1000	Fire
53.3	All	Weak	NA	0/1000	Fire
53	All	Weak	NA	1/1000	Fire
52.4	All	Weak	NA	2/1000	Fire
53.3	Partial	Weak	NA	0/1000	Fire
52.82	Partial	Weak	NA	1/1000	Fire
52.31	Partial	Weak	NA	2/1000	Fire

3.6 Conclusions

This study reviewed one of the wall assembly tests done by Kolarkar [1]. A numerical model was built in ABAQUS to simulate the experiment. The numerical model implemented parametric analysis with several varying parameters including: the effect of the stiffness provided by the gypsum boards at ambient temperature; different magnitudes of imperfection of the steel stud ("0/1000", "1/1000" and "2/1000"); the difference between in-situ

mechanical properties of steel and the design mechanical properties of steel ("Strong" and "Weak" steel); and different boundary conditions ("All" and "Partial"). The numerical results obtained from each stud model with its set of parameters are compared with each other and with the experimental results. The results are plotted and tabulated in this study. From the comparison, several conclusions can be drawn:

1. The gypsum boards themselves provided little to no effect in the response of the gypsum board wall assembly in both the ambient and fire tests. In the fire test, the temperature increase of the wall assembly severely decreases the stiffness of the gypsum boards and therefore the resistance of the gypsum boards can be rightfully neglected. In the ambient test, the responses of the stud with or without the spring elements, representing the stiffness of the gypsum boards, were virtually identical and are given in Figure 3.14.

2. The magnitudes of imperfection of the stud can contribute significantly to the response of the gypsum board wall assemblies. For example, as shown in the Numerical Modeling section, zero imperfection, coupled with in-situ mechanical properties of the G500 grade steel, had a much higher failure load (93.3 kN with "Partial" boundary condition) than the experimental failure load (79 kN). The model did not fail at the temperature at the time of failure, as shown in Figure 3.7.

3. The boundary condition representing the nail spacing condition between the gypsum boards and the stud had a negligent effect on the response of the wall assembly, as long as the spacing was 100 mm or smaller. The stud with the "All" boundary condition generated a slightly higher failure load than the stud with the "Partial" boundary condition. Both boundary conditions were demonstrated in Figure 3.6. Therefore, the use of the "All" boundary condition can provide quick insight into how the wall assembly will respond to both the ambient and fire tests.

4. A properly chosen combination of the mechanical properties of steel (in-situ values or design values) with the corresponding imperfection values can generate numerical results similar to the experimental results of the gypsum board wall assembly in the fire test. In the study, two combinations of the aforementioned properties were selected and the results of the stud model with the combination of these parameters were plotted against experimental results as shown in Figure 3.15 and Figure 3.16 (a) and (b). It was found that the in-situ mechanical properties ("Strong") coupled with "2/1000" as the magnitude of imperfection, or the design mechanical properties ("Weak") coupled with either "1/1000" as the magnitude of imperfection can generate the closest results to the experimental results among all the models simulated. The "All" boundary condition can be handily chosen due to its convenience.

5. Overall, this study demonstrated that using numerical simulation, with the correct combination of parameters, it is possible to predict the structural behavior of a gypsum board wall assembly in both ambient and fire tests.

3.7 References

[1]. Kolarkar, Prakash, Structural and Thermal Performance of Cold-formed Steel Stud Wall Systems under Fire Conditions, 2010

[2]. Hamilton, R. Scott, Performance-based Fire Engineering for Steel Framed Structures: a Probabilistic Methodology, 2011

[3]. Rahmanian, Ima, Thermal and Mechanical Properties of Gypsum Boards and Their Influences on Fire Resistance of Gypsum Board Based Systems, 2011

[4]. ASTM E 119-16: "Standard Test Methods for Fire Tests of Building Construction Materials," ASTM International, West Conshohocken, PA, 2016

[5]. Manzello, Samuel, et at., Analysis of Inter-laboratory Testing of Non-load-bearing Gypsum/Steel-Stud Wall Assemblies, 2007

[6]. Manzello, Samuel, et al., Furnace Testing of Full-scale Gypsum Steel Stud Non-load-bearing Wall Assemblies: Results of Multi-laboratory Testing in Canada, Japan and USA, 2009

[7]. Nassif, Ayman Y., et at., Full-scale fire testing and numerical modelling of the transient thermo-mechanical behaviour of steel-stud gypsum board partition walls, 2014

[8]. Standards Australia (SA), AS 2291, Methods for the Tensile Testing of Metals at Elevated Temperatures, Sydney, Australia, 1979

[9]. Kesawan, Sivakumar, and Mahendran, Mahen, Fire Tests of Load-bearing LSF Walls Made of Hollow Flange Channel Sections, 2015

[10]. Chen, Wei, et al., Full-scale Fire Experiments on Load-bearing Cold-formed Steel Walls Lined with Different Panels, 2012

[11]. Chen, Wei, et al., Improved Fire Resistant Performance of Load-bearing Cold-formed Steel Interior and Exterior Wall Systems, 2013

[12]. Vieira Jr., Luiz Carlos Marcos Vieira Junior, Behavior and Design of Sheathed Cold-formed Steel Stud Walls under Compression, 2010

[13]. Abedi, Karim, et al., Numerical Modeling and Finite Element Analysis of Steel Sheathed Cold-Formed Steel Shear Walls, 2012

[14]. ASTM, E 8M-04, Standard Test Methods for Tension Testing of Metallic Materials (Metric). 2004, ASTM International: West Conshohocken, PA.

[15]. Kankanamge, Nirosha and Mahendran, Mahen, Mechanical Properties of Cold-formed Steels at Elevated Temperatures, 2015

[16]. Young, Ben and Chen, Ju, Mechanical Properties of Cold-formed Steel at Elevated Temperatures, 2004

[17]. Lee, Jinwoo, Elevated-temperature Properties of ASTM A992 Steel for Structural-fire Engineering Analysis, 2012

[18]. Landesmann, Alexandre, Experimental Investigation of the Mechanical Properties of ZAR-345 Cold-Formed Steel at Elevated Temperatures, 2014

[19]. Zhao, et al., Calculation Rules of Lightweight Steel Sections in Fire Situations, 2005

[20]. Gunalan, Shanmuganathan and Mahendran, Shanmuganathan, Finite Element Modelling of Load Bearing Cold-formed Steel Wall Systems under Fire Conditions Shanmuganathan Gunalan and Mahen Mahendran, 2013

Chapter 4   Numerical Evaluation of Fire Ratings: Composite Steel-EPS Wall Assemblies[3]

4.1 Abstract

Wall assemblies constructed with gypsum boards are widely used as load-bearing and non-load-bearing walls for structures in modern construction, particularly for mid-rise, commercial, industrial and residential building construction. Gypsum board wall assemblies are known for their relatively high strength-to-weight ratio, ease of prefabrication, quick erection and good insulation. In the past, the Fire Resistance Rating (FRR) for specific gypsum board assemblies could only be determined by subjecting wall assemblies to furnace fire testing according to standards set forth in documents such as E119. However, conducting such tests is both expensive and time consuming. Therefore, it is shown in this study that numerical methods are a reliable way to assess FRR for composite, structurally insulated wall assemblies. The insulation in this study had a density of 1.5 pcf. This alternative approach to experimental fire testing can be very promising because it could potentially save the high level of expense and time associated with conducting traditional fire tests.

4.2 Introduction

Modern buildings require construction materials to possess certain positive traits, such as a high strength-to-weight ratio, ease of prefabrication, fast erection and good insulation, especially in the age of high rise buildings [1]. Since the attack on the World Trade Center in 2001, the fire resistance of construction members has become an increasingly important trait and gypsum boards have been found to be a very good thermal insulation material [2]. Before any construction material or structural element can be used in construction, its Fire Resistance Rating (FRR) has to be evaluated [3]. Traditional, the FRR of a gypsum board assembly, or any other construction material or structural element, is determined via a standard furnace fire test performed in accordance with standardized documents, such as E119 in the US. Conducting such tests can be very difficult due to the high level of cost and the large amount of time needed. In order to get a general idea of how well the material or the structure will behave under the standard furnace fire test, researchers have been investigating other means to accurately estimate the FRR before conducting such tests. Among these means, numerical analysis is one of the most promising [4].

---

[3] This chapter will be submitted for publication as Quan, Zhili, Hulsey, Leroy, Journal of Structural Fire Engineering.

This study was developed for the specific purpose of giving architects, engineers, code writers, and contractors an alternative to conducting expensive fire tests. An ASTM E119 fire test was numerically simulated on a new composite, load-bearing gypsum board wall assembly and the results of this new wall assembly are presented in this study.

In this study, a 12 ft X 12 ft X 7.5 in panel of the new wall assembly was numerically evaluated for its thermal behavior (temperature variation within the panel) and mechanical behavior (failure load and deflection of the panel). The study was conducted with ABAQUS V6.14, a finite element program. A numerical model was built in ABAQUS to simulate the wall assembly being subjected to a standard furnace fire test according to E119, and the responses of the wall assembly were obtained through the modeling analysis. The responses were thoroughly studied and the FRR of the wall assembly was deduced.

As introduced before, the performance of construction materials and structural elements under fire must be tested via standard testing methodology before any practical implementation. ASTM E119 [3] serves as the standard for fire furnace testing methodology in the US. Gypsum board wall assemblies, like any other structural elements, require the E119 fire testing to determine their FRR and different researchers have carried out fire tests to deduce the FRR and study the thermal and structural behaviors of these wall assemblies under fire. Manzello, et al. [5] did a series of fire tests in the US to study the thermal behaviors of several gypsum board wall assemblies. The wall assemblies consisted of 10 samples of the same configuration: a 10 ft (3.05 m) X 10 ft (3.05 m) single layer gypsum board wall assembly with 9 20 gauge steel studs inside; the gypsum boards were 5/8 in (16 mm) thick; the studs were 16 in (40.64 cm) O.C. except the two studs on the far ends which were 12 in (30.5 cm) from the ones next to them. Manzello, et al. [5] recorded the temperatures of the unexposed side of the gypsum boards of the wall assemblies from the beginning of the tests until the wall assemblies failed according to the failure criteria given in ASTM E119 [3]. In 2007, Manzello, et al. [6] did another set of tests in Japan with the exact same configuration for the gypsum board wall assemblies in order to compare the North American Laboratory results with the Japanese Laboratory results. Their research captured the thermal behavior of the gypsum board wall assemblies by recording the rise in temperature of the unexposed side of the gypsum boards, but not the mechanical behavior of the wall assemblies, such as the vertical and lateral deflections.

Experimental test results from both the US and Japan demonstrated some of the key features of a wall assembly when gypsum boards were used to improve the FRR according to Manzello, et al. [5, 6]. It is worth noting

that only the thermal behavior of the wall assembly was recorded because the study featured only non-load-bearing gypsum board wall assemblies. Some researchers have conducted experiments to study both the thermal behavior and mechanical behavior of gypsum board wall assemblies. Allam [7] and Kolarkar [1] each did furnace fire tests to study the thermal and mechanical behaviors of their gypsum board wall assemblies. Kesawan and Mahendran [8] and Chen, et al. [9, 10] each did a series of furnace fire tests for gypsum board assemblies with varying factors such as the thickness of the gypsum boards and the types of the gypsum boards. Some researchers, such as Vieira Jr. [11], did thorough and detailed experiments on gypsum board wall assemblies at ambient temperature instead of in standard furnace fire tests. The experiments were meant to study the mechanical behavior of the gypsum boards at ambient temperature and can be used as a great resource for the mechanical behavior of gypsum boards under fire tests.

In addition to subjecting gypsum board wall assemblies to standard furnace fire tests, numerical simulation studies have also been done on some wall assemblies. Vieira Jr. [11] numerically simulated all of his experiments on gypsum board wall assemblies in order to verify his numerical methodology by comparing the numerical results with experimental results. Allam [7] conducted a fire test on a gypsum board assembly and consequently simulated the fire test in ABAQUS. The numerical results were compared to the experimental results with a high degree of accuracy.

Kolarkar [1] investigated the mechanical properties of the steel used in gypsum board wall assemblies at elevated temperatures. The tested steel was grade G500 with an assumed minimum design yield strength of 500 MPa (72.5 ksi) and a Young's modulus of 200 GPa (29,000 ksi) at ambient temperature. Kolarkar was able to test the in-situ yield strength and Young's modulus of grade G500 steel, and found that the in-situ values were 5-15% greater than the design values at both the ambient and elevated temperatures. Vieira Jr. [11] also did a series of in-situ coupon tests of Grade A50 steel in the US. Again, the in-situ test values were higher than the design values: 50 ksi (345 MPa) for yield strength and 29,000 ksi (200 GPa) for Young's modulus. Other researchers [12, 13, 14, 15, 16] were able to get similar results in their in-situ tests as well. The thermal properties of steel have also been studied [17].

Manzello, et al. [5, 6] did extensive experiments on the thermal properties of gypsum boards made in North America. Ima [4] conducted detailed tests to study the thermal and mechanical properties of gypsum boards at different temperatures. The tested gypsum boards were British products. Some researchers like Allam [7] and Vieira

Jr. [11] did thorough literature reviews on the mechanical properties of gypsum boards at ambient and elevated temperatures.

The new gypsum board wall assembly studied here contains steel studs framed with Expanded Polystyrene (EPS) in order to provide additional insulation. The steel studs are braced with phenolic resin. Therefore, the mechanical and thermal properties of EPS and phenolic resin need to be studied as well. Properties such as density, thermal conductivity, specific heat, latent heat of fusion and the melting point of EPS were studied extensively before any numerical analysis took place [18, 19, 20, 21, 22]. Phenolic resin is only designed to be used as a bracing device. However, it loses surface mass at elevated temperatures [23]. Phenolic resin is widely used as an ablative material which sacrifices some surface mass to protect internal components in a traditional thermal protection system. Phenolic resin has long been used in many fields due to many desirable traits it possesses, namely, lightness, low thermal conductivity, high allowable stress and thermal stability.

The objective of this study is to assess the FRR when 5/8 in Type X gypsum boards are installed on each face of the steel-stud-framed EPS in the new wall assembly design. The structural response of a simulated fire test for the new wall system was studied. The insulation in this wall assembly is made of EPS with a density of 1.5 pcf. A numerical model in ABAQUS was built to model the standard furnace fire test according to E119 on the wall assembly. Numerical responses of the wall assembly in the simulated furnace fire test were obtained and studied. The responses shed great light on the thermal and mechanical behavior of this new composite wall assembly under fire. In the future, it is proposed that the numerical load-bearing capabilities of this new wall assembly be compared to the experimental results of the wall assembly undergoing a standard fire test.

4.3 Structural Composite Insulated Wall Assembly

A single wall assembly unit consists of gypsum boards between top and bottom steel tracks, with composite steel-EPS insulation and phenolic resin bracing. The composite steel-EPS insulation consists of 4 pairs of steel studs facing each other and Expanded Polystyrene (EPS) framed by the steel studs. Each wall assembly unit has dimensions of 12 ft X 4 ft X 7.5 in and has a male and female connector to connect multiple composite steel-EPS insulation panels together. The front and back of the composite steel-EPS insulation are covered with single, double or triple layers of gypsum boards. Braces made of phenolic resin are installed on the steel studs to prevent global buckling. The two bracing conditions introduced in the study are unbraced lengths of 3 ft and 6 ft. The top and

bottom tracks are used to fix different components together and do not act as strength-supporting elements. The steel studs are CSJ channels and specified as 362S162-54 or 362S162-33. These studs are light gauge steel and they are consistent with the American Iron and Steel Institute (AISI) and the Steel Stud Manufactures Association (SSMA). 362S162-54 is a 3.625 in X 1.625 in X 0.5 in, 16 gauge (0.0566 in thickness) steel stud and 362S162-33 is a 3.625 in X 1.625 in X 0.5 in, 20 gauge (0.0346 in thickness) steel stud. Top and bottom tracks are 7.5 in X 1.25 in, 20 gauge channels. All the steel components are made of Grade A33 steel. The whole assembly is fastened together with No.10 self-tapping screws. The plan view of a unit of wall assembly insulated with single layer of gypsum boards and with composite steel-EPS insulation is given in Figures 4.1 (a), along with a typical cross section of a CSJ stud in Figure 4.1 (b). Figure 4.2 and Figure 4.3 give the elevation view of a single layer of gypsum board wall assembly with 3 ft O.C. and 6 ft O.C. transverse bracing.
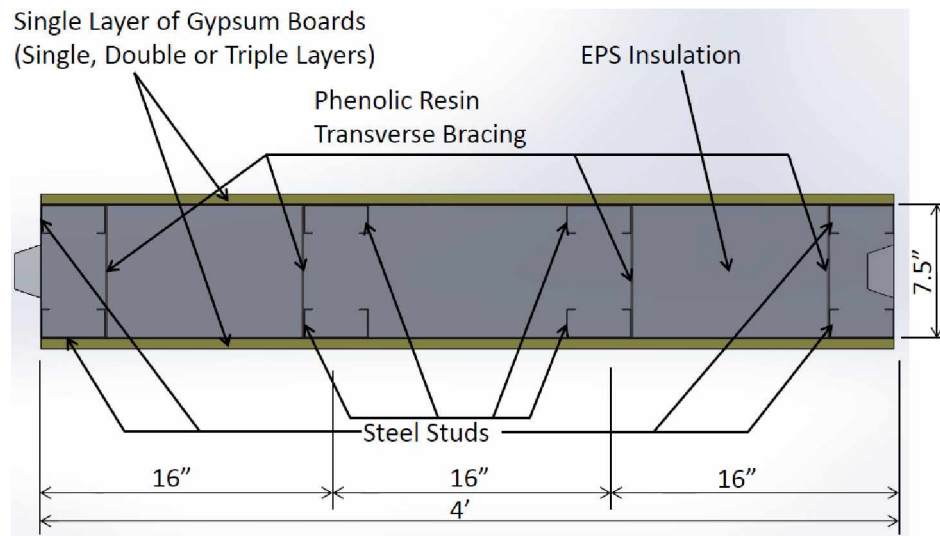
(a)
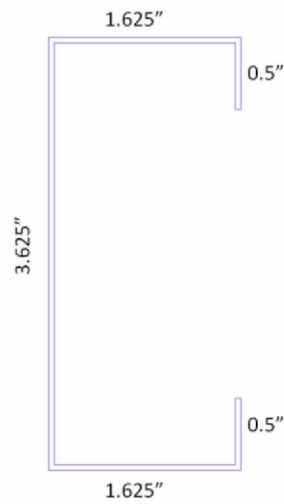
(b)

Figure 4.1: (a) Plan view of a single unit of wall assembly; (b) a typical cross-section for a CSJ stud
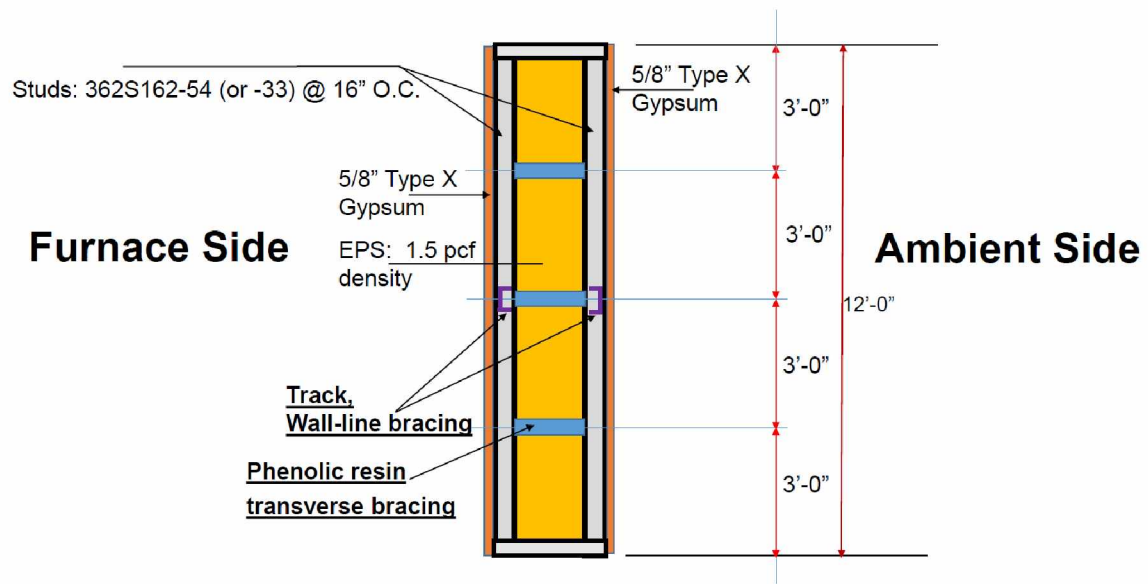
Figure 4.2: Elevation view of a single layer of gypsum board wall assembly with 3 ft O.C. transverse bracing
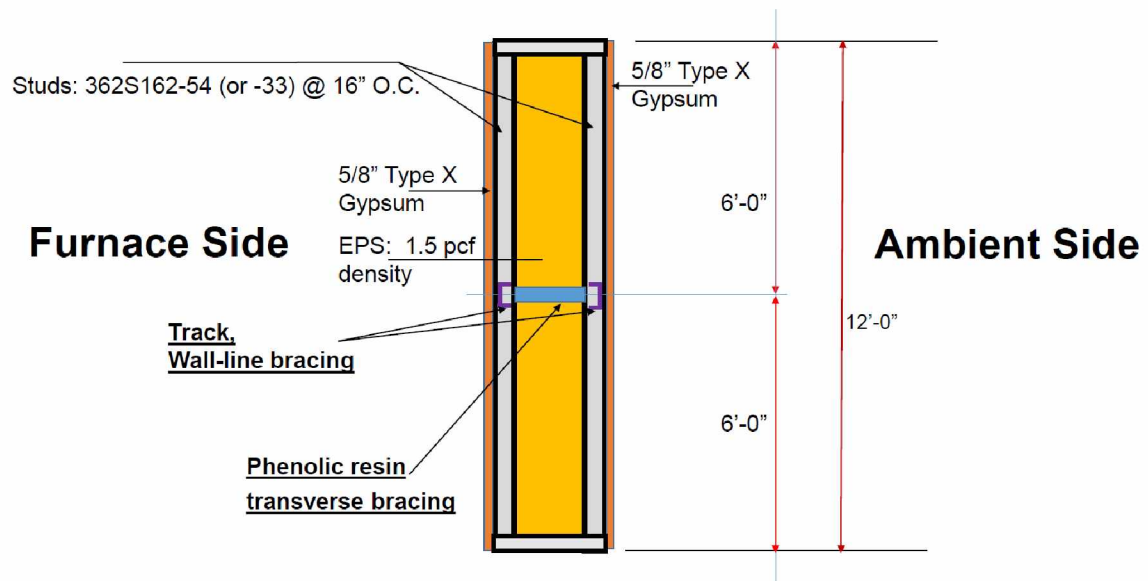
Figure 4.3: Side view of a single layer of gypsum board wall assembly with 6 ft O.C. transverse bracing

4.4 Standard Furnace Fire Test

It is important in the construction industry to understand how materials or wall assemblies will behavior under fire. Therefore, it is typical that the FRR for a given construction material or any structural element, such as walls, columns and floors, are tested using a standard furnace fire test [3]. In the US, the standard fire test methodology is coded in ASTM E119. ASTM E119 prescribes a standard for exposing construction materials and structural elements to a fire of controlled extent and severity. Performance is defined as the elapsed period of resistance for the material or elements exposed to the fire before any of the failure criteria is observed. The standard for exposing a wall assembly to a fire of controlled extent and severity is with a furnace specifically set up according to E119.

According to E119, the three failure criteria to test the FRR of a specific structural member can be categorized as such:

a) the average temperature rise or the maximum temperature rise of the ambient side gypsum board exceeds certain values (thermal insulation);

b) a breach occurs on the tested structural member so that flames can escape and spread (thermal integrity);

c) the structural member fails under the specified loading condition in the fire test due to the degradation of the mechanical properties of the structural member (structural integrity).

Therefore, by subjecting a construction material or structural element to the standard furnace fire test prescribed by E119, the FRR can be determined as the elapsed time when any of the above three failure criteria is met. In a typical standard furnace fire test, the gypsum board wall assembly to be tested is mounted on the furnace as given in Figure 4.4 [5]. The flame will initiate in the furnace and the temperature in the furnace will be controlled to match the temperature vs time function given in E119. The thermal and mechanical behavior of the construction material or structural element will be recorded through the test until any of three failure criteria takes place.

Figure 4.4: Gypsum board wall assembly being mounted on the furnace [2]

4.5 Numerical Analysis Methodology

4.5.1 General Description

In this study, the numerical simulation of the furnace fire test of this new wall assembly was carried out in ABAQUS. The numerical simulation was carried out in two separate modeling procedures. It was assumed that the thermal analysis of the wall assembly and mechanical analysis of steel studs under elevated temperature are uncoupled. The temperature response obtained from the thermal analysis was inputted as the thermal condition for

the mechanical analysis of the steel studs. The thermal analysis was conducted in 2D modeling, and it was assumed the temperature only varied across the thickness of the wall assembly but not along the height or width. The mechanical analysis of the steel studs was conducted in 3D modeling and the response of the steel studs was obtained after the thermal response and loading condition were applied.

4.5.2 Properties of Steel

All the materials involved in the wall assembly, including: Grade A33 steel, Expanded Polystyrene (EPS), gypsum boards and phenolic resin, have been studied regarding their mechanical and thermal properties before any numerical modeling took place. The thermal and mechanical properties of the steel at different temperatures are given in Table 4.1.

Table 4.1: Mechanical properties of Grade A33 steel [24]

Temperature T (F)	Young's Modulus E (ksi)	Yield Stress Fy (ksi)	Temperature T (C)	Young's Modulus E (GPa)	Yield Stress Fy (MPa)
68	29,000	33	20	500	227.53
200	29,000	33	93	500	227.53
400	26,100	26.4	204	450	182.02
600	22,620	19.14	316	390	131.97
750	20,300	13.86	399	350	95.56
800	19,430	13.2	427	335	91.01
1,000	14,210	9.57	538	245	65.98
1,200	6,380	4.29	649	110	29.58
1,400	3,190	1.98	760	55	13.65
1,600	2,030	1.32	871	35	9.10
1,800	1,450	0.99	982	25	6.83
2,000	580	0.33	1093	10	2.28
2,200	0	0	1204	0	0.00

The chosen Poisson's ratio of steel was 0.3 [24], and the chosen coefficient of thermal expansion was 6.5 E-6/F or 11.7 E-6/C, independent of temperature. The average thermal properties of the steel are given in Table 4.2.

Table 4.2: Thermal properties of steel [17]

Thermal conductivity	45 W/m*C	26 Btu/h*ft*F
Specific heat	600 J/kg*C	0.143 Btu/lb*f

4.5.3 Properties of EPS

The mechanical properties of EPS were introduced in the Literature Review section and were found to be negligible (730 psi Young's modulus) [22] compared to that of steel (29,000,000 psi Young's modulus). Therefore, EPS was ignored in the mechanical analysis as a strength supporting component. However, EPS plays an important role in the heat transfer part of the numerical modeling and its thermal properties are given in Table 4.3 and Table 4.4. The density of the gypsum board is given as 1.5 pcf (24 kg/m^3) by the manufacturer.

It is worth noting that EPS is not a crystalline material, and it doesn't undergo the same phase change as other crystalline materials, such as steel. It softens when heated to 100 C and becomes fully liquid at 240 C [19], unlike crystalline materials, such as ice or steel, which melt at a definitive temperature after latent heat of fusion is released. Different studies have different values for the latent heat of fusion [18, 19] for EPS. The melting temperature of EPS was chosen as 240 C [19]. Table 4.3 gives the thermal conductivity of EPS and Table 4.4 gives the specific heat.

Table 4.3: Thermal conductivity of EPS [18]

Temperature (C)	Thermal Conductivity (W/m*k)	Temperature (F)	Thermal Conductivity (Btu/h*ft*F)
20	0.038	68	0.022
85	0.048	185	0.028

Table 4.4: Specific heat of EPS [21]

Temperature (C)	Cp (kJ/kg*K)	Temperature (F)	Cp (Btu/lb*f)
16.85	1.18	62.33	0.34
26.85	1.22	80.33	0.36
36.85	1.27	98.33	0.37
46.85	1.31	116.33	0.38
56.85	1.36	134.33	0.40
66.85	1.40	152.33	0.41
76.85	1.45	170.33	0.43
86.85	1.50	188.33	0.44
96.85	1.54	206.33	0.45
106.85	1.85	224.33	0.54
116.85	1.87	242.33	0.55
126.85	1.91	260.33	0.56
136.85	1.93	278.33	0.56
146.85	1.97	296.33	0.58
156.85	1.99	314.33	0.58
166.85	2.03	332.33	0.59
176.85	2.05	350.33	0.60
186.85	2.09	368.33	0.61
196.85	2.11	386.33	0.62

4.5.4 Properties of Gypsum Boards

The mechanical properties of gypsum boards were also found to be negligible compared to that of steel. The Young's modulus of gypsum boards is only 70 ksi/480 MPa, which is barely more than 0.2% of that of steel (29,000 ksi/200 GPa) [7]. Therefore, it is also not included in the mechanical analysis. Gypsum boards, like EPS, also plays an important role in the heat transfer part of the numerical modeling. The thermal properties are given below. Table 4.5 gives the thermal conductivity of gypsum boards [5] and Figure 4.5 gives the original and modified specific heat of gypsum boards [5]. It is worth noting that the specific heat of the gypsum boards has been modified such that the two spikes in the original specific heat of the gypsum boards are spread over a wider temperature range with a constant specific heat. The purpose of modifying the specific heat is to avoid numerical instability in the numerical analysis due to the sharp increase in the specific heat of gypsum boards after chemically bound water is released and then vaporized due to the rise in temperature. Additionally, a shift in the specific heat peak temperature

range was designed to deal with the "thermal delay" effect in the heat transfer analysis of the gypsum board wall assembly in the fire test.

Table 4.5: Thermal conductivity of gypsum boards [5]

Temperature (C)	Thermal Conductivity (W/m*K)	Temperature (F)	Thermal Conductivity (Btu/h*ft*F)
29.70	0.17	85.46	0.10
49.62	0.15	121.32	0.09
75.13	0.15	167.24	0.09
100.02	0.16	212.04	0.09
150.43	0.17	302.77	0.10
200.21	0.17	392.37	0.10
249.98	0.18	481.97	0.11
299.76	0.19	571.58	0.11
350.17	0.20	662.30	0.11
399.95	0.20	751.91	0.12
450.35	0.21	842.63	0.12
500.13	0.22	932.23	0.13
549.91	0.23	1021.84	0.13
600.31	0.24	1112.55	0.14
649.46	0.26	1201.02	0.15
699.85	0.27	1291.74	0.16
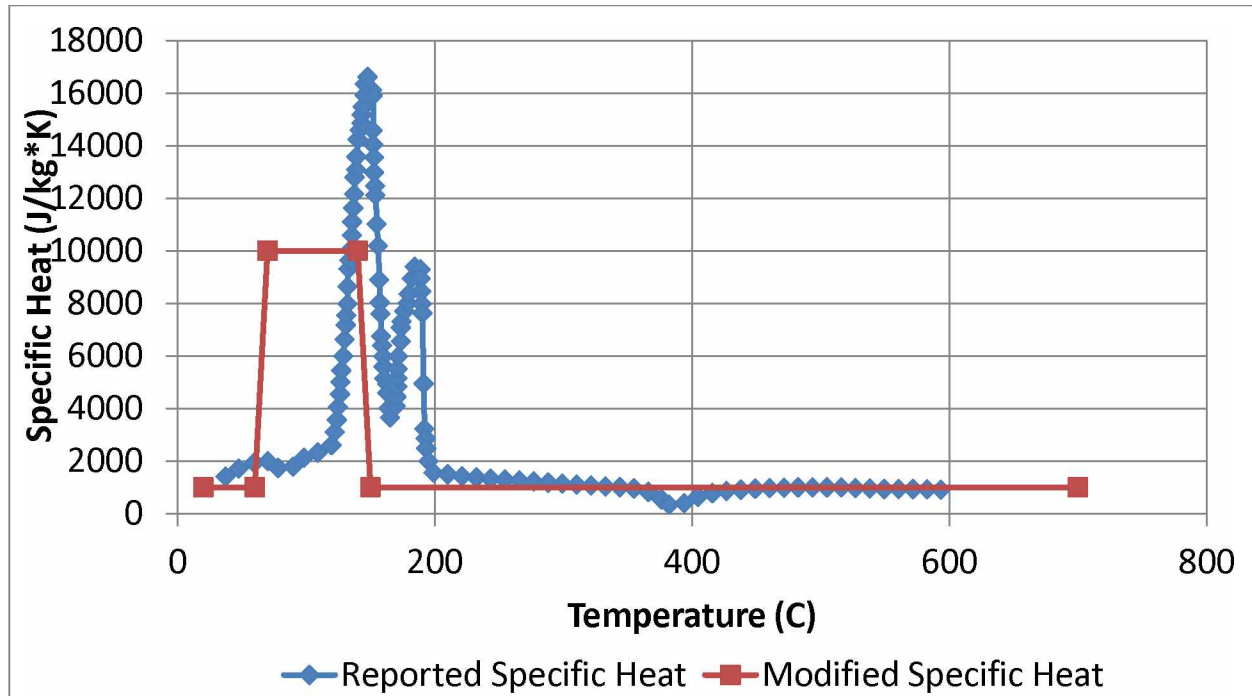
Figure 4.5: Specific heat of gypsum boards (only in SI unis)

4.5.5 Phenolic Resin

Phenolic resin braces are located throughout the thickness of the wall assembly. Phenolic resin is only used as a bracing device, so its thermal and mechanical behaviors are qualitatively studied but not quantitatively tabulated like other materials. As introduced here in the Literature Review section, phenolic resin is widely used as an ablative material to sacrifice some surface mass to protect internal components in a traditional thermal protection system. Phenolic resin is often used as a bracing device because it possesses many positive traits such as lightness, low thermal conductivity, high allowable stress and thermal stability. Phenolic resin loses 11.5% of its weight in the temperature range from 297 C (566.6 F) to 485 C (905 F), 29% of its weight from 485 C (905 F) to 622 C (1151.6 F) and 54.5% of its weight from 622 C (1151.6 F) to 820 C (1508 F) [23]. After the analysis, it was found that the temperature across the gypsum boards is not high enough to burn off 29% of the phenolic resin bracing and the remaining phenolic resin will be strong enough to brace the steel studs from buckling globally.

4.5.6 Thermal Analysis Model and Mechanical Analysis Model

The schematic demonstration of the new gypsum board wall assembly with composite steel-EPS insulation is given in Figures 4.1, 4.2 and 4.3. The wall assembly will be mounted on a furnace, and fire will start burning in the furnace to heat up the wall assembly, as shown in Figure 4.4. The temperature of the furnace has to be controlled according to E119. In the thermal analysis part of the modeling, the wall assembly was modeled in 2D and it was assumed that the temperature only varies throughout the thickness of the wall. The model is given in Figure 4.6. The 7.5 in thick EPS insulation was divided into 20 pieces to simulate melting. It is noted that the steel studs were not included in the thermal analysis. The reason for that is steel studs have very little effect on the thermal behavior of the gypsum boards due to their thinness (0.0566 in or 0.0346 in) and steel's high thermal conductivity (45 W/m*C or 26 Btu/h*ft*F). The structural analysis was done in 3D with each pair of steel studs, against the front and back gypsum boards, connected together by phenolic resin braces. A single steel stud model is given in Figure 4.7 (left) and two steel studs acting together as a single unit to withstand the vertical load was modeled and given in Figure 4.7 (right). Both models in Figure 4.7 have a 36 in unbraced length.
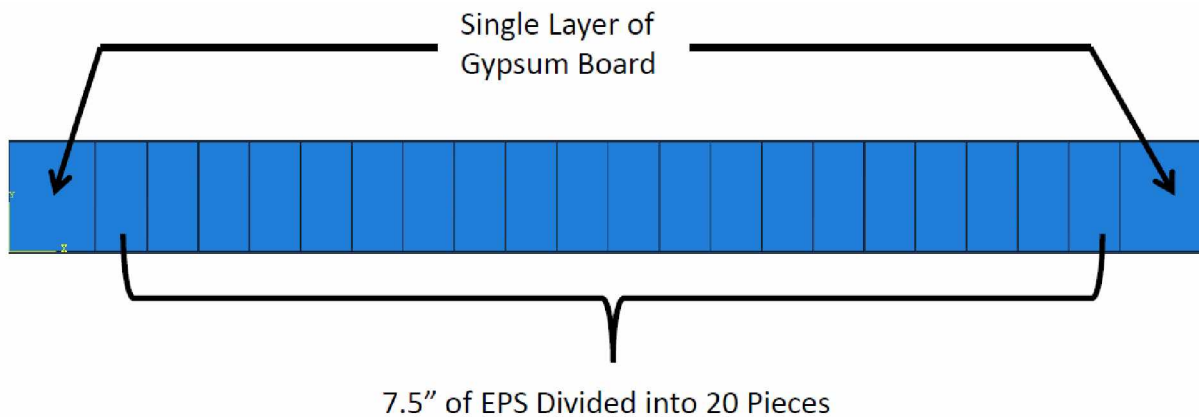
Figure 4.6: 2D model of gypsum board wall assembly for thermal analysis
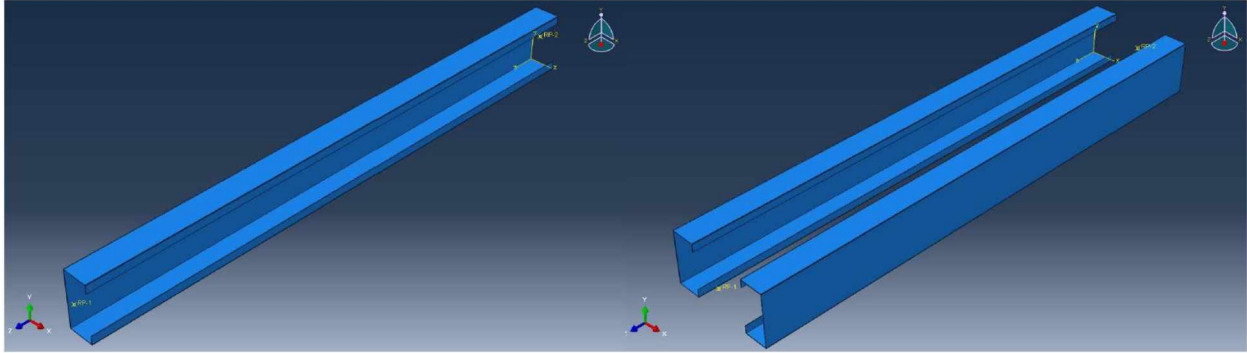
Figure 4.7: 3D model of single steel stud (left) and two facing studs braced together (right) with 36 in unbraced length

The furnace temperature table for a given fire test is presented in Table 4.6. That is, the temperature inside the furnace should be controlled such that it follows Table 4.6.

Table 4.6: E119 temperature vs time

t (min)	T (F)	T (C)	t (min)	T (F)	T (C)
0	68	20	95	1804	984
5	1000	538	100	1815	991
10	1300	704	105	1826	997
15	1399	759	110	1835	1002
20	1462	794	115	1843	1006
25	1510	821	120	1850	1010
30	1550	843	125	1856	1013
35	1584	862	130	1862	1017
40	1613	878	135	1869	1020
45	1638	892	140	1875	1024
50	1661	905	145	1882	1028
55	1681	916	150	1888	1031
60	1700	927	155	1894	1034
65	1718	937	160	1900	1038
70	1735	946	165	1906	1041
75	1750	954	170	1912	1044
80	1765	963	175	1919	1048
85	1779	971	180	1925	1052
90	1792	978	185	1932	1055

4.5.7 Heat Transfer Modeling

The thermal analysis was done to calculate the temperature distribution of the wall assembly in the furnace fire test. Heat transfer takes place in three forms: thermal conduction, thermal convection and thermal radiation [25]. Thermal conduction takes place in the gypsum boards and EPS. Thermal convection and thermal radiation take place on the surfaces of the gypsum boards and the surface of the melting EPS. The convective heat transfer coefficient chosen was 25 W/m^2*K [26] on the fire side of the gypsum board. The chosen emissivities of the gypsum boards and EPS were 0.9 under all conditions [26, 27]. The convective heat transfer coefficient chosen was 10 W/m^2*K [26] on the ambient side of the gypsum board. The ambient temperature chosen was 20 C/68 F and the furnace temperature is given in Table 4.6. The heat transfer across the wall assembly is completely in the form of thermal conduction before the EPS starts melting. After the EPS starts melting, thermal convection and thermal radiation begin to take place in the gap between the gypsum board on the furnace side and the melting EPS. Eventually, all the EPS melts away and thermal convection and thermal radiation take place on the interior surfaces of the gypsum boards on both the fire and ambient sides.

In the heat transfer modeling, the thermal radiation was magnified by a factor of $1 + C$ to account for the thermal convection, which occurs in the cavity when the EPS starts melting and was not explicitly modeled in the analysis. Therefore, the thermal magnifying factor C accounts for the thermal convection that was not explicitly modeled. C varies as the EPS melts away and was derived through principles of heat transfer. The mathematical expression of total heat transfer in the cavity of gypsum boards is given in Equation 3.1. The convective heat transfer and radiative heat transfer are given in Equations 3.2 and 3.3. The thermal magnifying factor accounting for convective heat transfer is given in Equation 4.4.

$$\dot{Q}_{total} = \dot{Q}_{conv} + \dot{Q}_{rad} = (1 + C)\dot{Q}_{rad} \tag{3.1}$$

$$\dot{Q}_{conv=}(T_1 - T_2)\frac{K_{eff}}{L}A \tag{3.2}$$

$$\dot{Q}_{rad} = (T_1^4 - T_2^4)\varepsilon\sigma FA \tag{3.3}$$

$$C = \frac{(T_1 - T_2)\frac{K_{eff}}{L}A}{(T_1^4 - T_2^4)\varepsilon\sigma FA} \tag{3.4}$$

Where:

$\dot{Q}_{total}$ is the total heat transfer in the cavity of the gypsum board wall assembly;

$\dot{Q}_{conv}$ is the convective heat transfer in the cavity of gypsum board wall assembly;

$\dot{Q}_{rad}$ is the radiative heat transfer in the cavity of gypsum board wall assembly.

C is the thermal magnifying factor accounting for convective heat transfer;

T_1 is the temperature of the surface of cavity on the fire side;

T_2 is the temperature of the surface of cavity on the ambient side;

L is the distance of the cavity in the gypsum board wall assembly caused by melting EPS insulation;

K_{eff} is the effective thermal conductivity of air in the cavity of melting EPS insulation;

ε is thermal emissivity of gypsum board, 0.9; and

σ is the Stefan Boltzmann constant, $5.67*10^{-8}$ W/m^2*K^4 or 1.714×10^{-9} BTU/hr*ft^2*R^4.

Figure 4.8 demonstrates the heat transfer mechanism as the EPS is melting away. It is worth noting that the steel studs are neglected in the thermal analysis due to their thinness (0.0566 in or 0.346 in) and high thermal conductivity.
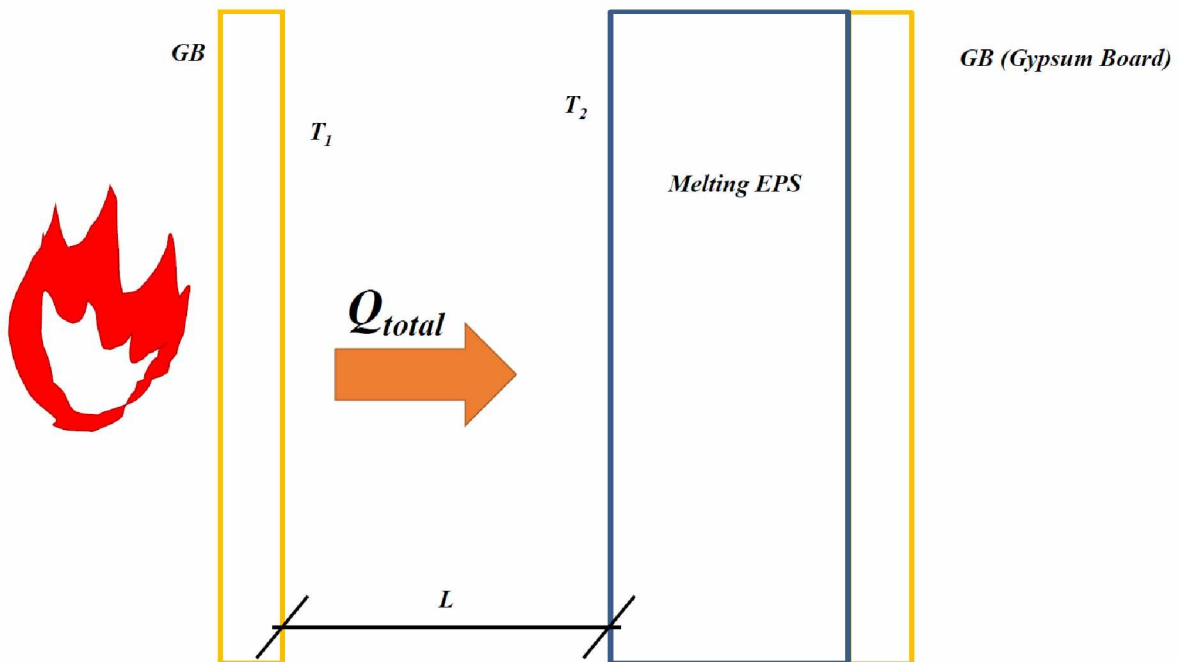

Figure 4.8: Schematic of heat transfer mechanism in the cavity of wall assembly with EPS insulation

K_{eff} is the effective thermal conductivity of the air between the gypsum board on the fire side and the melting EPS (or the gypsum board on the ambient side when the entire EPS melts away). The convective heat transfer in the cavity of the wall assembly after the EPS starts melting is treated as pure thermal conduction with an effective thermal conductivity in the medium of length L. The effective thermal conductivity K_{eff} is given in Equation 3.5. K_{air} is the thermal conductivity of air and Nu is the Nusselt number in the cavity of the wall assembly where thermal convection takes place. Using the Nusselt number can greatly simplify the convective heat transfer analysis and the Nusselt number for the cavity between two rectangular plates can be calculated with Equations 3.6 and 3.7.

$$K_{eff} = K_{air} Nu \tag{3.5}$$

$$Nu = 0.46 Ra_L^{1/3} \tag{3.6}$$

$$Ra_L = \frac{g\beta(T_1 - T_2)L_c^3}{v^2} Pr \tag{3.7}$$

Where:

Ra_L is the Rayleigh number;

g is the gravitational acceleration, m/s² or ft/s²;

β is the coefficient of volume expansion, $1/K$ ($\beta = 1/T$ for ideal gas);

L_c is the characteristic length, m or ft ($L_c = L$ in this case);

v is the kinematic viscosity of the fluid, m²/s or ft²/s; and

Pr is the Prandtl number.

The view factor between any two parallel plates is calculated according to Equation 3.8.

$$F = \frac{1}{\pi w^2}\left(ln\frac{x^4}{1+2w^2} + 4wy\right) \tag{3.8}$$

Where:

$$w = H/L \tag{3.9}$$

H: height of the gypsum boards, 12 ft or 3.6576 m in this case

$$x = \sqrt{1 + w^2} \tag{3.10}$$

$$y = x \cdot arctan(\frac{w}{x}) - arctan(w) \qquad\qquad (3.11)$$

The equations given above were implemented in ABAQUS recursively until the results converged with negligible difference. In the first simulation, the thermal convection was completely neglected, which means C was equal to be zero. In the second simulation, the thermal magnifying factor was calculated based on the thermal result from the first simulation and implemented into ABAQUS as a function of time. The process was repeated until the difference between the current results and the previous results was negligible.

4.5.8 Simulation of Melting of EPS

EPS starts softening at 100 C (212 F) and melts completely at 240 C (464 F) [19]. EPS is not a crystalline material so it does not have a definitive melting temperature like steel or ice. The specific heat of EPS is given in Table 4.4. In this study, it is assumed the EPS becomes a jelly-like material above 100 C until 240 C when it becomes fully liquefied. The softened, jelly-like material can still act as thermal insulation to absorb heat from the furnace until it becomes completely liquefied. In order to simulate the melting phenomenon, the 7.5 in thick EPS was divided into 20 equal pieces, as shown in Figure 4.6. Each piece was deleted from the analysis after the "cold" side (the side towards the ambient side of the gypsum board) reached 240 C. Moreover, the thermal properties of EPS were replaced by the thermal properties of air when the temperature of any EPS element exceeded 240 C.

4.5.9 Recursive Analysis of Thermal Magnifying Factor C

As introduced previously, the thermal magnifying factor C was calculated with recursive analysis. The first thermal magnifying factor as a function of time was calculated based on the thermal results obtained by assuming $C = 0$. The iteration was repeated until C converged with negligible difference.

Figure 4.9 shows the converged magnifying factors for wall assemblies with 1, 2 and 3 layers of gypsum boards after only 3 iterations. It can be seen that the magnifying factor C was zero until the EPS started melting and rising rapidly. It then flattened to a constant value until the EPS melted away completely, at which point it decreased rapidly (except in the case of the wall assembly with 3 layers of gypsum boards). The magnifying factor C dropped in the wall assemblies with 1 and 2 layers of gypsum boards because radiative heat transfer becomes significant when the temperature is high. The EPS in the wall assembly with 3 layers of gypsum boards never melted completely, so the magnifying factor only flattened in the 3-hour fire test simulation. It can also be seen in Figure

4.9 that the differences between zero convective heat transfer (Nu_0), the first iteration (Nu_I1) and the second iteration (Nu_I2) were almost negligible.

In the analysis, the final thermal magnifying factor C was chosen to be the average integrated value for either the EPS melting phase or the post-EPS melting phase, as shown in Figure 4.9. The average integrated magnifying factor C was calculated to be 0.4382 for the wall assembly with 1 layer of gypsum boards, 0.4323 for the assembly with 2 layers of gypsum boards and 0.4207 for the assembly with 3 layers of gypsum boards, all in the EPS melting phase. The average magnifying factor C was calculated to be 0.1105 for the wall assembly with 1 layer of gypsum boards and 0.2 for the wall assembly with 2 layers of gypsum boards, both in the post-EPS melting phase.
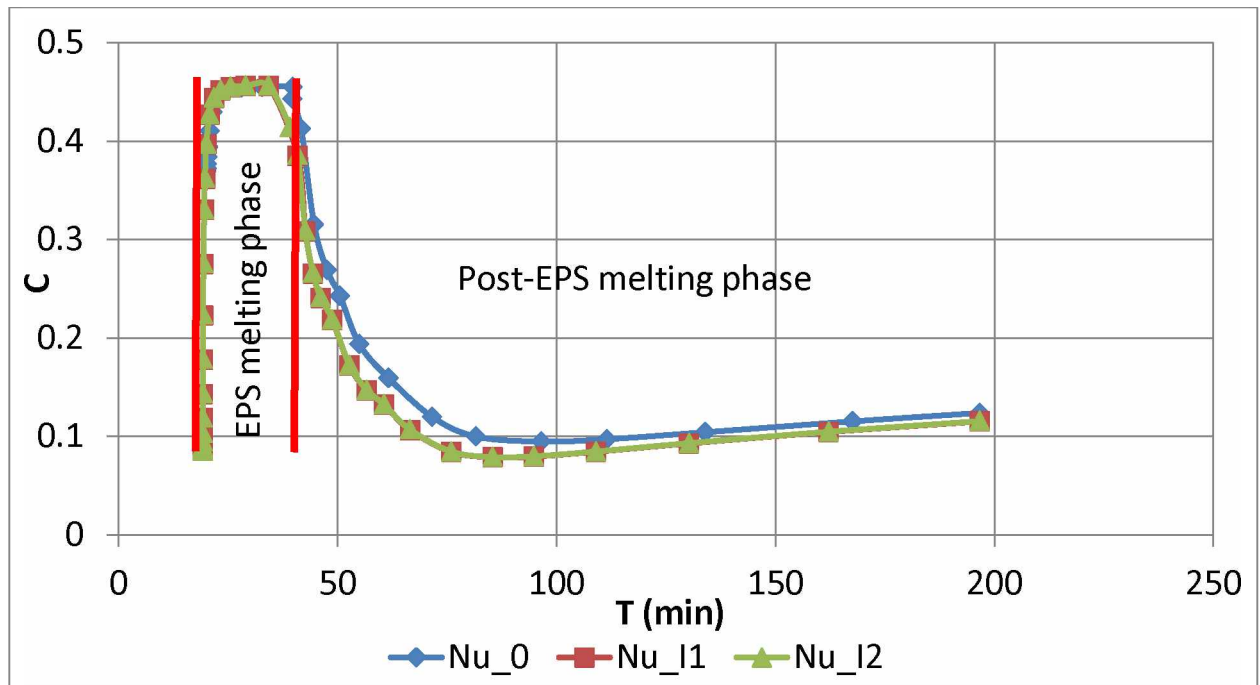
(a)
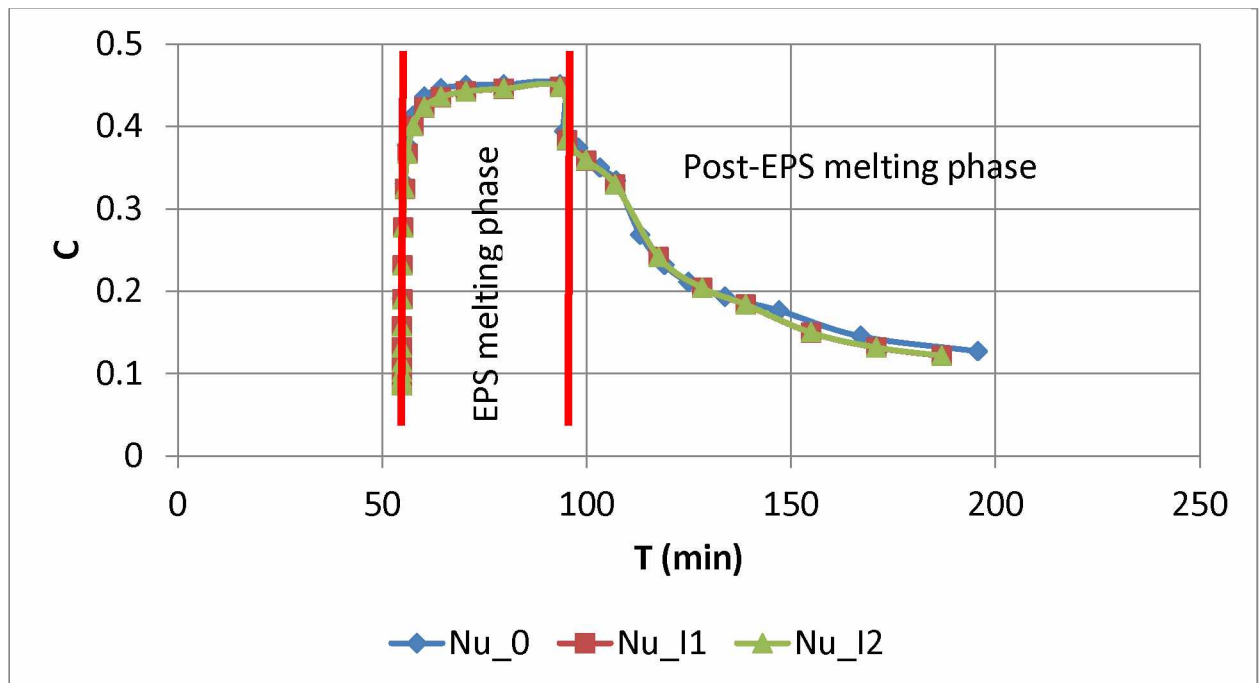
(b)
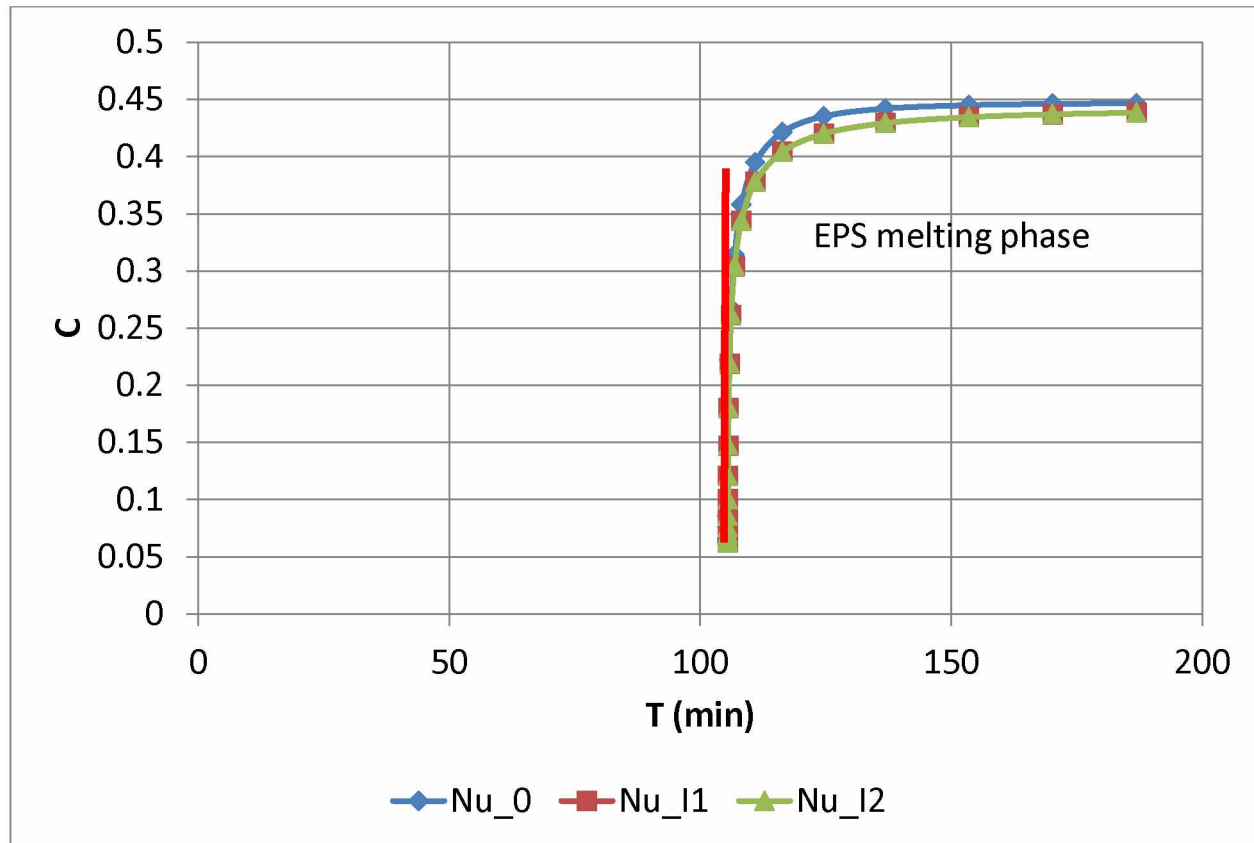
(c)

Figure 4.9: (a) Thermal magnifying factor C for wall assembly with 1 layer of gypsum boards; (b) Thermal magnifying factor C for wall assembly with 2 layers of gypsum boards; (c) Thermal magnifying factor C for wall assembly with 3 layers of gypsum boards

4.5.10 Failure Analysis of Steel Studs

Each steel stud was modeled in ABAQUS and is given in Figure 4.7 (left), and two steel studs facing each other were connected by phenolic resin braces and are shown in Figure 4.7 (right). The failure load of two braced steel studs was calculated at different times of the simulated furnace fire in a nonlinear post-buckling analysis in ABAQUS.

4.5.11 Finite Element Models, Meshing and Boundary Conditions of Thermal Analysis in ABAQUS

The thermal analysis model of the gypsum board wall assembly, excluding the steel studs, was given previously in Figure 4.6. It was assumed that heat only transfers across the gypsum board in one direction and the

model was done in 2D. The final meshing of the models of the gypsum board wall assemblies with one, two and three layers of gypsum boards is given in Figure 4.10. All the models were composed entirely of DC2D4 elements. The model with one layer of gypsum boards had 88 elements and 198 nodes. The model with two layers of gypsum boards had 96 elements and 216 nodes. The model with three layers of gypsum boards had 104 elements and 234 nodes. The elapsed times for wall assemblies with 1, 2 and 3 layers of gypsum boards were 1511 s, 2021 s and 1824.7 s.
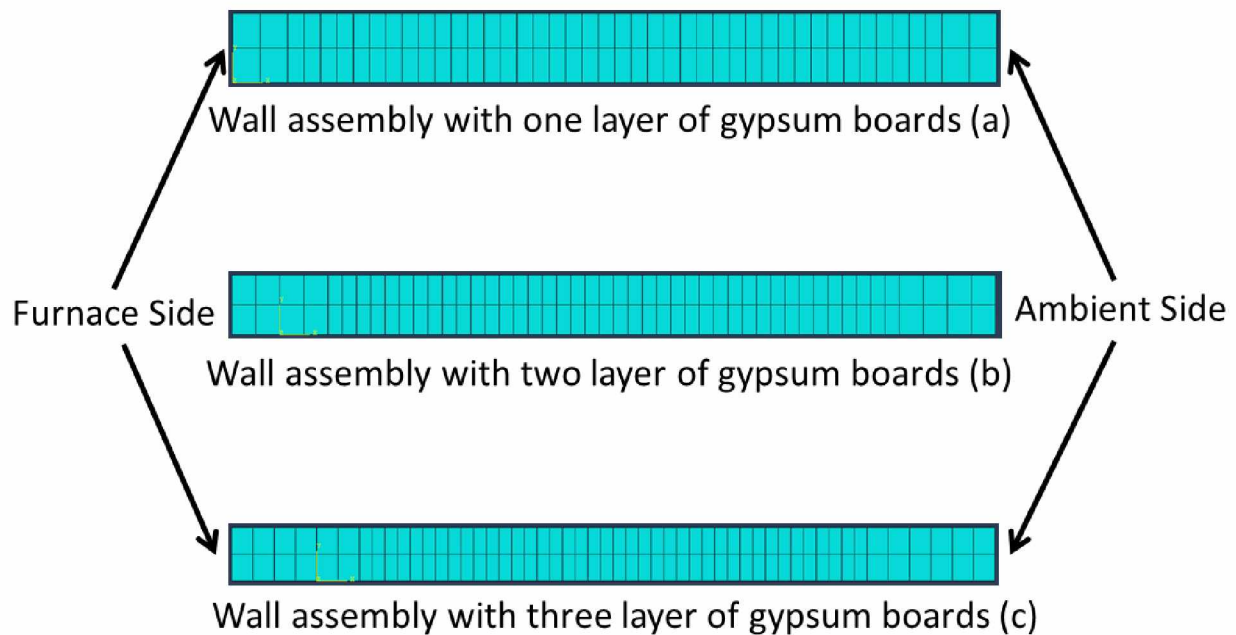
Figure 4.10: Meshing of the wall assembly models with one, two and three layers of gypsum boards

The boundary conditions of the wall assembly models were given in Figure 4.8. In the simulation, the furnace side of the wall assembly was subjected to the convective heat transfer and radiative heat transfer from the furnace fire, and the ambient side of the assembly was subjected to the convective heat transfer and radiative heat transfer at ambient temperature. The thermal coefficients and emissivities for both the furnace side and ambient side were introduced in the heat transfer modeling section.

4.5.12 Finite Element Models, Meshing and Boundary Conditions of Mechanical Analysis in ABAQUS

The final meshing of a single stud and two studs braced together is given in Figure 4.11. For two steel studs connected together, the centroids on both the top and bottom of the steel stud assembly were pin-connected to the top and bottom ends of both studs. A vertical load was imposed on the top centroid for the two steel studs connected together as a single unit. The middle-line nodes for both steel studs are fixed in the y direction to simulate the screws connecting the studs with the gypsum boards. The screws act as a means to prevent buckling in the undesired y direction. Figure 4.12 gives the boundary conditions of both the top and bottom (left) and middle-line nodes (right) for two steel studs connected together by phenolic resin with a 36 in unbraced length.
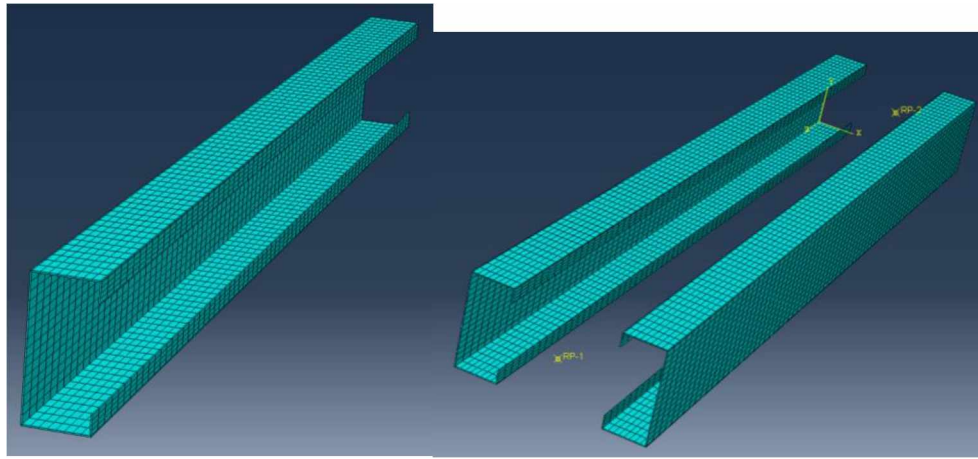

Figure 4.11: Meshing of a single steel stud (left) and two steel studs braced together (right) with each model having 36 in unbraced length
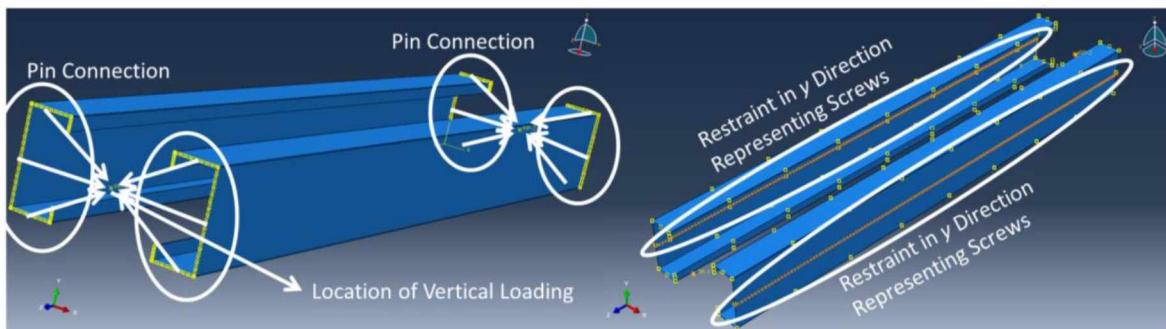

Figure 4.12: Boundary conditions for two steel studs braced together with 36 in unbraced length: top and bottom (left) and middle-line nodes restraint (right)

The final model of two steel studs connected together with 36 in unbraced length had 3,168 C3D20R elements and 22,984 nodes. The final model of two steel studs connected together with 72 in unbraced length had 6,336 C3D20R elements and 45,518 nodes.

4.6 Numerical Modeling Results

4.6.1 Thermal Analysis Results

The thermal analysis result was meant to determine the temperature of the steel studs on the fire and ambient sides as time elapses. It is assumed that the temperature of the steel studs is the same as the temperature of the EPS insulation where the studs are in contact with the EPS before the EPS melts away. Once the EPS melts away completely, the temperature of the steel studs is assumed to be uniform [28] and equal to the temperature of the gypsum boards that they are leaning against, whether it is the fire side gypsum board or the ambient side gypsum board. This assumption is due to the thinness of the steel studs (0.0566 in or 0.0346 in), short flange length (1.625 in) and the high thermal conductivity of steel. Figure 4.13 shows 4 locations where temperature was measured in the 2D thermal analysis. This study examined the influence of the number of layers of gypsum boards on the temperature response of the wall assemblies. Figure 4.14, Figure 4.15 and Figure 4.16 show the temperature at the 4 locations as a function of time for single, double and triple layers of gypsum boards.
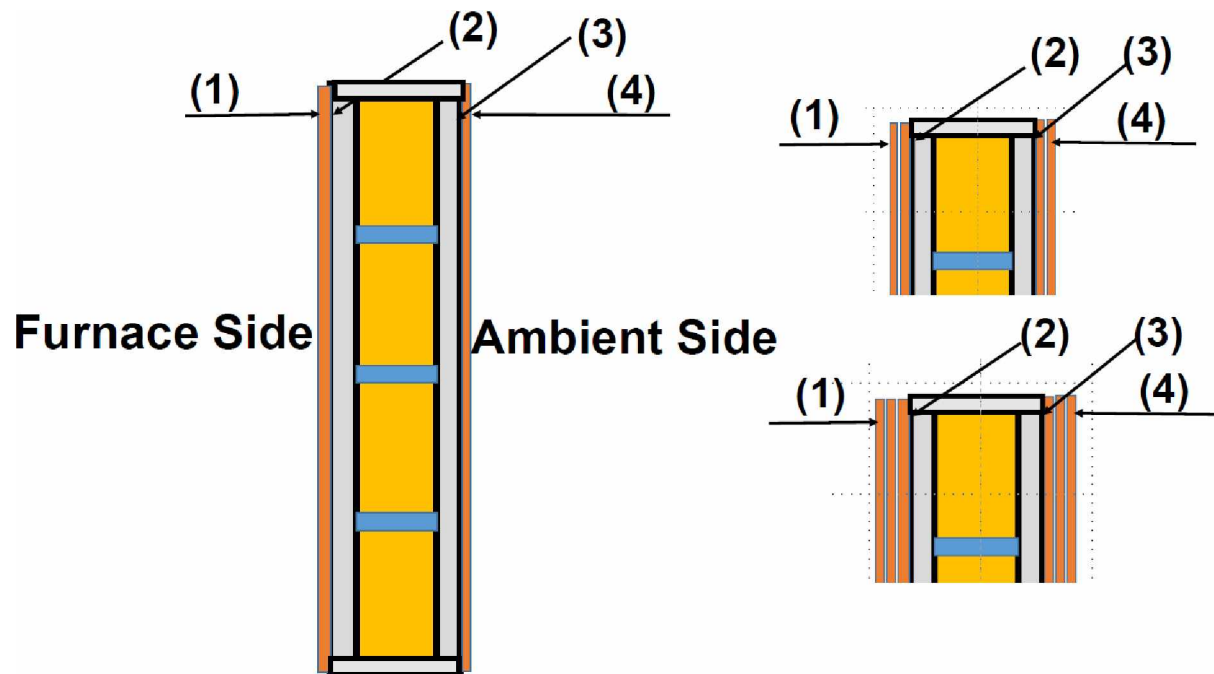
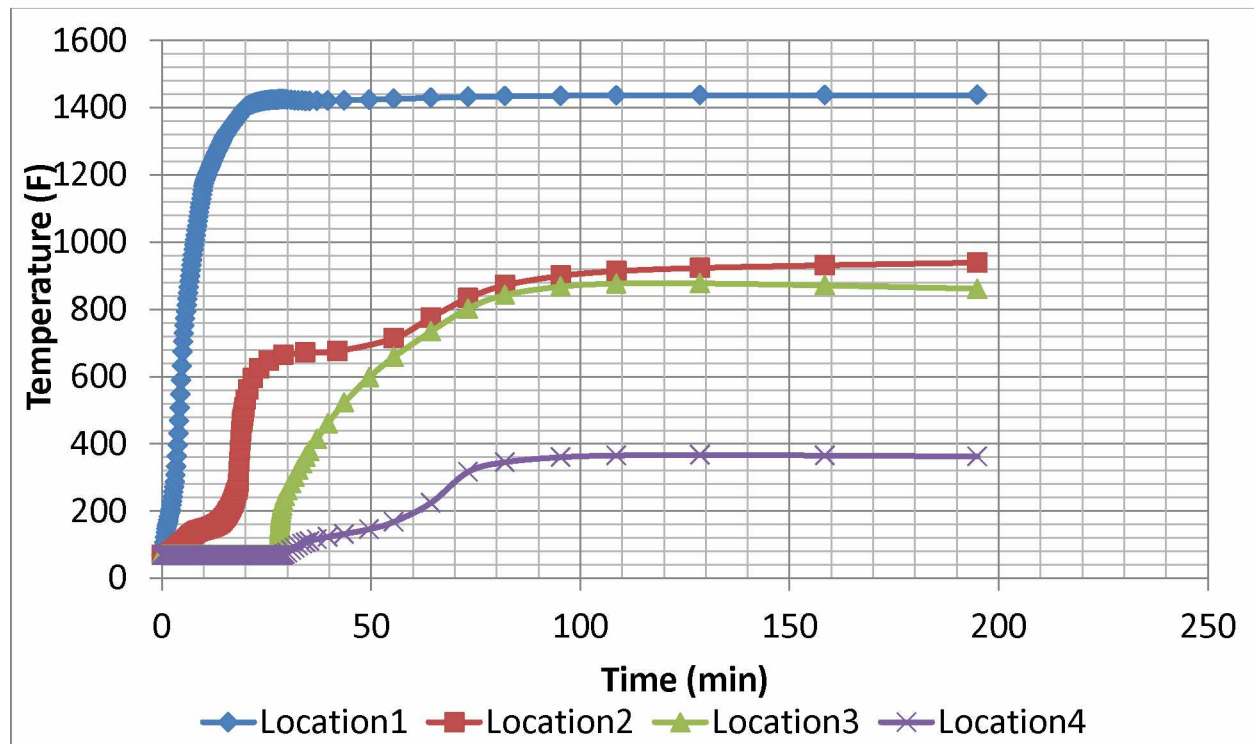Figure 4.13: Locations for the temperature measurement in the wall assembly

Figure 4.14: Temperature of the 4 chosen locations vs time (single layer)
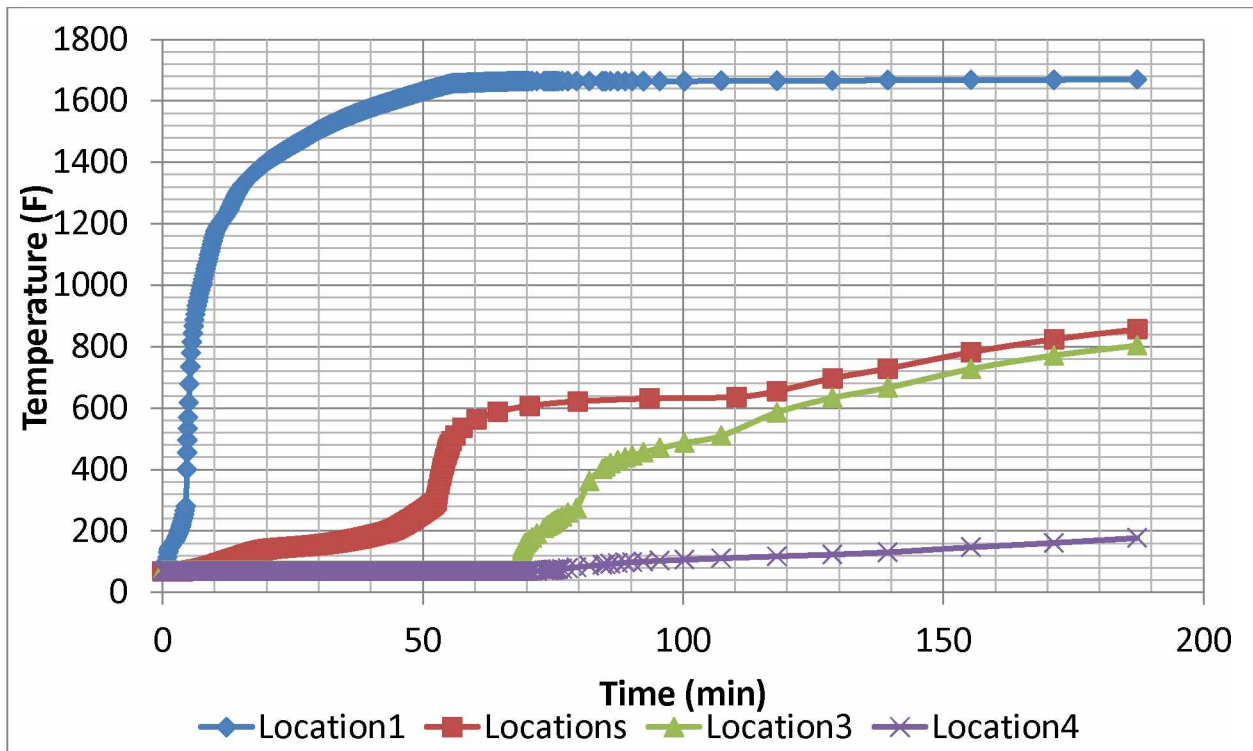
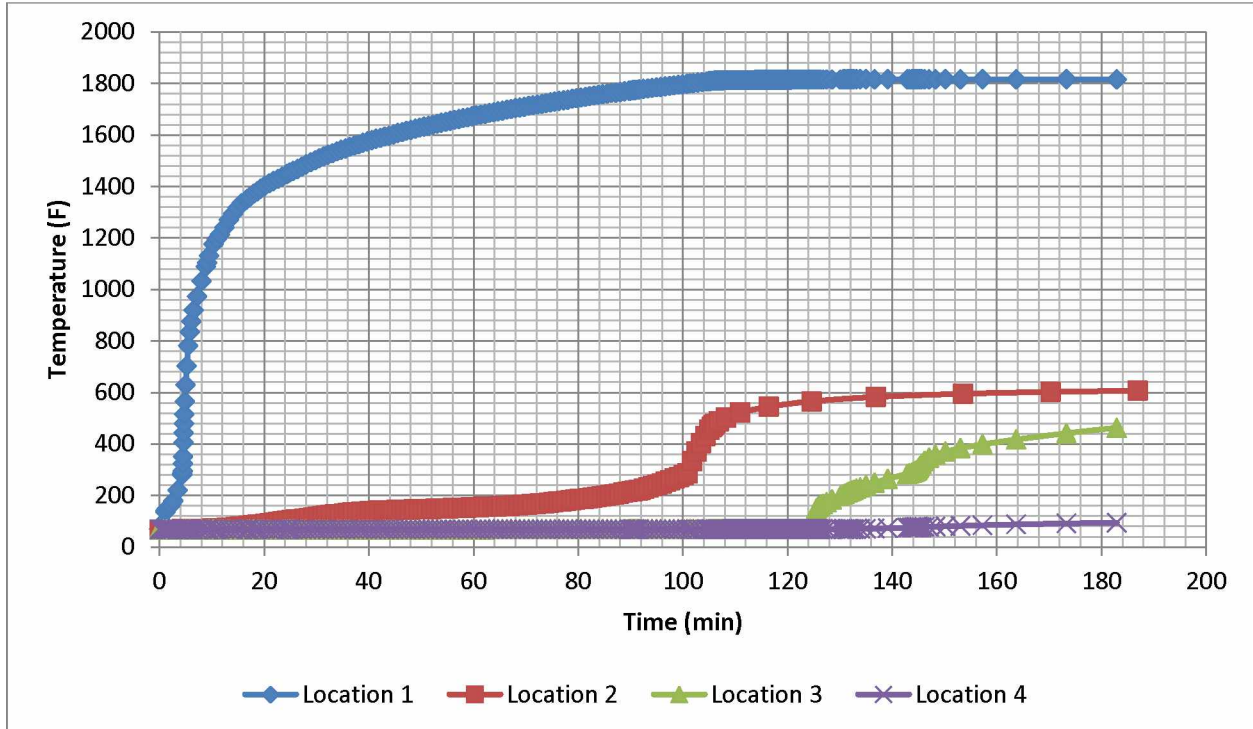Figure 4.15: Temperature of the 4 chosen locations vs time (double layers)

Figure 4.16: Temperature of the 4 chosen locations vs time (triple layers)

4.6.2 Mechanical Analysis Results

A failure analysis of the steel studs in the wall assembly at 1, 2 and 3 hours was examined. The temperatures obtained from the thermal analysis were inputted as the thermal boundary conditions for the steel studs. The temperatures measured at Location 2 were inputted as the overall temperature of the steel stud close to the fire. The temperatures measured at Location 3 were inputted as the overall temperature of the steel stud away from the fire. The two different unbraced lengths chosen were 36 in and 72 in, and the bracings are demonstrated in Figure 4.2 and Figure 4.3. Two different sized studs, 362S162-54 (16 gauge) and 362S162-33 (20 gauge), were used in the analysis. The chosen magnitude of imperfection of all the steel studs was L/1000. Therefore, the 36 in unbraced length had a largest initial deflection of 0.036 in, and the 72 in unbraced length had a largest initial deflection of 0.072 in. The first buckling mode of a given unbraced length (36 in or 72 in) of a two-connected-stud model was chosen as the imperfection shape for the two-connected-stud model with that unbraced length. Figure 4.17 (left) gives the buckling analysis for two connected studs with a 36 in unbraced length connected to single layer of gypsum boards after 1 hour of fire. It can be seen that only the stud close to the fire buckled. The load imposed on the top centroid, as shown in Figure 4.12, kept increasing until the steel studs failed in ABAQUS. Figure 4.17 (right) gives the failure shape of the same two steel studs connected together with a 36 in unbraced length, and again, only the stud close to the fire failed.

The failure analysis obtained failure loads for the two-connected-stud models, with 36 in and 72 in unbraced lengths, at 1, 2 and 3 hours into the furnace fire test. Figure 4.18 and Figure 4.19 give the failure loads of the two studs connected together as a function of time for both 362S162-33 and 362S162-54 CSJ studs. Figure 4.20 demonstrates the load path of two 362S162-54 studs connected together with 1 layer of gypsum boards at 1 hour of fire. The failure load of a model with two connected studs is defined as the largest compressive load the model can withstand before bifurcation takes place. After bifurcation the compressive load decreases with increased deflection, as shown in Figure 4.20. Tables 4.7 and 4.8 give the elapsed analysis times for the models constructed with both 362S162-54 and 362S162-33 steel studs with varying parameters. It should be noted that the elapsed analysis time for a model was the overall time elapsed before ABAQUS aborted the process due to numerical non-convergence. The failure loads were obtained for all the models with different parameters, but different models failed at different times in the post-buckling analysis due to numerical non-convergence, after the failure load was achieved. Therefore, the elapsed times given in Tables 4.7 and 4.8 do not represent the times at which the failure loads, like

the one shown in Figure 4.20, occurred. It can be seen that the elapsed times varied by a very large degree for models with different parameters. Table 4.9 gives the summary of the buckling loads and failure loads of the two steel studs with different parameters, with 362S162-33 signified as G20 and 362S162-54 as G16 in the Table.

The buckling behavior of the steel studs was thoroughly analyzed and studied. Appendix D gives further detail on the buckling analysis of steel stud 362S162-33.
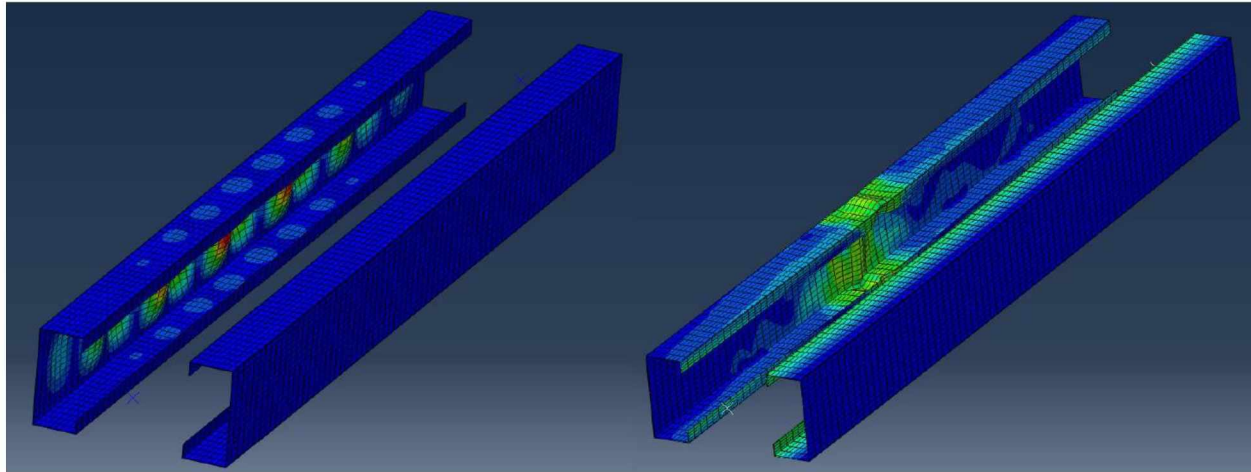
Figure 4.17: Buckling shape (left) and failure shape (right) of two steel studs connected together with 36 in unbraced length
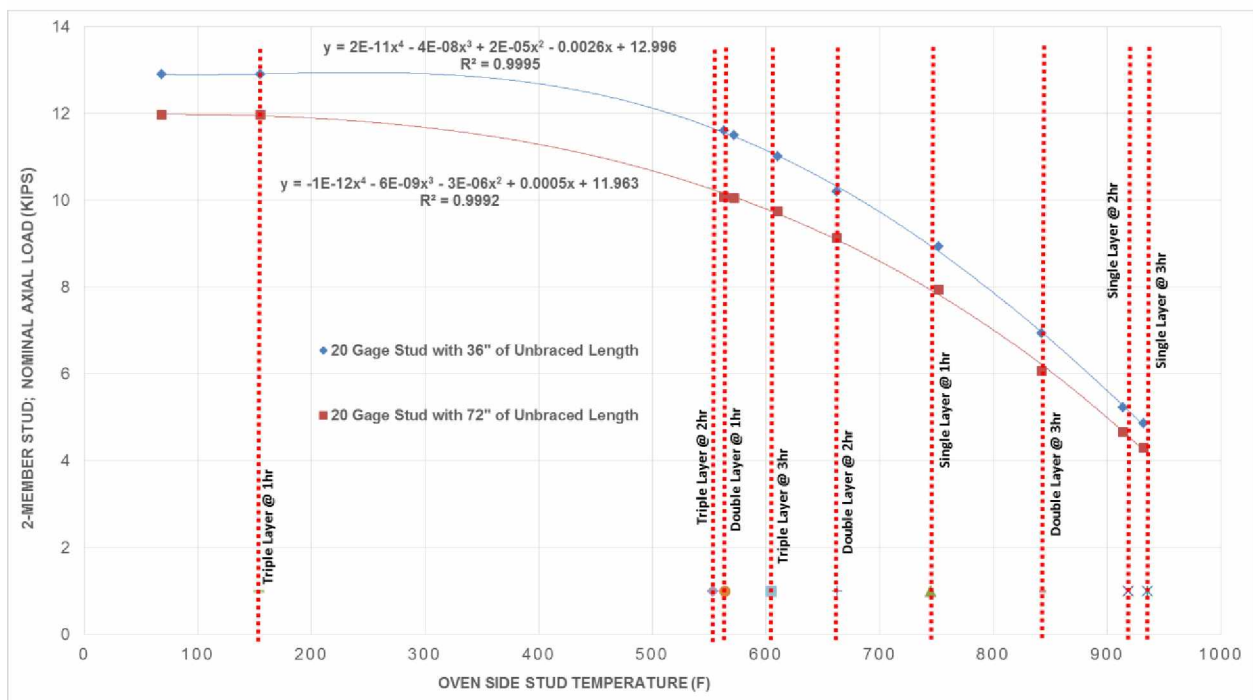
Figure 4.18: Load capacity for two 362S162-33 studs connected together
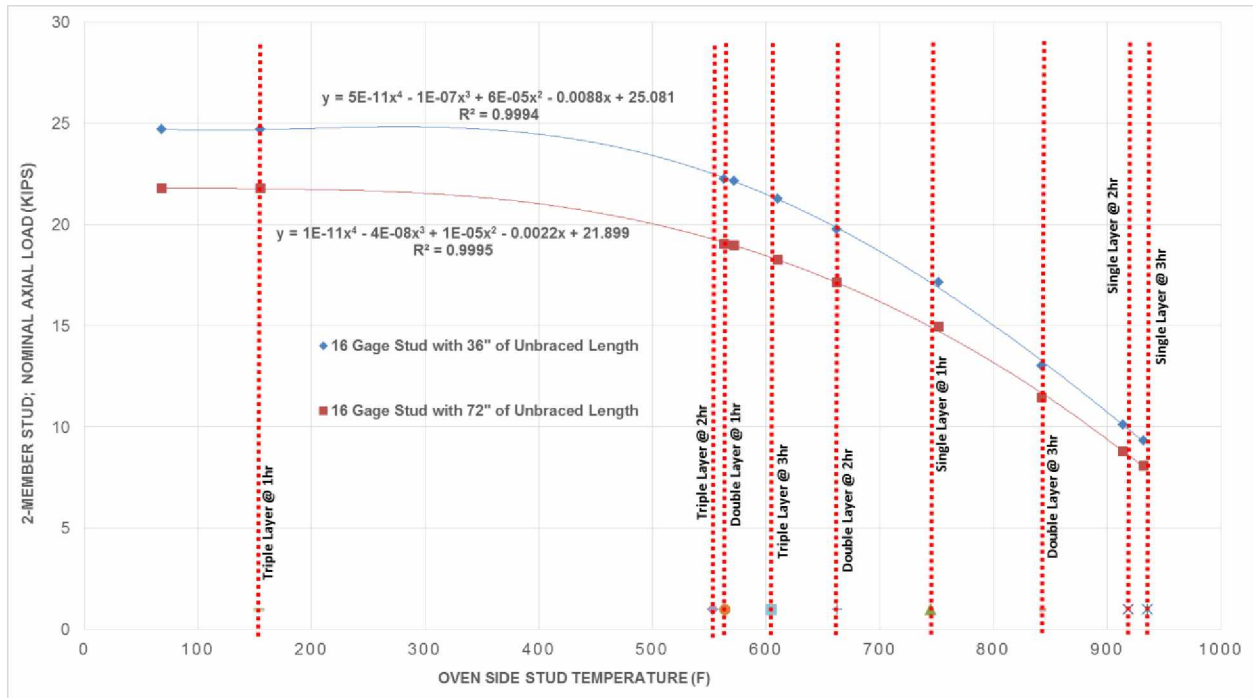
Figure 4.19: Load capacity for two 362S162-54 studs connected together
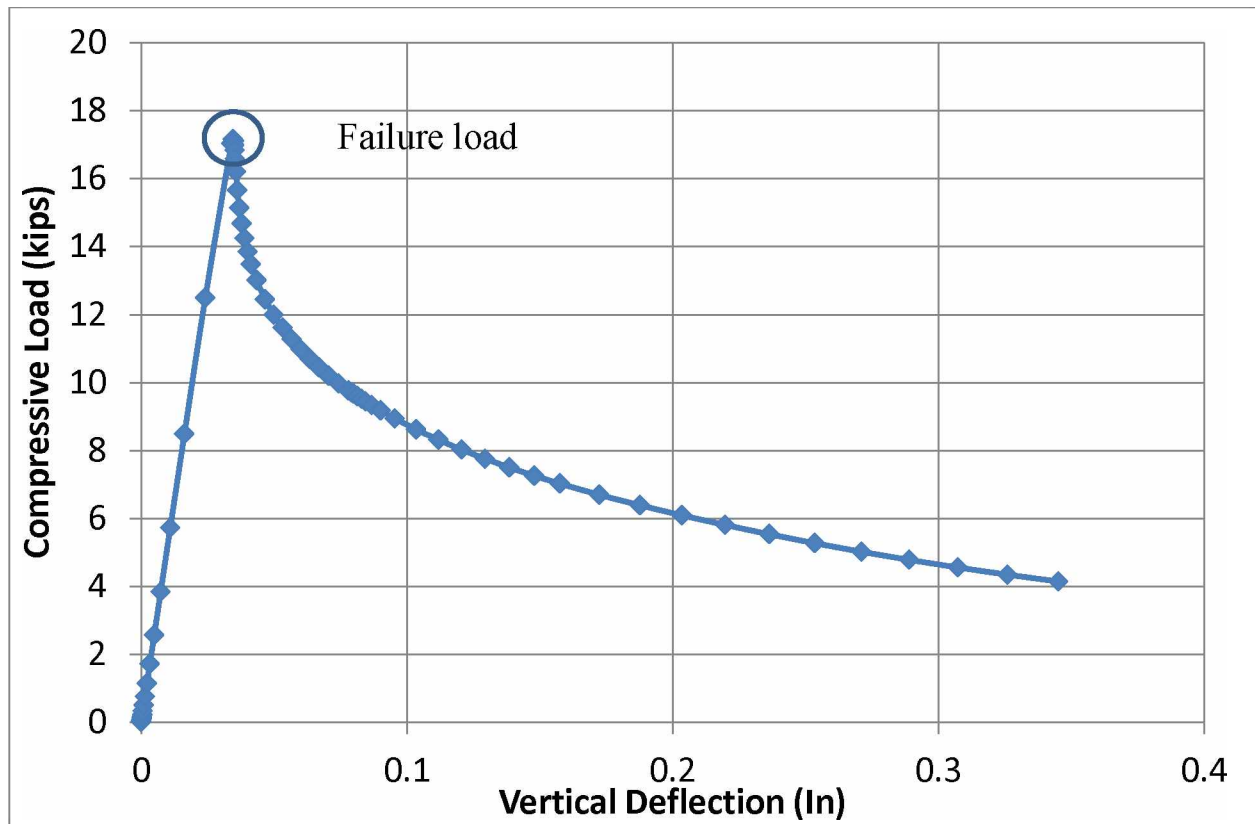
Figure 4.20: Loading path of two 362S162-54 studs connected together with 36 in of unbraced length and 1 layer of gypsum boards at 1 hour fire

Table 4.7: Elapsed time of analysis of 362S162-54 stud with varying parameters

Elapsed time (s)	Layers of Gypsum boards	Hours of Fire	Unbraced Length (in)
29,155	1	1	36
11,274	1	2	36
11,405	1	3	36
17,990	2	1	36
49,554	2	2	36
26,732	2	3	36
4,649	3	1	36
19,171	3	2	36
4,429	3	3	36
4,649	NA (Ambient Temperature)		36
61,677	1	1	72
35,802	1	2	72
39,548	1	3	72
37,916	2	1	72
2,704	2	2	72
7,947	2	3	72
15,711	3	1	72
2,458	3	2	72
5,248	3	3	72
15,711	NA (Ambient Temperature)		72

Table 4.8: Elapsed time of analysis of 362S162-33 stud with varying parameters

Elapsed time (s)	Layers of Gypsum boards	Hours of Fire	Unbraced Length (in)
2,016	1	1	36
2,481	1	2	36
1,480	1	3	36
2,415	2	1	36
1,011	2	2	36
12,563	2	3	36
1,713	3	1	36
3,086	3	2	36
1,700	3	3	36
1,649	NA (Ambient Temperature)		36
5,304	1	1	72
3,053	1	2	72
3,651	1	3	72
37,916	2	1	72
11,052	2	2	72
2,425	2	3	72
9,490	3	1	72
7,640	3	2	72
4,276	3	3	72
9,490	NA (Ambient Temperature)		72

Table 4.9: Summary of buckling and failure loads of the studs with varying parameters

G16 (36" Unbraced Length)			G16 (72" Unbraced Length)		
Buckling Load (kips)	Failure Load (kips)	Temperature (F)	Buckling Load (kips)	Failure Load (kips)	Temperature (F)
32.207	24.7	68	32.055	21.788	68
32.207	24.7	155	32.055	21.788	155
25.018	22.23	563	24.9	19.032	563
24.809	22.16	572	24.691	18.965	572
24.557	21.25	610	24.441	18.258	610
24.112	19.77	662	23.997	17.144	662
23.165	17.154	752	23.055	14.944	752
17.848	13.02	842	17.763	11.452	842
13.758	10.11	914	13.692	8.797	914
12.685	9.33	932	12.625	8.094	932
G20 (36" Unbraced Length)			G20 (72" Unbraced Length)		
Buckling Load (kips)	Failure Load (kips)	Temperature (F)	Buckling Load (kips)	Failure Load (kips)	Temperature (F)
7.3539	12.9	68	7.3205	11.965	68
7.3539	12.9	155	7.3205	11.965	155
5.7133	11.6	563	5.6873	10.07	563
5.6708	11.49	572	5.6398	10.047	572
5.6076	11	610	5.5848	9.738	610
5.5055	10.2	662	5.4805	9.126	662
5.2892	8.935	752	5.2652	7.941	752
4.0757	6.93	842	4.0572	6.056	842
3.1416	5.215	914	3.1274	4.658	914
2.8969	4.854	932	2.8837	4.292	932

4.7 Results Discussion

4.7.1 Thermal Analysis Result

It can be seen in Figure 4.14, Figure 4.15 and Figure 4.16 that the temperature on the exterior fire side of the gypsum board (Location 1) increases rapidly and eventually plateaus. The temperature increase varies with the number of layers of gypsum boards for all 4 locations. The temperature rises the fastest for the single layer gypsum board wall assembly, less so for the double layer wall assembly and the slowest in the triple layer assembly.

The temperature at Location 2 increases slowly before 212 F (100 C). After reaching 212 F, the temperature increases rapidly until it reaches over 600 F (316 C) before it slows down again. The slow increase of

the temperature before 212 F is due to the release and vaporization of the chemically bound water in the gypsum board. After all the water vaporizes, the temperature rises rapidly until reaching around 600 F, at which point the temperature remains rather constant for 1, 2 and 3 layers of gypsum boards for different periods of times. The reason temperature stays constant is because the EPS reaches 240 C (464 F) and starts melting away. The melting of EPS functions similarly to the release and vaporization of chemically bound water in the gypsum boards. Heat is absorbed but the temperature stays rather constant. It can be seen that for a single layer gypsum board wall assembly, the temperature slowly reaches 212 F about 15 minutes into the fire test and starts rising rapidly. Then the temperature stays constant until about 50 minutes due to the melting EPS. After 50 minutes, the temperature starts rising quickly again and eventually plateaus. The temperature of the double layer gypsum board wall assembly follows a very similar pattern but the timings are different. The temperature reaches 212 F at around 46 minutes before it rises rapidly. It then stays constant until about 110 minutes due to the melting EPS. After 110 minutes, the temperature starts rising fast again. For the triple layer gypsum board wall assembly, it takes 100 minutes before the temperature at Location 2 reaches 212 F and starts rising rapidly. After 180 minutes (3 hours) of the fire test, the EPS in the triple layer gypsum boards has not melted away. The second rapid temperature increase, like the ones shown in Figure 4.14 and Figure 4.15 in the post-EPS melting phase, is never observed in Figure 4.16.

The temperature at Location 3 stays at 68 F (20 C) for a while until it begins to increase for single, double and triple layers gypsum board wall assemblies. Once EPS melts away completely, the lack of thermal insulation increases the heat transfer via thermal radiation and thermal convection. The temperature at Location 3 starts getting close to the temperature at Location 2. The temperature at Location 4 varies considerably for single, double and triple layer gypsum board wall assemblies. The temperature at Location 4 for the single layer wall assembly stays constant at 68 F. After 30 minutes, the temperature starts rising slowly to about 145 F (63 C) until around 50 minutes. After that, the temperature rises quickly to about 360 F (182 C) until 90 minutes, when the temperature stabilizes until the end of the 3 hours. The temperature at Location 4 for the double layer wall assembly stays at 68 F, then increases linearly at a slow pace and never reaches 200 F at the end of 3 hours. The temperature at Location 4 for triple layer wall assembly never exceeds 100 F during the entire 3 hours.

The highest temperatures at Location 2 of the single, double and triple layers gypsum boards wall assemblies after 3 hours of furnace fire test are 932 F (500 C), 842 F (450 C) and 610 F (321 C), respectively. As introduced before, phenolic resin only loses 11.5% of its weight in the temperature range from 297 C (566.6 F) to

485 C (905 F) and loses 29% of its weight from 485 C (905 F) to 622 C (1151.6 F) [23]. Therefore, the phenolic resin bracing will stay effective during the entire 3 hours.

It is concluded that gypsum boards have a significant thermal insulation effect on the wall assembly due to their low thermal conductivity and the release and vaporization of chemically bound water. EPS effectively slows down the temperature rise due to its low thermal conductivity and the absorption of heat when it is melting away. Phenolic resin can be effective during the entire 3 hours even for the wall assembly with a single layer of gypsum boards.

4.7.2 Mechanical Analysis Result

The buckling shape and failure shape of the two-connected-steel-stud are given in Figure 4.17. The connected-steel-stud assembly failed at the middle section of the steel stud close to the fire side of the gypsum board (higher temperature). As shown in Figure 4.17 (right), the failure happened at the middle section of the stud due to the default ABAQUS setting. The largest deflection always occurs at the middle section in the buckling analysis in ABAQUS. In reality, the failure is most likely to happen at locations of stress concentration [1]. The ultimate failure loads of the connected-steel-stud assemblies are given as functions of temperature in Figure 4.18 (362S162-33) and Figure 4.19 (362S162-54). It can be seen that as temperature increases, the patterns of the ultimate failure loads vs temperature are almost identical for 362S162-33 and 362S162-54. The ultimate failure loads for 362S162-54 studs are about twice as high as that for 362S162-33 studs for the same unbraced length.

It is concluded that temperature has a significant effect on the ultimate failure loads of steel studs. This is because the mechanical properties of steel (yield stress and Young's modulus) degrade with increase in temperature. Different gauges or sizes of steel studs significantly affect the ultimate failure loads as demonstrated by the comparison between 362S162-33 and 362S162-54. Different bracing lengths can also be helpful to boost the failure load of the wall assembly as demonstrated in Figure 4.18 and Figure 4.19. The failure loads for the 36 in unbraced length are about 10% higher than the 72 in unbraced length.

Table 4.9 gives the comparison of the buckling loads and failure loads of the steel studs with different parameters. It can be observed that the local buckling loads for the same steel stud are almost always identical regardless of the unbraced length at a fixed temperature, and it is because local buckling load is independent of the unbraced length, unlike global buckling. On the other hand, different unbraced lengths can influence the failure load

of the steel stud, due to post-buckling behavior where inelasticity of the material (steel) takes into effect. However, it can also be seen that the buckling loads of 362S162-54 (16G) are higher than the failure loads of the studs, whereas it is the opposite for 362S162-33 (20G). The explanation for this behavior is that 362S162-54 is a compact member and 362S162-33 is a non-compact member. The elastic buckling analysis does not consider the inelastic yielding of the steel and will generate higher loads for buckling than for failure, in the case of compact structural members.

4.8 Conclusions

This study introduced a numerical modeling methodology for evaluating the thermal and mechanical behaviors of a new composite steel-EPS wall assembly insulated with varying layers of gypsum boards. The wall assembly consisted of light gauge steel studs, EPS insulation and gypsum boards. The EPS insulation had the thickness of 7.5 in, and the steel studs used in simulation were 362S162-33 and 362S162-54. The chosen unbraced lengths were 36 in and 72 in. The fire performance of any new gypsum board wall assembly is typically determined by a standard furnace fire test before it can be used in the construction industry. The author proposed an alternative of numerical analysis and obtained numerical results for the new composite gypsum board wall assemblies with varying parameters. Several conclusions can be drawn from these results.

1. Gypsum boards have a significant thermal insulation effect on the wall assembly due to their low thermal conductivity and the vaporization of chemically bound water.

2. EPS effectively slows down the temperature rise due to its low thermal conductivity and the heat absorption when it is melting away.

3. The temperature of the cavity of the wall assembly will not be high enough to melt the phenolic resin bracing.

4. The ultimate failure load of the steel studs can be significantly affected by the temperature of the studs.

5. Different stud sizes can also significantly affect the ultimate failure loads of the wall assemblies.

6. Phenolic resin can be used as bracing devices to increase the ultimate failure loads of the wall assemblies.

7. Numerical analysis can be used to predict the thermal and mechanical response of the new gypsum board wall assembly, but a standard furnace fire test should be considered before the wall assembly can be used in the construction industry.

4.9 References

[1]. Kolarkar, Prakash, Structural and Thermal Performance of Cold-formed Steel Stud Wall Systems under Fire Conditions, 2010

[2]. Hamilton, R. Scott, Performance-based Fire Engineering for Steel Framed Structures: a Probabilistic Methodology, 2011

[3]. ASTM E 119-16: "Standard Test Methods for Fire Tests of Building Construction Materials," ASTM International, West Conshohocken, PA, 20162

[4]. Rahmanian, Ima, Thermal and Mechanical Properties of Gypsum Boards and Their Influences on Fire Resistance of Gypsum Board Based Systems, 2011

[5]. Manzello, Samuel, et al., Analysis of Inter-laboratory Testing of Non-load-bearing Gypsum/Steel-Stud Wall Assemblies, 2007

[6]. Manzello, Samuel, et al., Furnace Testing of Full-scale Gypsum Steel Stud Non-load-bearing Wall Assemblies: Results of Multi-laboratory Testing in Canada, Japan and USA, 2009

[7]. Allam, Ahmed, et al., Full-scale Fire Testing and Numerical Modelling of the Transient Thermal-Mechanical Behavior of Steel-stud Gypsum Board Partition Walls, 2014

[8]. Kesawan, Sivakumar, and Mahendran, Mahen, Fire Tests of Load-bearing LSF Walls Made of Hollow Flange Channel Sections, 2015

[9]. Chen, Wei, et al., Full-scale Fire Experiments on Load-bearing Cold-formed Steel Walls Lined with Different Panels, 2012

[10]. Chen, Wei, et al., Improved Fire Resistant Performance of Load-bearing Cold-formed Steel Interior and Exterior Wall Systems, 2013

[11]. Vieira Jr., Luiz Carlos Marcos Vieira Junior, Behavior and Design of Sheathed Cold-formed Steel Stud Walls under Compression, 2010

[12]. ASTM, E 8M-04, Standard Test Methods for Tension Testing of Metallic Materials (Metric). 2004, ASTM International: West Conshohocken, PA.

[13]. Kankanamge, Nirosha and Mahendran, Mahen, Mechanical Properties of Cold-formed Steels at Elevated Temperatures, 2015

[14]. Young, Ben and Chen, Ju, Mechanical Properties of Cold-formed Steel at Elevated Temperatures, 2004

[15]. Lee, Jinwoo, Elevated-temperature Properties of ASTM A992 Steel for Structural-fire Engineering Analysis, 2012

[16]. Landesmann, Alexandre, Experimental Investigation of the Mechanical Properties of ZAR-345 Cold-Formed Steel at Elevated Temperatures, 2014

[17]. Eurocode 4 - Design of composite steel and concrete structures - Part 1-2: General rules - Structural fire design, 2005

[18]. Karjala, P.J., et al., Thermal Properties of Syndiotactic Polystyrene, 1991

[19]. Brandrup, J. et al., Polymer Handbook, 4th Edition, 2004

[20]. Jansson, Robert, Measurement of Thermal Properties at Elevated Temperatures – Brandforsk Project 328-031, 2004

[21]. Moukhina, E, et al., Specific heat Functions Of Polystyrene in Glassy and in Liquid Amorphous State and Glass Transition DSC and TMDSC Study, 2006

[22]. Elragi, Ahmed, Selected Engineering Properties and Applications of EPS Geofoam, 2006

[23]. Chen, Xiong, Mechanical Properties with High Temperature and the Microstructure of Carbon/Phenolic Ablative Composites, 2012

[24]. AISC, Steel Construction Manual, 14th Edition, 2011

[25]. Cengel, Y and Ghajar, Afshin, Heat and Mass Transfer, 2011

[26]. Moro, L. et al., Influence of Surface Emissivity and of Low Emissivity Shields on the Thermal Properties of Low Density Insulating Materials, 2011

[27]. Keerthan, P. and Mahendran, M., Numerical Studies of Gypsum Plasterboard Panels under Standard Fire Conditions, Fire Safety Journal 53: 105-119, 2012

[28]. Gunalan, Shanmuganathan and Mahendran, Mahen, Finite Element Modelling of Load-bearing Cold-formed Steel Wall Systems under Fire Conditions, 2013

Chapter 5   Summary, Conclusion and Future Work

5.1 Summary

This dissertation gave a detailed numerical analysis of a new composite steel-EPS gypsum board wall assembly by using verified thermal and mechanical modeling methodology of existing experimental fire tests of a non-load-bearing and a load-bearing gypsum board wall assemblies. The thermal and mechanical behaviors of the new wall assembly were thoroughly studied, and subsequently the ultimate failure loads of the new wall assemblies with varying layers of gypsum boards at 1, 2 and 3 hours of fire were obtained.

The first chapter introduced the concept of fire safety design and its ever rising importance as an engineering subject, especially since 9/11 attack [1]. The chapter then introduced the increasing popularity of using gypsum boards as compartmentation devices [2]. The reason behind the increasing popularity is the positive traits gypsum boards possess such as high strength-to-weight ratio, easy installation and high thermal insulation. In practice, gypsum boards are usually framed with steel studs inside to form gypsum board wall assemblies with or without insulation in the cavity [2]. ASTM E119 was introduced as the standard document for fire tests of building materials or structural elements for their FRR assessment in the US [3].

The chapter went on to explain the objective of the dissertation. The goal was to use verified numerical simulation methodology of existing fire tests of gypsum board wall assemblies to simulate the fire test of the new wall assembly. The outline of the dissertation was subsequently given.

Chapter 2 gave one set of existing fire tests of a non-load-bearing gypsum board wall assembly. Manzello [4] did a series of fire tests to test the FRR of one specific non-load-bearing gypsum board wall assembly in both the US and Japan. All the fire tests were supposed to be identical. They recorded the temperature on the unexposed side of the gypsum boards but did not record the mechanical response of the gypsum board at all. The author of this study was able to numerically simulate the fire test of the non-load-bearing gypsum board wall assembly and was able to obtain numerical results very similar to Manzello's experimental results, by adjusting the reported thermal properties of the gypsum boards and using creative heat transfer techniques. Therefore, the thermal modeling methodology was verified.

Chapter 3 introduced another set of existing fire tests of a load-bearing gypsum board wall assembly. Kolarkar [2] peformed numerous fire tests of different gypsum board wall assemblies with varying parameters such

as the thickness, the number of layers and the types of the gypsum boards. Kolarkar [2] also did fire tests for both non-load-bearing and load-bearing gypsum board wall assemblies. The author of this study numerically simulated one of the load-bearing gypsum board wall assemblies, and again was able to obtain very similar numerical results against Kolarkar's experimental results by using selected parameters. The selected parameters included the mechanical properties of the steel studs, the boundary conditions and the magnitude of imperfection assigned to the steel studs. The author also investigated the importance of the stiffness provided by the gypsum boards and the effect of nailing spacing between the gypsum boards and the studs. The mechanical modeling methodology was thus also verified.

In Chapter 4, after the verification of both the thermal and mechanical modeling methodology, the author simulated the standard fire test of the new composite steel-EPS gypsum board wall assembly. The author was able to obtain the numerically simulated temperature and deflection of the wall assembly at various locations. A detailed discussion section was given on the simulated results. The ultimate failure loads of the new gypsum board wall assemblies with single, double and triple layers of gypsum boards were deduced at 1, 2 and 3 hours of the fire test.

5.2 Conclusion

Chapter 2 drew several conclusions regarding the simulation of fire tests of non-load-bearing gypsum board wall assemblies. The thermal conductivity and specific heat of gypsum boards in numerical simulation can and will always be different from measured values via experiments. The reported thermal conductivity by Manzello was only measured after the gypsum board was dehydrated unlike the condition in the fire tests, during which the majority of the thermal insulation effect takes place between 100 C and 200 C when gypsum boards lose chemically bound water. In addition, several other factors, such as the migration of water vapor, also could potentially change the thermal properties of gypsum boards in the fire tests. By adjusting the specific heat alone, it is possible to achieve numerical results that are very similar to the experimental ones, which results in a plausible thermal modeling methodology. The integrated specific heat across the temperature domain is the enthalpy of the gypsum board and thus cannot be changed due to conservation of energy.

Chapter 3 introduced the simulation of one existing fire test of one specific non-load-bearing gypsum board wall assembly. Gypsum boards provided little stiffness to the steel stud in the fire test performed by Kolarkar. The numerical results were very similar with or without the stiffness added by the gypsum boards. Gypsum boards did

however function as a bracing device to keep the steel stud from global buckling. The magnitude of imperfection could significantly affect the load carrying capacity of the steel studs in vertical loading test at ambient temperature, according to the simulated numerical results. However, the magnitude of imperfection did not affect the overall responses of the stud as much in the fire test where thermal bowing and thermal degradation of the steel stud were the major contributors to the time of failure. The spacing of the nails connecting gypsum boards with steel studs had only a minor effect on the overall response of the steel stud in both ambient and fire tests, given if the spacing was 100 mm or less. The right combination of different parameters inputted into the numerical model can generate the desired numerical results. The study achieved an implementable numerical simulation methodology for mechanical analysis of gypsum board wall assemblies.

A numerical simulation of the new composite steel-EPS gypsum board wall assembly was introduced in Chapter 4. Gypsum boards had a very significant thermal insulation effect on the wall assembly due to their low thermal conductivity and absorption of heat during the release and vaporization of chemically bound water. EPS, due to its low thermal conductivity and heat absorption when being melted away, also effectively slowed down the temperature rise of the wall assembly. Even with only one layer of gypsum board as insulation, the temperature of the wall assembly was not high enough to melt away the phenolic resin bracing after 3 hours of fire. Different stud sizes and unbraced lengths could greatly influence the load carrying capacity of wall assemblies.

5.3 Future Work

Regarding future work, a list of studies or improvements can be done.

1. More numerical simulations should be conducted on other existing fire tests of non-load-bearing and load-bearing gypsum board wall assemblies. This would further verify the numerical modeling methodology by comparing numerical results with experimental results.

2. More numerical simulations should also be done on a variety of the new composite steel-EPS gypsum board wall assemblies. Varying parameters, such as the thickness of the composite insulation, the size and type of the steel studs and different types and number of layers of gypsum boards, should be considered.

3. Fire tests should be done on the new composite steel-EPS gypsum board wall assemblies to verify the numerical simulation methodology.

5.4 References

[1]. Hamilton, R. Scott, Performance-based Fire Engineering for Steel Framed Structures: a Probabilistic Methodology, 2011

[2]. Kolarkar, Prakash, Structural and Thermal Performance of Cold-formed Steel Stud Wall Systems under Fire Conditions, 2010

[3]. ASTM E 119-16: "Standard Test Methods for Fire Tests of Building Construction Materials," ASTM International, West Conshohocken, PA, 20162

[4]. Manzello, Samuel, et al., Furnace Testing of Full-scale Gypsum Steel Stud Non-load-bearing Wall Assemblies: Results of Multi-laboratory Testing in Canada, Japan and USA, 2009

Appendix A   Verification of Heat Transfer in ABAQUS

The following content gives the theoretical results vs numerical results in ABAQUS for the three basic forms of heat transfer: conduction, convection and radiation. All three forms of heat transfer require a temperature difference. It is worth noting that only one dimensional thermal analysis verification is given in this appendix because only one dimensional heat transfer was assumed to take place in the thermal analysis of the gypsum board wall assemblies.

The first three sections of the appendix give the verification of numerical results against theoretical results for steady state heat transfer analysis of conduction, convection and radiation. Steady state heat transfer takes place when the temperature at any point of the system doesn't change with time. The last section of the appendix gives the verification of numerical results against theoretical results for transient convective heat transfer analysis. It is worth noting that the model of the 1D heat transfer analysis was modeled in 3D with DC3D8 elements in ABAQUS. Heat was assumed to only transfer in the longitudinal direction of the models given in this Appendix, as no temperature difference existed in the other two dimensions.

A1 Steady State Conductive Heat Transfer in 1D

Heat transfer can take place in the form of thermal conduction. Conduction is the transfer of energy from the more energetic particles of a substance to the adjacent, less energetic ones as a result of interactions between the particles. In the case presented here, a block with the dimension of 1 m X 1 m X 20 m was analyzed. The temperature on one side of the block was 100 C and on the other side was 0 C. The material properties of the block were chosen as such: 1 W/m*K for thermal conductivity, 1000 kg/m^3 for density and 1000 J/kg*C for specific heat. The model and its boundary conditions for temperature are shown in Figure A1.
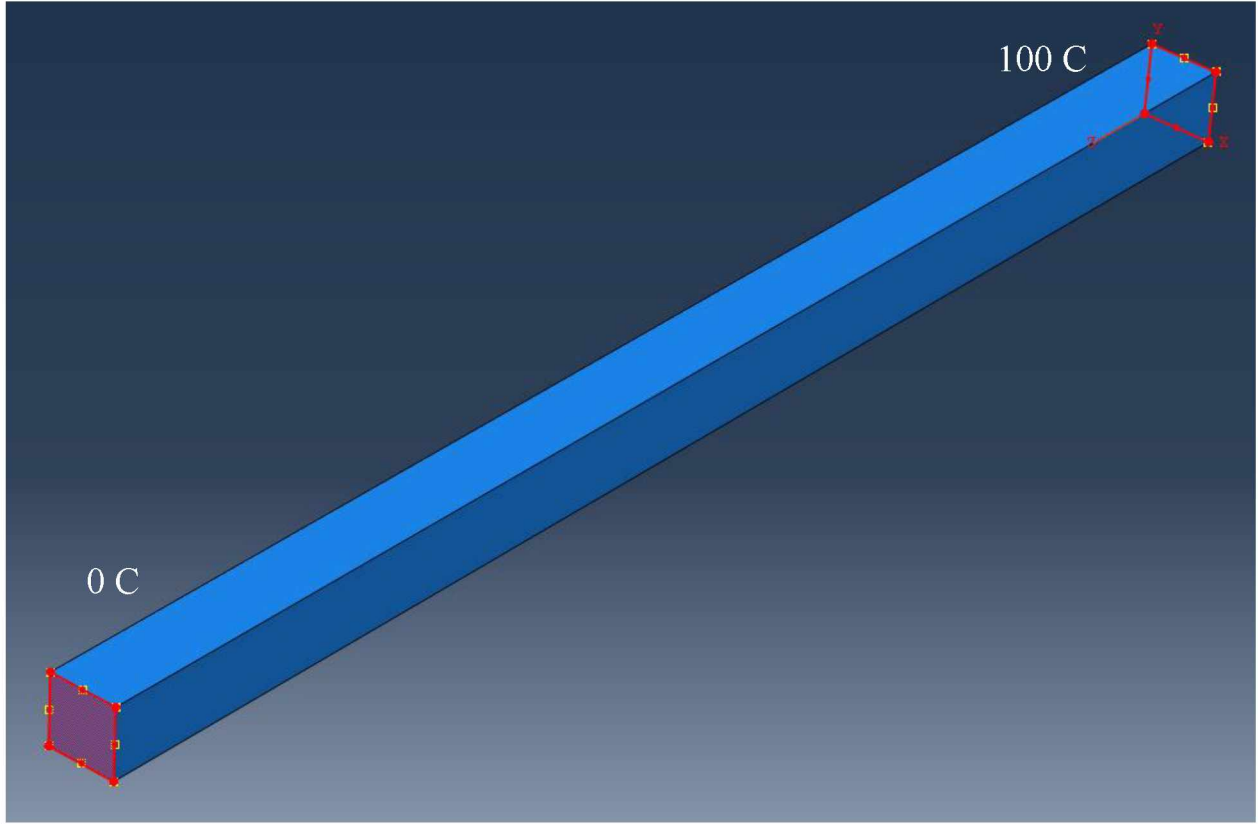
Figure A1: Thermal conduction model with boundary conditions

The theoretical heat flux for steady state heat flux can be calculated by Equation A1.

$$q = k * dT/dL = 1W/(m*K) * (100C - 0C)/20m = 5W/m^2 \quad \text{(A1)}$$

Figure A2 shows the numerical results for the heat influx of the model and Figure A3 shows the numerical results for temperature gradient. It can be observed that the theoretical results for steady state heat flux and numerical results calculated by ABAQUS are identical. The model consisted of 2,025 nodes and 1,280 elements with the typical element size 0.25 m X 0.25 m X 0.25 m. The total elapsed time for the analysis was 4 s.
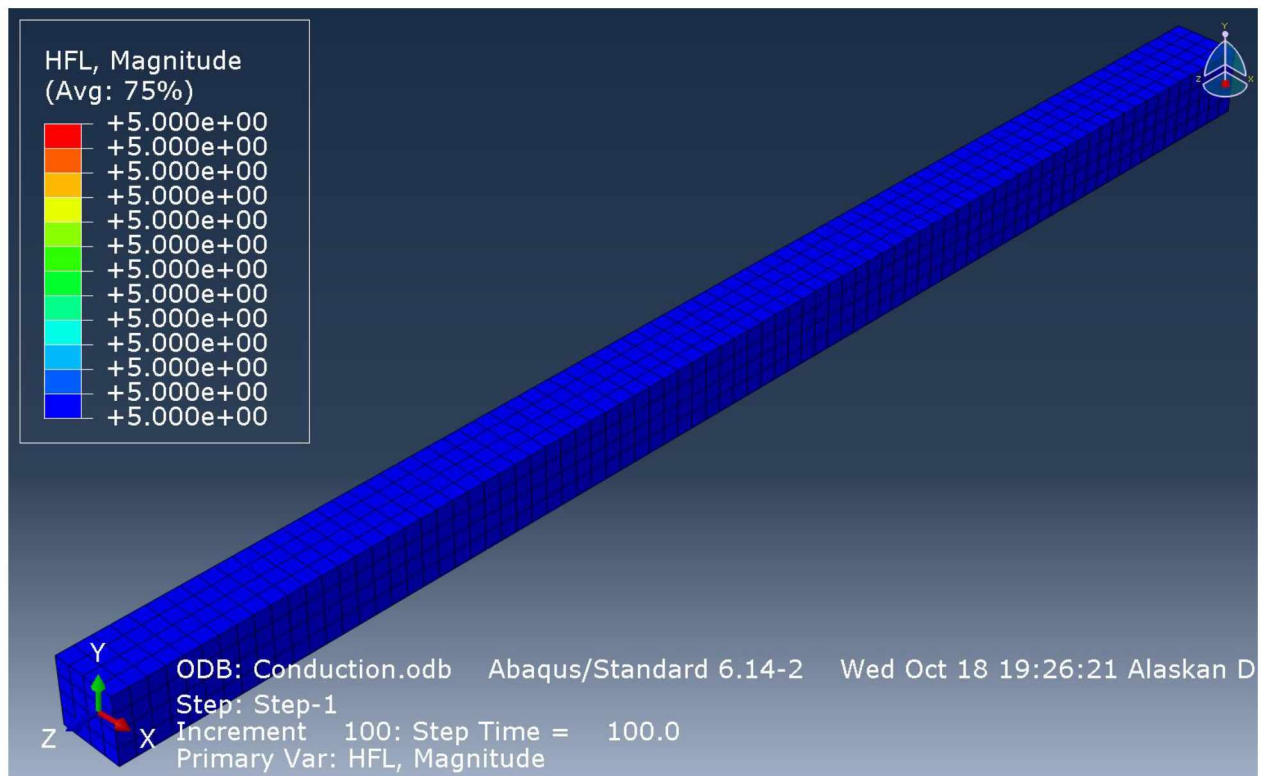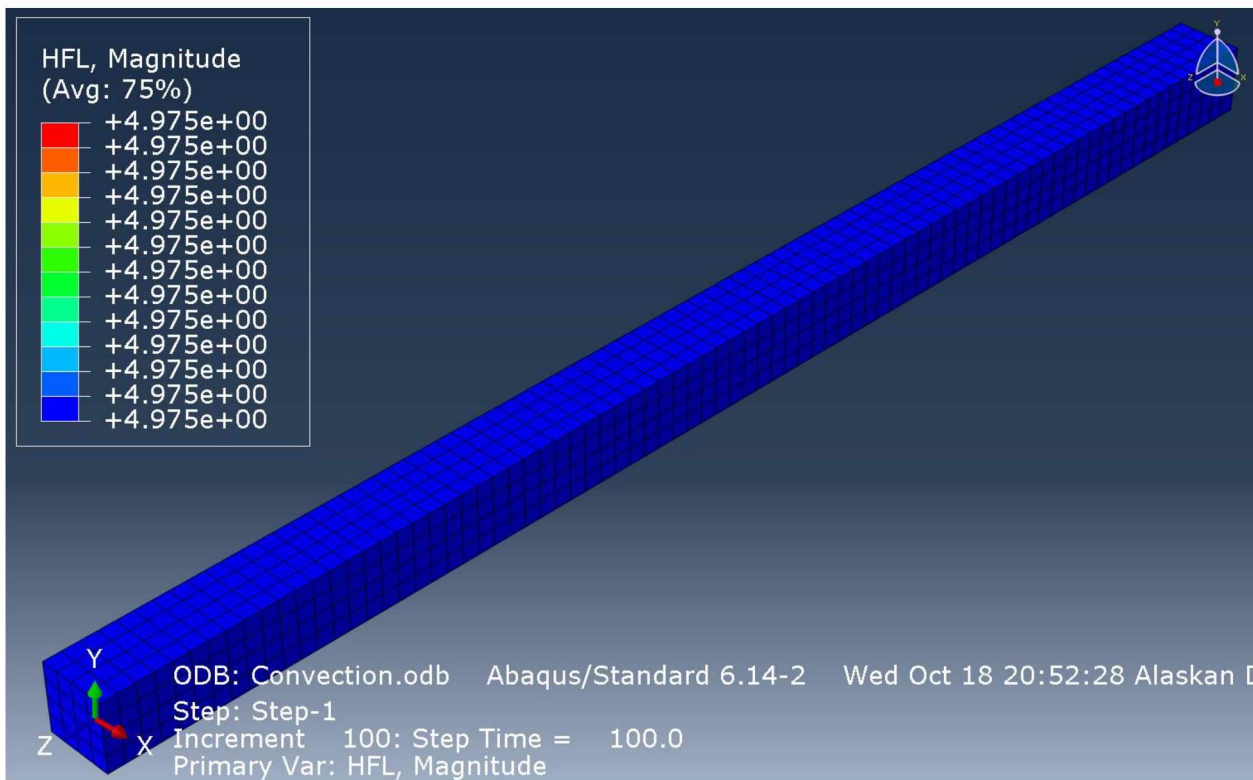
Figure A2: Numerical results of heat flux for the modeled thermal conduction
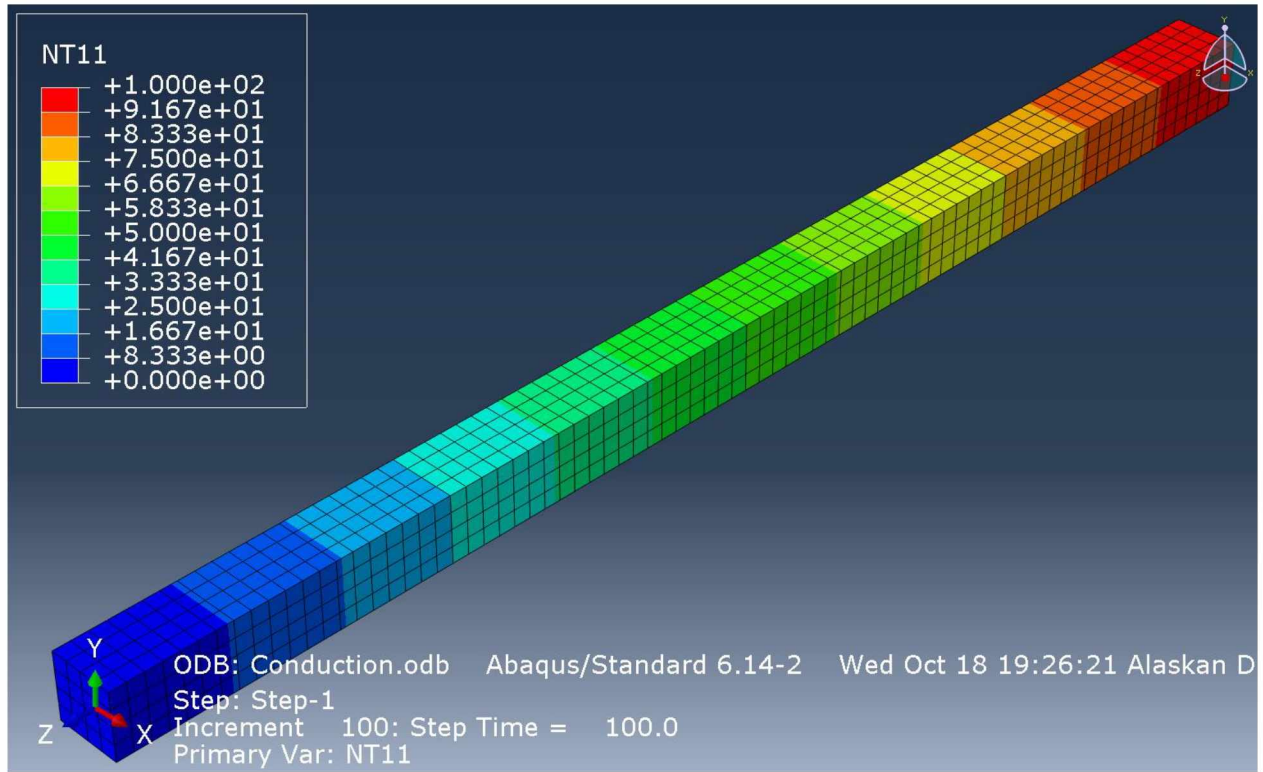
Figure A3: Numerical results of temperature gradient for the modeled thermal conduction

A2 Steady State Convective Heat Transfer in 1D

Convection is the mode of energy transfer between a solid surface and the adjacent liquid or gas that is in motion, and it involves the combined effects of conduction and fluid motion [18]. Despite the complexity regarding thermal convection, the rate of convective heat transfer is observed to be proportional to the temperature difference. The rate of heat transfer is conveniently expressed by Newton's law of cooling as given by Equation A2, where h is the convective heat transfer coefficient, T_s is the surface temperature and T_a is the ambient temperature. In the case analyzed here, the convective heat transfer model is exactly the same as the thermal conduction model with the same material properties. However, the boundary conditions are different. The temperature at one end stays at 0 C, and the other end is exposed to an ambient temperature of 100 C with a heat transfer coefficient of 10 W/m^2*K. The model is given in Figure A4. The numerical result for the heat flux is shown in Figure A5, and the numerical result for the temperature gradient is shown in Figure A6.
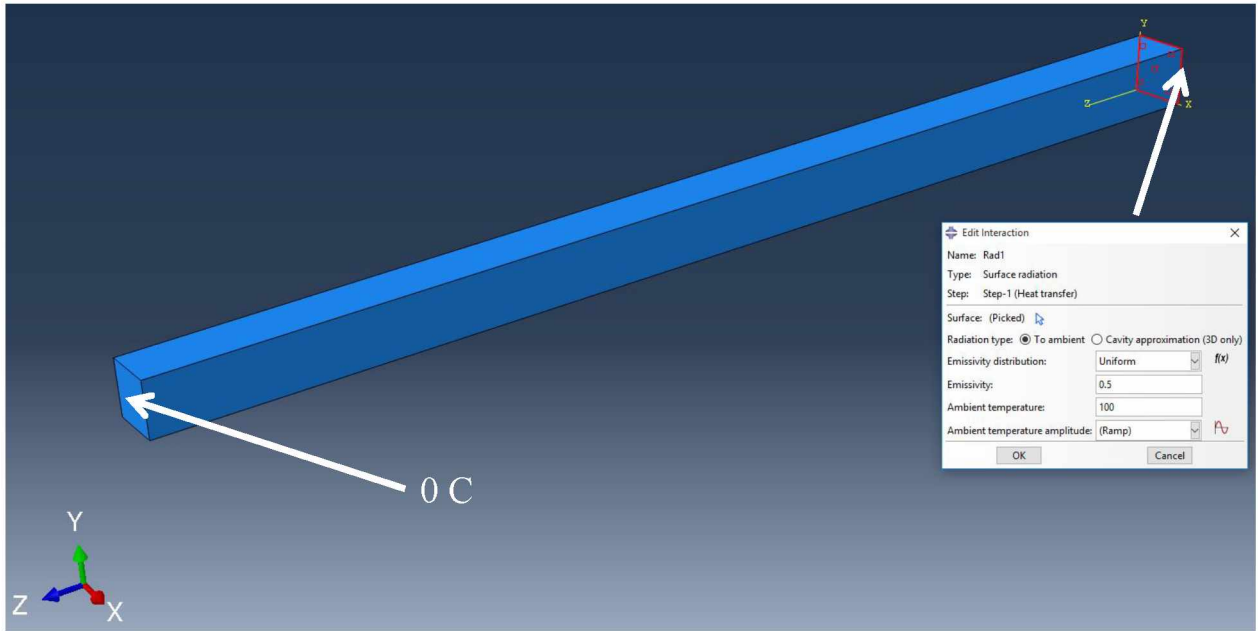
$$q = h * (T_s - T_a)$$ (A2)
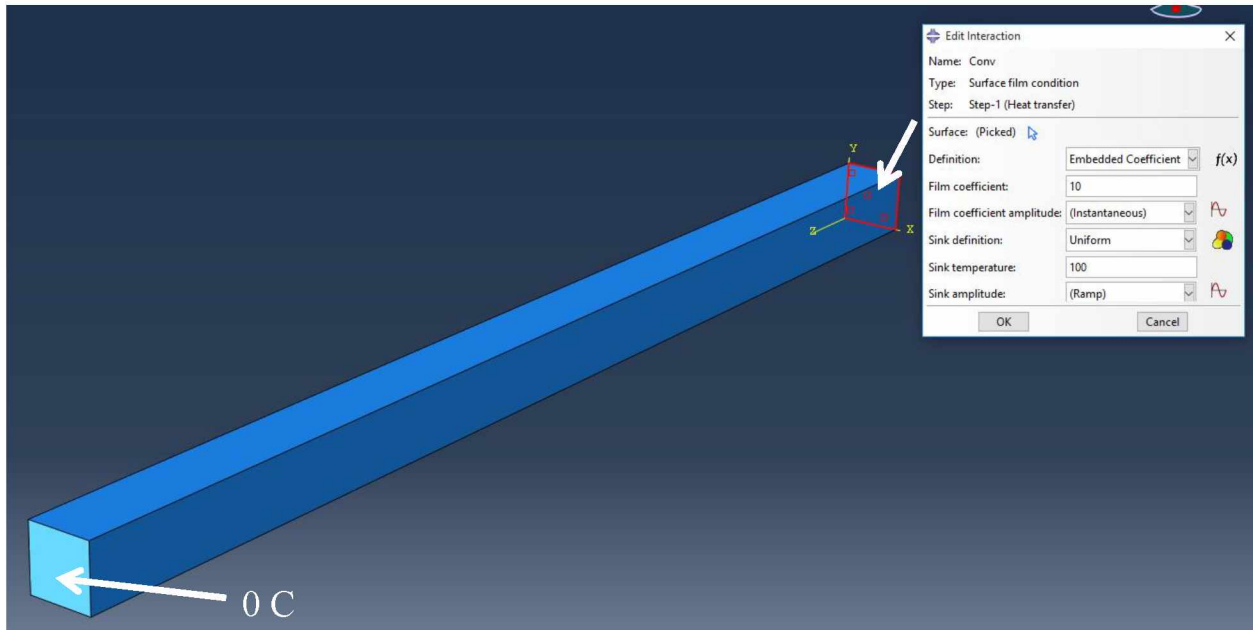
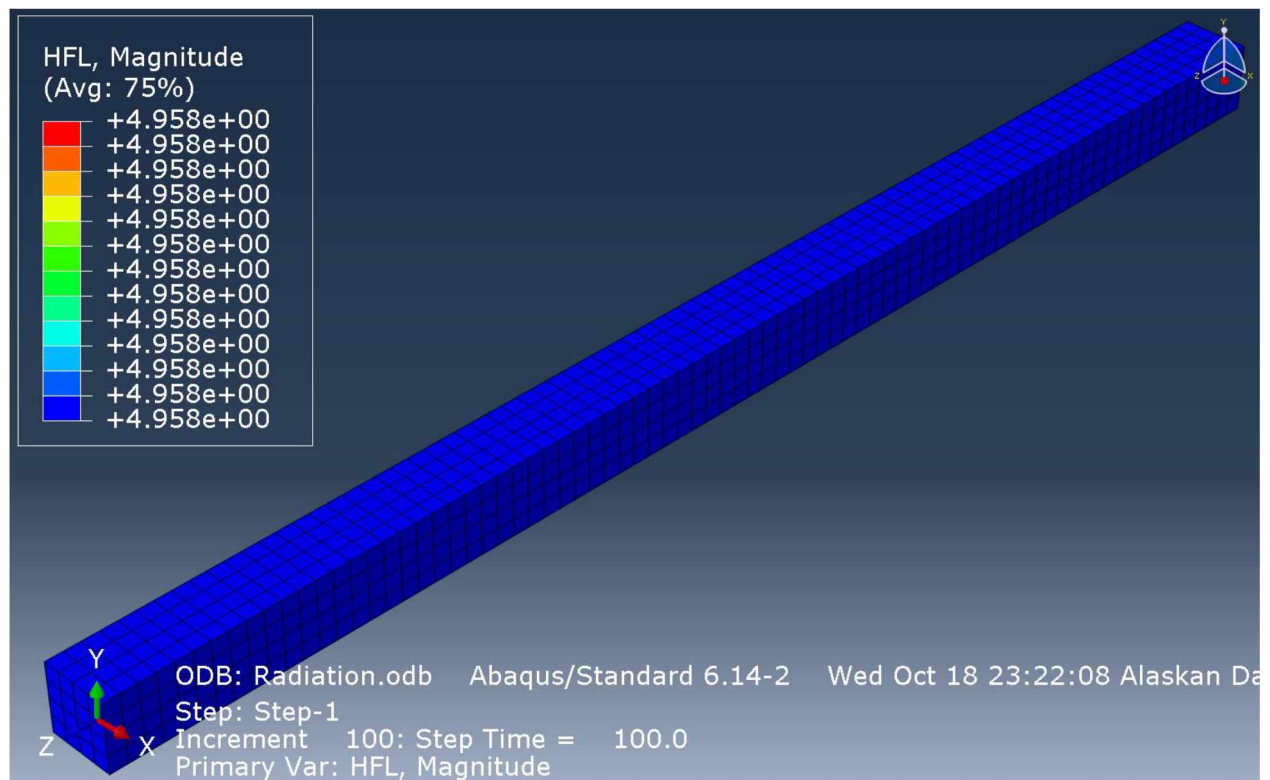Figure A4: Thermal convection model with boundary conditions

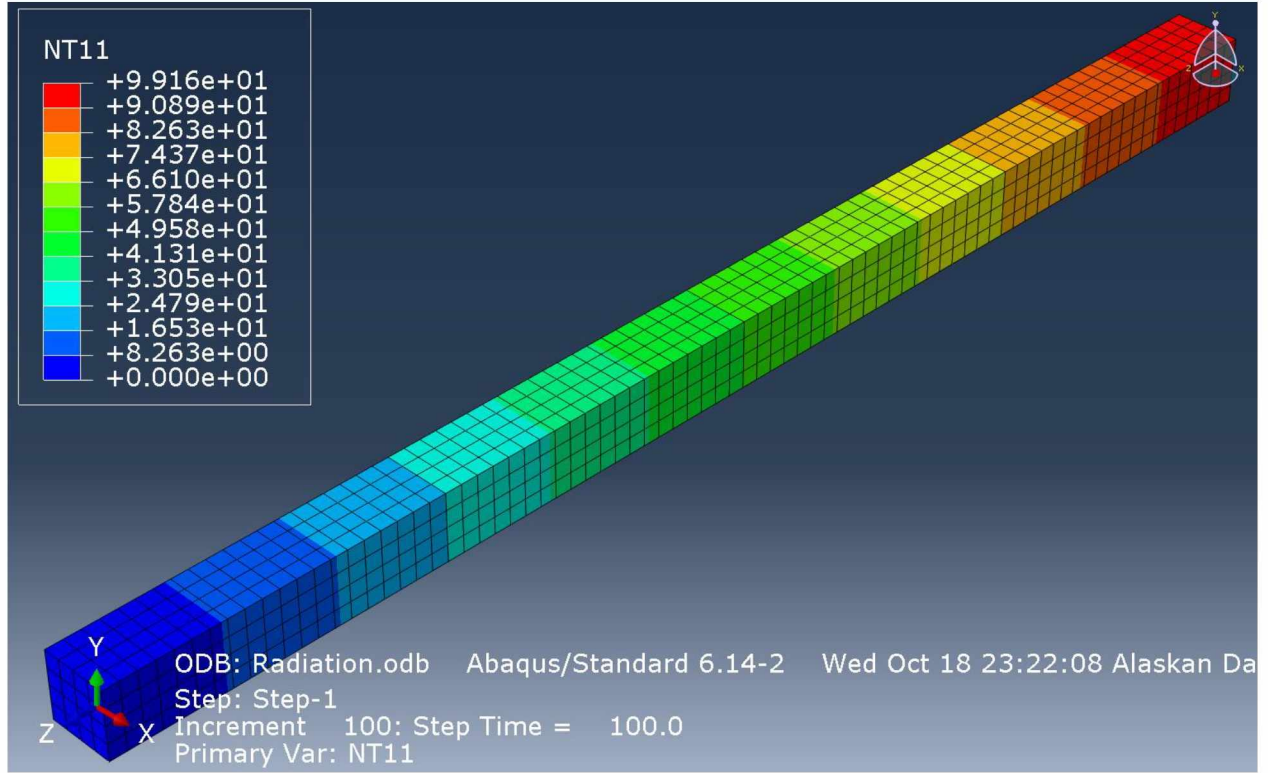Figure A5: Numerical results of heat flux for the modeled thermal convection
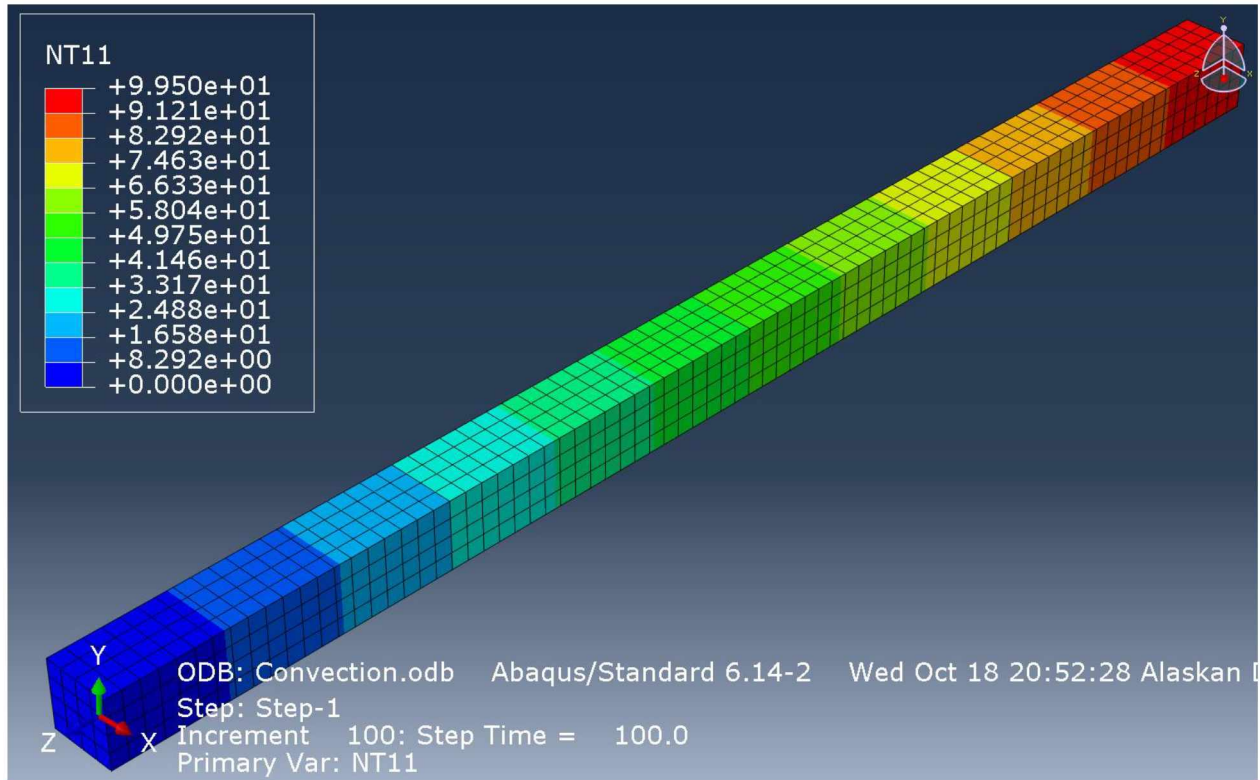
Figure A6: Numerical results of temperature gradient for the modeled thermal convection

The theoretical heat flux, calculated by Equation A3, resulted in the steady state surface temperature of 99.5025 C. The theoretical heat flux coincides with the numerical heat flux calculated from ABAQUS. The model consisted of 2,025 nodes and 1,280 elements with the typical element size 0.25 m X 0.25 m X 0.25 m. The total elapsed time for the analysis was 4 s.

$$q = h * (T_a - T_s) = 10 \left(\frac{W}{m^2} * K \right) * (100 \, C - 99.5025 \, C) = 4.975 \, W/m^2$$

(A3)

A3 Steady state radiative heat transfer in 1D

Radiation is the energy emitted by matter in the form of electromagnetic waves as a result of the changes in the electronic configurations of the atoms or molecules. Radiation is usually considered a surface phenomenon. When a surface of emissivity ε is enclosed by a much larger surface at thermodynamic temperature T_a and separated by a fluid, the net rate of radiative heat flux between these two surfaces is given by

$$q = \varepsilon\sigma(T_s^4 - T_a^4) \tag{A4}$$

where ε is the surface emissivity, σ = 5.670 E-8 W/m^2*K^4 is the Stefan-Boltzmann constant, T_s is the surface

temperature and T_a is the ambient temperature. The model used for this radiative heat transfer analysis was again the

same as the previous two models. The radiative heat transfer model had a temperature of 0 C at one end and a

temperature of 100 C at the other end, with 0.5 as the surface emissivity. Figure A7 shows the model in ABAQUS.

Figure A8 shows the numerical results for heat flux, and Figure A9 shows the numerical results for the temperature

gradient.

Figure A7: Thermal radiation model with boundary conditions

Figure A8: Numerical results of heat flux for the modeled thermal radiation

NT11
+9.916e+01
+9.089e+01
+8.263e+01
+7.437e+01
+6.610e+01
+5.784e+01
+4.958e+01
+4.131e+01
+3.305e+01
+2.479e+01
+1.653e+01
+8.263e+00
+0.000e+00

ODB: Radiation.odb   Abaqus/Standard 6.14-2   Wed Oct 18 23:22:08 Alaskan Da
Step: Step-1
Increment   100: Step Time =   100.0
Primary Var: NT11

Figure A9: Numerical results of temperature gradient for the modeled thermal radiation

The theoretical radiation heat flux can be calculated by Equation A5.

$$q = \varepsilon\sigma(T_s^4 - T_a^4) =$$

$$0.5 * 5.670E - \frac{8W}{m^2} * K^4 * \left[(100 + 273.15)K^4 - (99.1557 + 273.15)K^4\right] =$$

$$\frac{4.956W}{m^2} \tag{A5}$$

The result again coincides with the numerical heat flux. The model consisted of 2,025 nodes and 1,280 elements with the typical element size 0.25 m X 0.25 m X 0.25 m. The total elapsed time for the analysis was 4 s.

The second part of this appendix gives the validation of the numerical transient heat transfer analysis against theoretical transient heat transfer analysis. In steady state heat transfer analysis, thermal equilibrium is reached so temperature may vary at different locations but not with time. In transient heat transfer analysis, however, thermal equilibrium is not achieved and therefore temperature can change with locations and time. It is usually hard to analyze transient heat transfer because it involves solving partial differential equations which govern

125

the heat transfer mechanism. The independent variables are in dimensions (x, y and z) and in time (t), and the solution of the governing partial differential equations typically involves infinite series and transcendental equations. The section below demonstrates a 1D transient convective heat transfer analysis.

A4 Transient Convective Heat Transfer in 1D

Figure A10 shows a 1D plane wall with the thickness of *2L* and initial temperature T_i. At time *t=0*, the wall is immersed in a fluid at temperature T_a (ambient temperature) and is subjected to convective heat transfer from both sides with a convective coefficient of h. The height and the width of the wall are considered to be infinity. Therefore, the heat transfer can be modeled in 1D. Moreover, the model has thermal symmetry and the temperature gradient profile and heat flux profile must be symmetrical about the centerline, as shown in Figure A10. The problem can thus be simplified by reducing the wall thickness in half.
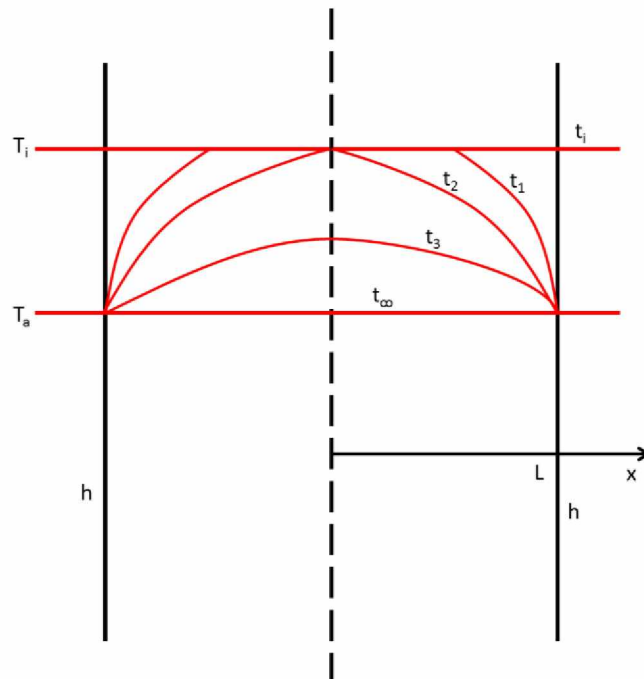
Figure A10: Transient heat transfer for a 1D plane wall

A4.1 Analytical Solution of the 1D Plane Wall Heat Transfer

The 1D transient convective heat transfer problem can be mathematically expressed by the following equations.

126

Differential equation:

$$\frac{d^2 T}{dx^2} = \left(\frac{1}{a}\right)\frac{dT}{dt} \tag{A7}$$

Boundary conditions:

$$\frac{dT(0,t)}{dx} = 0 \tag{A8}$$

$$-\frac{k\,dT(L,t)}{dx} = h\left[T(L,t) - T_a\right] \tag{A9}$$

Initial conditions:

$$T(x,0) = T_i \tag{A10}$$

where $a=k/(\rho * c_p)$ is the thermal diffusivity of the material. The density of the material ρ was chosen to be 1 kg/m³.

Equation A7 can be further simplified with dimensionless variables given below.

Dimensionless differential equation:

$$\frac{d\theta^2}{dX^2} = \frac{d\theta}{d\tau} \tag{A11}$$

Dimensionless boundary conditions:

$$\frac{d\theta(0,\tau)}{dX} = 0; \; \frac{d\theta(1,\tau)}{dX} = -Bi\theta(1,\tau) \tag{A12}$$

Dimensionless initial conditions:

$$\theta(X,0) = 1 \tag{A10}$$

Where:

$$\theta(X,\tau) = \frac{T(x,t) - T_a}{T_i - T_a} \tag{A11}$$

$$X = \frac{x}{L} \tag{A12}$$

$$Bi = \frac{hL}{k} \tag{A13}$$

$$\theta = \frac{\alpha t}{L^2} = Fo \tag{A14}$$

The solution of the problem has been solved and well documented and it takes the form as

$$\theta = \sum A_n e^{-\lambda_n \tau} \cos(\lambda_n X) \tag{A15}$$

Where:

$$A_n = 4 \frac{\sin(\lambda_n)}{2\lambda_n + \sin(2\lambda_n)} \tag{A16}$$

λ_n are the roots of $\lambda_n \tan(\lambda_n) = \text{Bi}$ (A17)

In this study, the variables are chosen as

$$L = 10 \, m \tag{A18}$$

$$0 \le t \le 10s \tag{A19}$$

$$h = 1 \, W/m^2 * K \tag{A20}$$

$$k = 1 \, W/m * K \tag{A21}$$

$$C_p = 1 \, J/kg * K \tag{A22}$$

$$T_i = 20 \, C \tag{A23}$$

$$T_a = 100 \, C \tag{A24}$$

$$Bi = \frac{hL}{k} = 10 \tag{A25}$$

Therefore, the analytical results of the problem can be calculated by inputting all the variables into the solution of the problem.

A4.2 Numerical Solution of the 1D Plane Wall Heat Transfer

The problem can also be solved numerically with finite difference method. The finite element scheme is written as

$$\frac{T\big(x(m+1),t(n)\big) + T\big(x(m-1),t(n)\big) - 2*T\big(x(m1),t(n)\big)}{dx^2} =$$

$$\frac{1}{a}\left(\frac{T\big(x(m),t(n+1)\big) - T\big(x(m),t(n)\big)}{dt}\right) \tag{A26}$$

$$T\big(x(m),t(n+1)\big) = a\frac{dt^2}{dx^2}\Big(T\big(x(m+1),t(n)\big) + T\big(x(m-1),t(n)\big) - 2T\big(x(m1),t(n)\big)\Big) +$$

$$T\big(x(m1),t(n)\big) \tag{A27}$$

$$\frac{T\big(x(1),t(n)\big) - T\big(x(0),t(n)\big)}{dx} = 0 \tag{A28}$$

$$T\big(x(1),t(n)\big) = T\big(x(0),t(n)\big) \tag{A29}$$

$$-k\frac{T\big(x(end),t(n)\big) - T\big(x(end-1),t(n)\big)}{dx} = h*\Big(T\big(x(end),t(n)\big) - Ta\Big) \tag{A30}$$

$$T\big(x(end),t(n)\big) = \frac{\frac{k}{dx*k}}{1+\frac{k}{dx*h}}T\big(x(end-1),t(n)\big) + \frac{Ta}{1+\frac{k}{dx*h}} \tag{A31}$$

$$T(x(m),0) = T_i \tag{A32}$$

The solution of the problem was calculated progressively with MATLAB.

A4.3 ABAQUS Simulation Results

The problem was also simulated in ABAQUS. The initial condition, boundary conditions and meshing are shown in Figure A11. It is worth noting that the model of the 1D plane wall, just like the models given in the previous section, was a 3D model in ABAQUS with thermal insulation and zero temperature difference in the other two dimensions. The heat could only flow in the longitudinal direction in the model. The model consisted of 12,221

nodes and 10,000 DC3D8 elements. The typical element size was 0.1 m X 0.1 m X 0.1 m. The elapsed time for the analysis was 15.7 s.
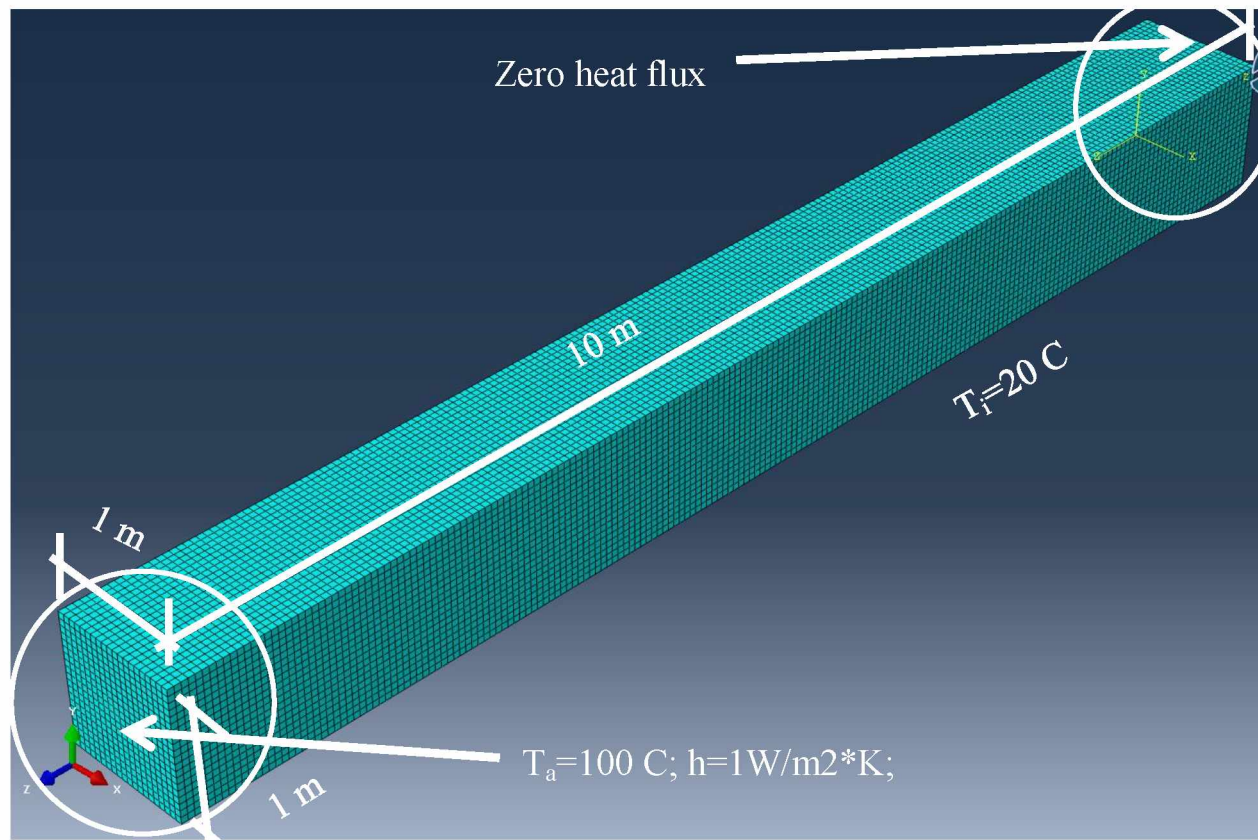
Figure A11: Initial conditions, boundary conditions and meshing of 1D plane wall

The results of analytical analysis, numerical analysis with finite difference method and ABAQUS simulation are shown in Figure A12. The results measured 10 s of simulation. It can be observed that the results from analytical analysis, numerical analysis with finite difference method and numerical simulation with ABAQUS are virtually identical.
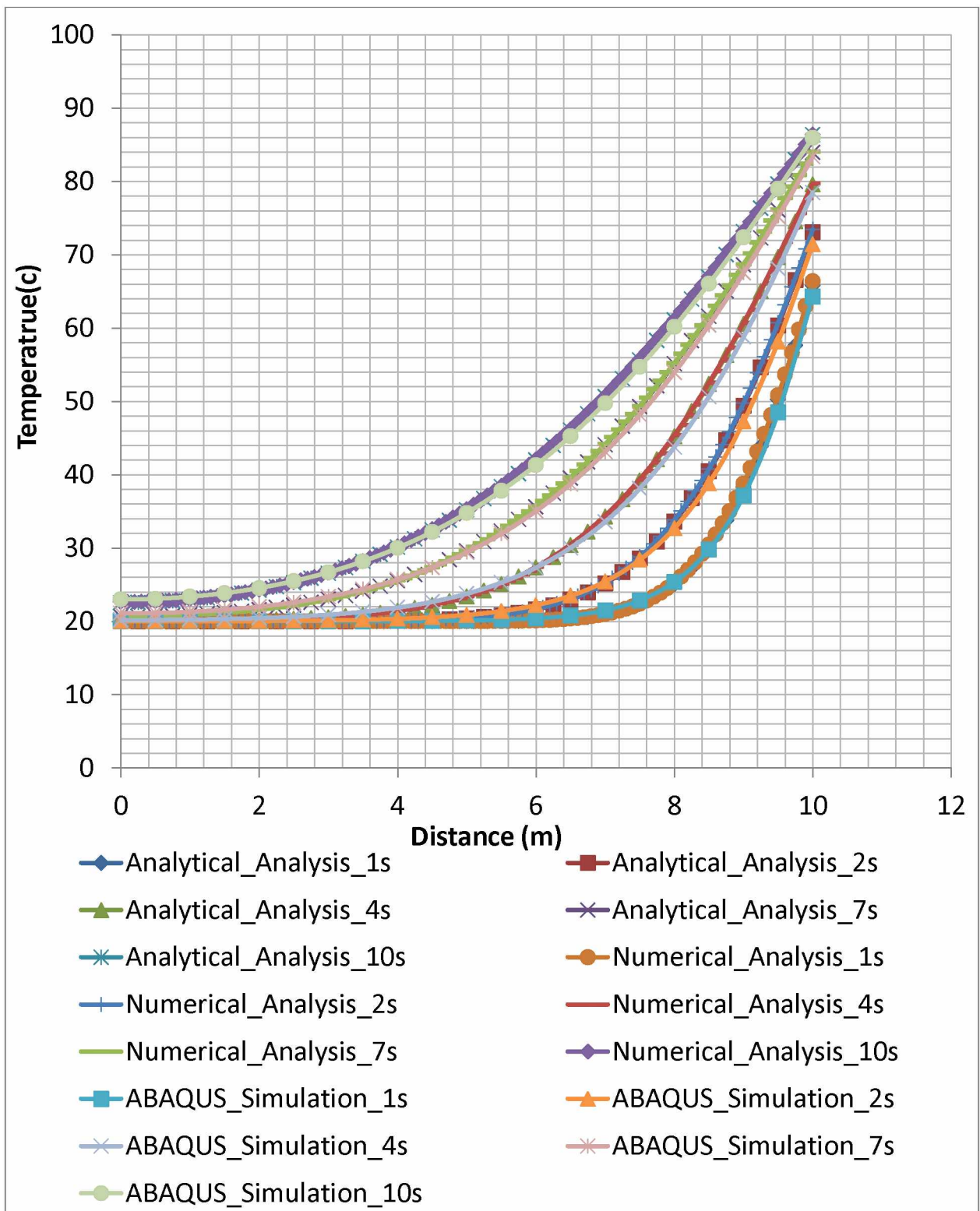
Figure A12: Analytical, numerical and ABAQUS simulated results of 1D plane wall

B1 Introduction

The following content gives the spring constant calculation of the stiffness provided by the gypsum boards in the y and z directions. It was assumed that the gypsum boards provided adequate restraint in the x direction. The demonstration of the spring stiffness provided by the gypsum boards to a stud is given in Figure B1.
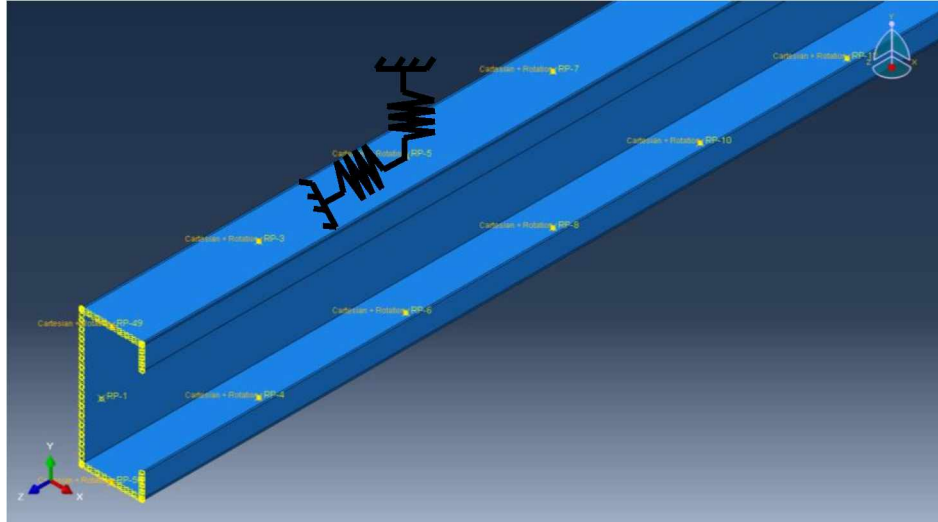
Figure B1: Steel stud strengthened by springs

B2 Spring Constant in the y Direction

The springs were further distributed evenly as elastic springs acting on a beam as shown in Figure B2 (left). The structure given in Figure B2 (left) should behave the same way as the steel stud, when stiffened by the tributary gypsum boards, should behave under the same uniformly distributed load, given in Figure B2 (right). The evenly distributed spring constant, k, in Figure B2 should follow Equation B1 with regard to each individual spring's constant, K_y.
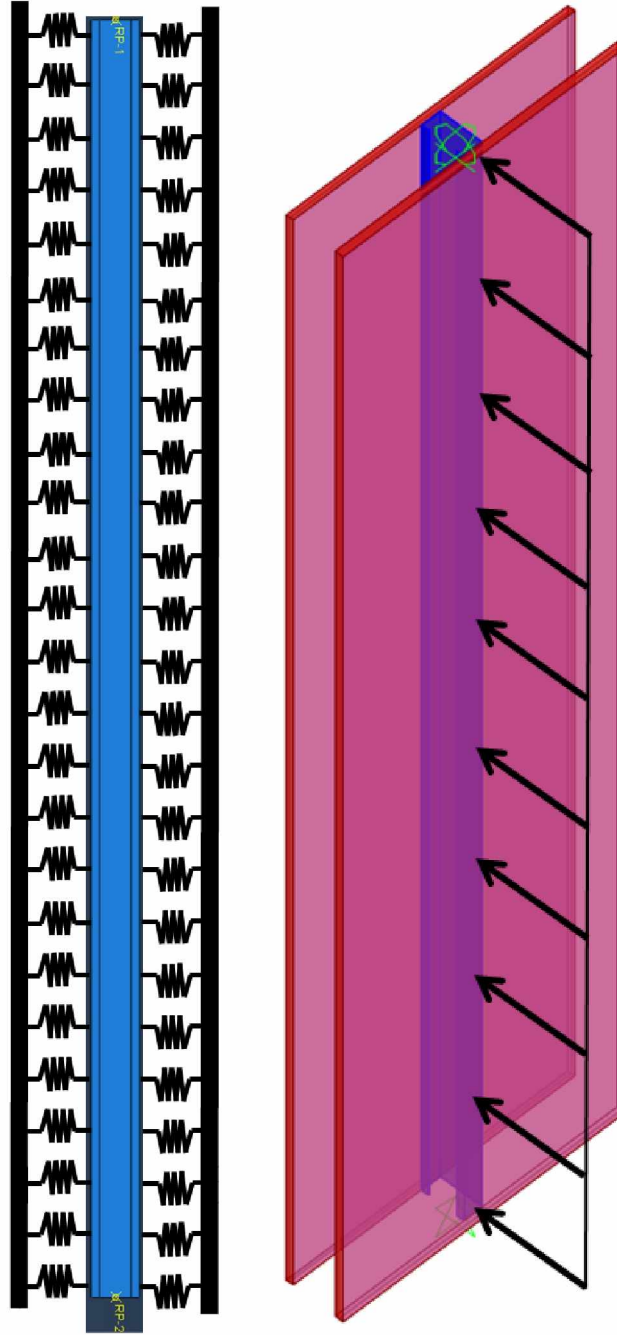
Figure B2: Steel stud stiffened by springs (left) and steel stud with tributary gypsum boards (right)

$$kL = K_y N \tag{B1}$$

Where:

K_y is the spring stiffness of a single spring element, provided by the gypsum boards;

k is the evenly distributed elastic spring constant representing the tributary gypsum boards; and

N is the number of springs representing screws on the studs; $N = 50$.

The cross section of the stud fastened with tributary gypsum boards is given in Figure B3 (a), and the transformed cross section for the stud with tributary gypsum boards is given in Figure B3 (b). The transformation of the section was based on the assumption that there was no relative movement between the stud and the gypsum boards. The Young's modulus of gypsum boards is only 0.2% of that of steel. 1.2 mm steel flanges were calculated by dividing the 600 mm wide gypsum boards by the ratio of the steel's Young's modulus to the gypsum board's Young's modulus. The transformed section in Figure B3 (b) uses two 1.2 mm thick steel flanges on top and bottom representing the 600 mm wide tributary gypsum boards.
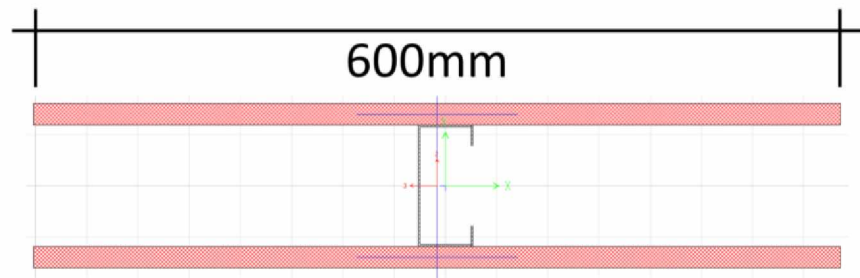
(a)
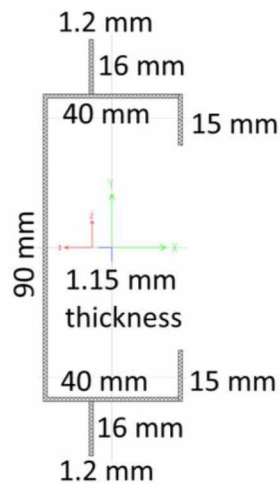
(b)

Figure B3: (a) Stud with tributary gypsum boards; (b) transformed section for the stud with tributary gypsum boards

The deflection of the transformed cross section given in Figure B3 (b) under a uniformly distributed load of 1000 N/m can be calculated by the following equation.

$$U_{mid} = \frac{5}{384}\frac{wL^4}{EI_t} = 0.0049 \, m \tag{B2}$$

Where:

U_{mid} is the deflection of the transformed cross section under the uniformly distributed load;

E is the measured Young's modulus for the steel stud, 214GPa;

w is the uniformly distributed load, 1000 N/m;

L is the height of the wall assembly, 2.4 m; and

I_t is the second moment of area of the transformed cross section given in Figure B3 (b) and is calculated in the following equation.

$$I_t = \left(\left(\frac{45^3*1.15}{12}\right) + 45*1.15*22.5^2\right) + \left(\left(\frac{40*1.15^3}{12}\right) + 40*1.15*40^2\right) +$$

$$\left(\left(\frac{15^3*1.15}{12}\right) + 15*1.15*37.5^2\right) + \left(\left(\frac{16^3*1.2}{12}\right) + 16*1.2*53^2\right) = 4.1402e-$$

$$07 \, m^4 \tag{B3}$$

The steel stud stiffened by linear springs in Figure B2 (left) should have the same deflection as the steel stud with tributary gypsum boards in Figure B3 (right). The governing differential equation for a beam on linear elastic foundation in Figure B4 is given by Equation B4 [1].
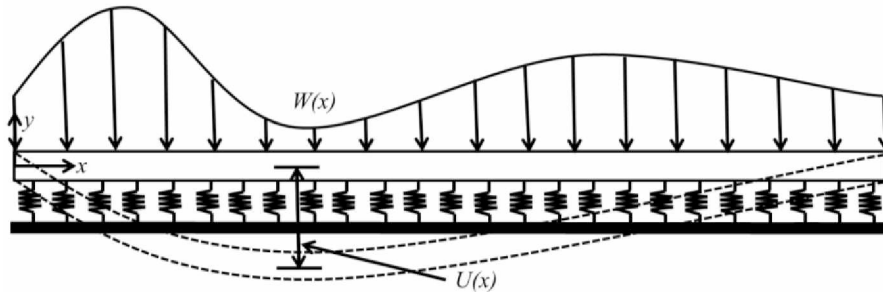
Figure B4: A beam on linear elastic foundation

$$EI\frac{d^4U(x)}{dx^4} + kU(x) = w(x) \tag{B4}$$

Where:

$U(x)$ is the deflection of the beam under the distributed load;

E is the measured Young's modulus of steel stud, 214 GPa;

$w(x)$ is the distributed load;

k is the spring constant for the elastic foundation;

L is the length of the beam, 2.4 m in this case; and

I is the second moment of area of the beam resting on the elastic foundation.

The beam in this case is the steel stud given in Figure B1. The second moment of area of the steel stud is calculated in the following equation.

$$I = \left(\left(\frac{45^3 * 1.15}{12}\right) + 45 * 1.15 * 22.5^2\right) + \left(\left(\frac{40 * 1.15^3}{12}\right) + 40 * 1.15 * 40^2\right) +$$

$$\left(\left(\frac{15^3 * 1.15}{12}\right) + 15 * 1.15 * 37.5^2\right) = 3.0534e - 07 \ m^4 \tag{B5}$$

The solution of the governing differential equation (Equation B4) with the uniformly distributed load w is given in the following equations.

$$U(x) = e^{ax}(C_1 sinax + C_2 cosax) + e^{-ax}(C_3 sinax + C_4 cosax) + \frac{w}{k} \tag{B6}$$

$$a = \left(\frac{k}{4EI}\right)^{\frac{1}{4}} \tag{B7}$$

The chosen boundary conditions of the differential equation in this case are expressed by the following equations.

$$U(0) = 0; U(L) = 0; \frac{d^2U}{dx^2}(0) = 0; \frac{d^2U}{dx^2}(L) = 0; \tag{B8}$$

The equations given above represent a pinned-pinned boundary condition. Equations B6 and B7 can be solved with boundary conditions (B8), the uniformly distributed load w and a given spring constant k. Table B1 gives the deflection of the stud at the mid-section with different spring constants under $w = 1000 \ N/m$. The coefficients in Equation B6 are also given in Table B1.

Table B1: Deflection of the studs at the mid-section with different spring constants under 1000 N/m

k (N/m/m)	a	C1	C2	C3	C4	U_{mid} (m)
1000	0.2487	-0.1398	-0.3426	-0.1398	-0.6574	0.0066
10000	0.4423	-0.0207	-0.0198	-0.0207	-0.0802	0.0063
65000	0.7062	-0.0028	-1.71E-04	-0.0028	-0.0152	0.0049
100000	0.7865	-0.0015	-2.61E-04	-0.0015	-0.0103	0.0043

Therefore, the linear elastic spring constant was calculated to be 65000 N/m/m and K_y was calculated to be 3120 N/m (20 lbs/in) according to Equation B1. In the study, K_y was conservatively chosen to be 3500 N/m.

B3 Spring Constant in the z Direction

It was assumed that the two gypsum boards acted like a column under compressive load, and the nails provided adequate restraint to prevent any movement between the gypsum boards and the steel studs. The stiffness provided by the gypsum boards is demonstrate in Figure B5 and calculated with Equation B9.
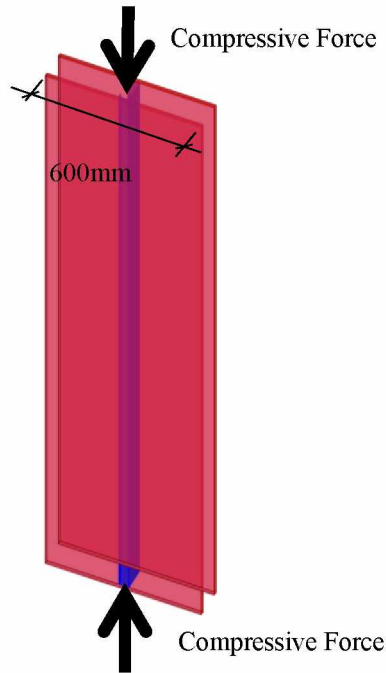
Figure B5: Demonstration of stiffness provided by gypsum boards in the z direction

$$K_z = \frac{EA}{NL} = 76{,}800 \frac{N}{m} = 438 \; lbs/in \tag{B9}$$

Where:

K_z is the spring stiffness provided by the gypsum boards;

E is the Young's modulus of the gypsum boards, 480MPa;

N is the number of springs representing screws on the studs; $N = 50$;

L is the height of the wall assembly, 2.4 m; and

A is the cross section area of the two tributary gypsum boards and is calculated as such:

$$A = 2bh = 0.0192 m^2 \tag{B10}$$

Where:

b is the width of the gypsum boards, 600 mm, as shown in Figure B5;

h is the thickness of the gypsum boards, 16 mm.

However, the individual springs created numerical instability due to large local nonlinear deflection. To solve this problem, the spring constants in both the y and z directions were evenly distributed at 9 locations, as given in Figure B6.

It can be seen that each sub-spring was assigned with the spring constants k_y and k_z and given in Equations B11 and B12.
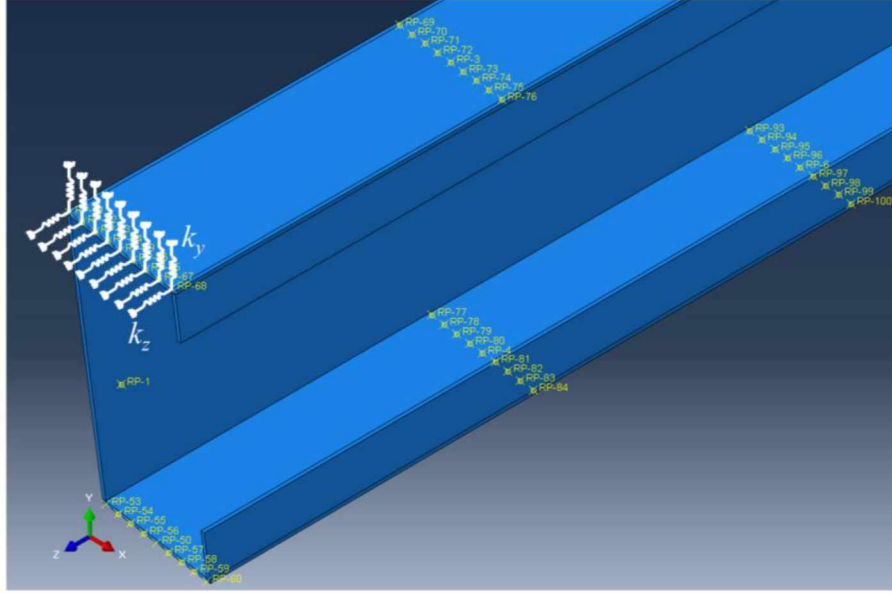
Figure B6: Distribution of spring constants at each screw location

$$k_y = \frac{K_y}{9} = 350 \ N/m \tag{B11}$$

$$k_z = \frac{K_z}{9} = 9000 \ N/m \tag{B12}$$

References

[1]. Hetenyi, M. Beams on Elastic Foundation. Waverly Press, Baltimore, 1946

Appendix C   Convergence Test Analysis

C1 Introduction

This appendix gives the convergence test of two 72 in long 362S162-33 cold-formed steel studs connected together. Each stud has an unbraced length of 72 in. Figure C1 gives the profile of a 362S162-33 steel stud.

Figure C1: 362S162-33 cold-formed steel stud

C2 Converge Test with Progressively Finer Meshing

A pair of connected 362S162-33 cold-formed steel studs was built in ABAQUS and given in Figure C2. The boundary conditions of the braced steel studs are given in Figure C3.
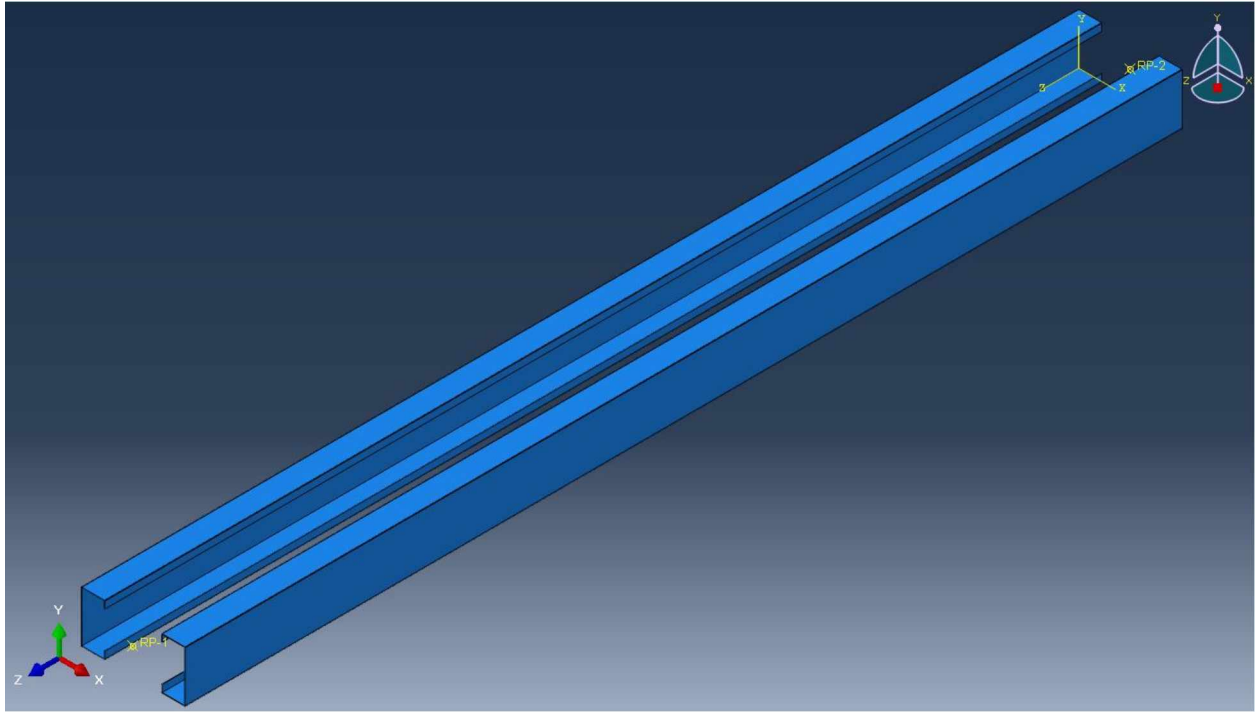
Figure C2: Two 72 in long 362S162-33 cold-formed steel studs connected together without lateral bracing
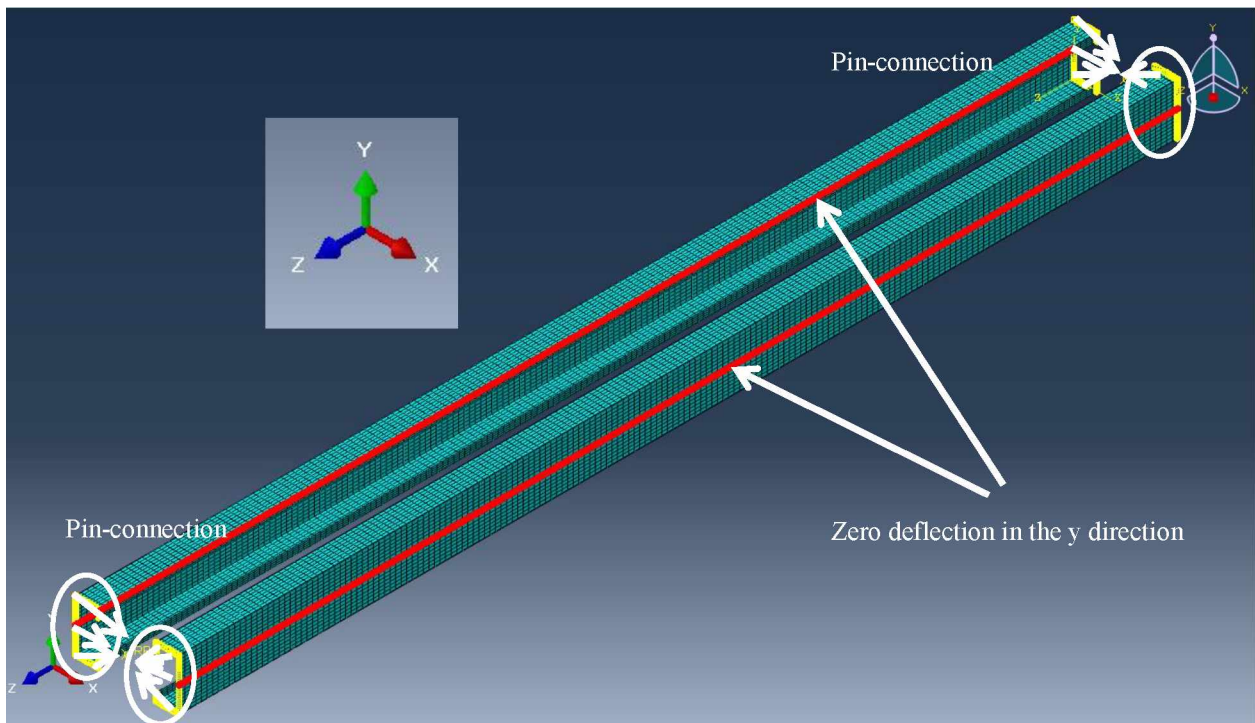
Figure C3: Boundary conditions of the two steel studs connected together

Figure C4 gives the first buckling load of the connected steel studs' vs the number of elements used, Figure C5 gives the load-deflection path of the non-linear analysis of the model under compressive load with 4 different numbers of elements and Figure C6 gives the failure load of the model vs the number of elements used. As shown in Figure C5, the failure load is the maximum load in the load-deflection path right before numerical bifurcation, at the moment the connected steel studs buckle. All the elements were C3D20R. The elapsed times for different models with different sizes of elements are given in Table C1.
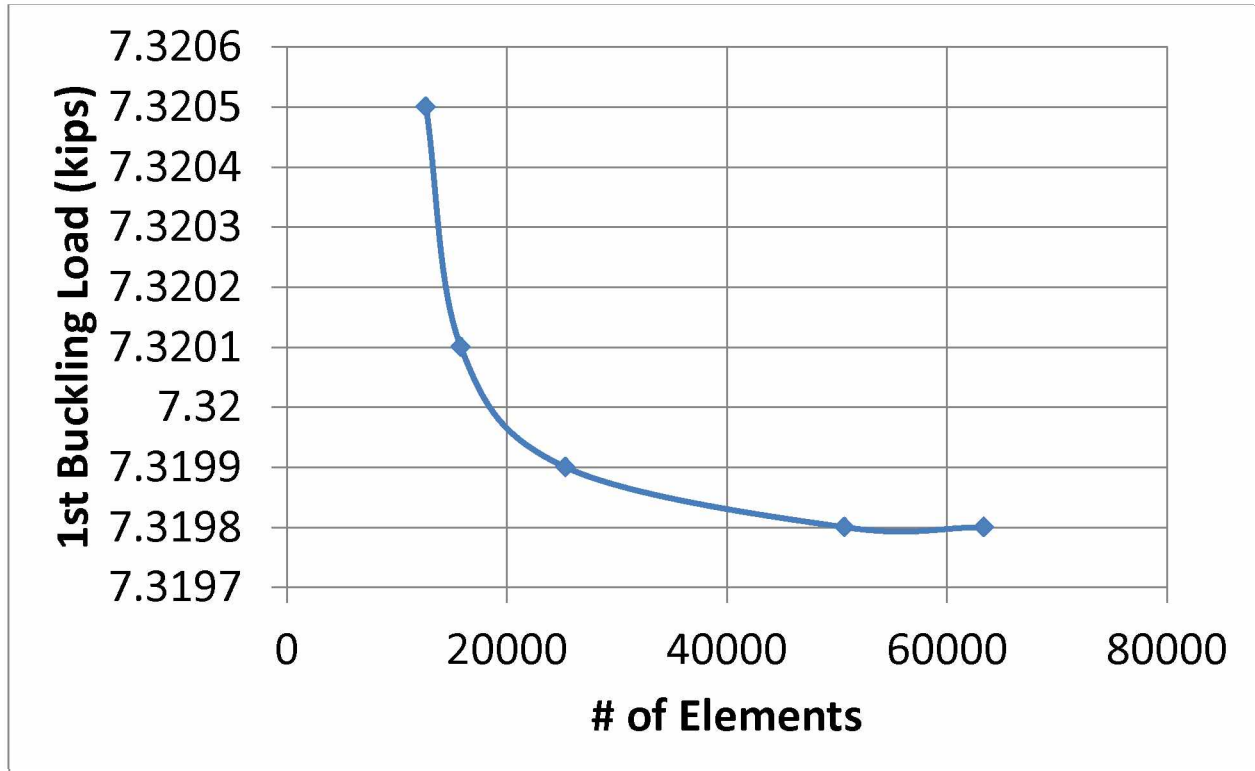
Figure C4: First buckling load of the two connected steel studs' vs number of elements
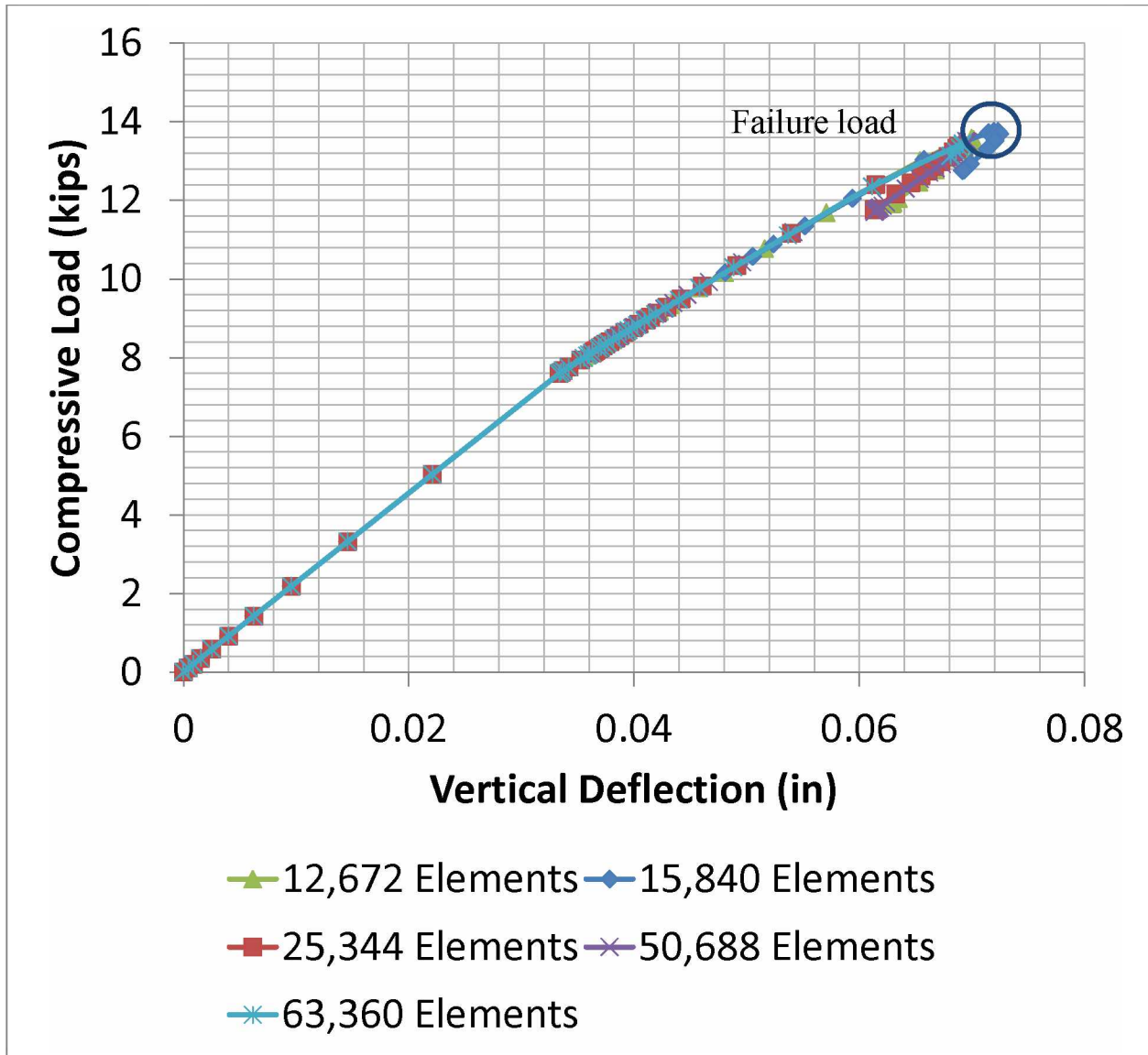
Figure C5: The loading path of the connected steel studs under compressive load with different numbers of elements
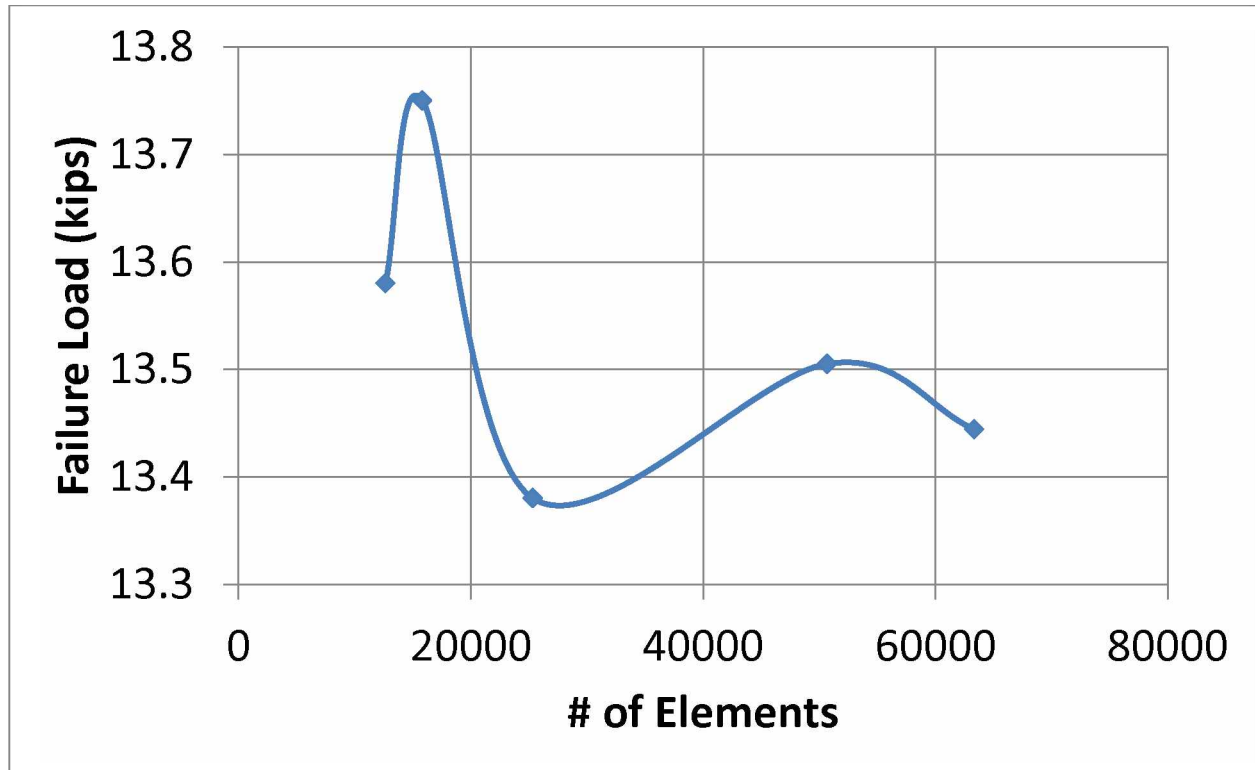
Figure C6: Failure load of the model vs number of elements

Table C1: Elapsed times of models with different sizes of elements

Number of Elements	Elapsed Time(s)
12672	2432
15840	3121.8
25344	6943.5
50688	12406
63360	13244

It can be seen in Figure C4 that the first buckling load of the model converged as the number of elements increased. Figure C5 demonstrates that, even as the number of elements increased, the failure load only varied slightly and the load-deflection paths were almost always identical. Figure C6 gives the oscillatory converging pattern of the failure load of the model as the number of elements increased.

Roache [1] proposed a new method for grid refinement studies. He introduced the concept of Grid Convergence Index (GCI) and used the following equations to study the convergence of a finite element model.

$$\epsilon = \frac{f_2 - f_1}{f_1} \tag{C1}$$

$$GCI(fine\ grid) = \frac{3|\epsilon|}{r^p - 1} \tag{C2}$$

$$GCI(coarse\ grid) = \frac{3|\epsilon|r^p}{r^p - 1} \tag{C3}$$

Where:

f_1 is the discrete numerical solution of fine grid;

f_2 is the discrete numerical solution of coarse grid;

r is the grid refinement ratio h_2/h_1 ;

h_1 is the typical spacing of fine grid;

h_2 is the typical spacing of coarse grid; and

p is the number of the order of the GCI method, e. g. $p = 1, 2, 3$, etc.

According to the numerical results given above, a GCI table is given in Table C2.

Table C2: GCI for two-362S162-33 steel stud-braced-together model

1st Buckling Load	Fine Grid GCI			Coarse Grid GCI		
p r	4	2	1.25	4	2	1.25
1	0.0096%	0.0246%	0.0656%	0.0383%	0.0492%	0.0820%
2	0.0019%	0.0082%	0.0291%	0.0306%	0.0328%	0.0455%
3	0.0005%	0.0035%	0.0172%	0.0291%	0.0281%	0.0336%
4	0.0001%	0.0016%	0.0114%	0.0288%	0.0262%	0.0278%
Failure Load	Fine Grid GCI			Coarse Grid GCI		
p r	4	2	1.25	4	2	1.25
1	0.5553%	4.4843%	14.8364%	2.2214%	8.9686%	18.5455%
2	0.1111%	1.4948%	6.5939%	1.7771%	5.9791%	10.3030%
3	0.0264%	0.6406%	3.8915%	1.6925%	5.1249%	7.6006%
4	0.0065%	0.2990%	2.5732%	1.6726%	4.7833%	6.2823%

It can be seen in Table C2 that all the GCI values decreased as the r and p values increased. In the analysis of both the first buckling load and the failure load, the fine grid GCI values were less than the coarse grid GCI values. The GCI values for the first buckling load analysis, for both fine grid and coarse grid, decreased at a faster rate than the GCI values of the failure load analysis. Therefore, it can be safely concluded that, though the first buckling load converged faster, both numerical results were converging.

It is worth noting that convergence test analysis for more models may be needed for the purpose of publishing several chapters of this dissertation, if required by the journals.

C4 References

[1]. Roache, P. J., Perspective: A Method for Uniform Reporting of Grid Refinement Studies, 1994.

Appendix D   Buckling Analysis of Steel Studs

D1 Introduction

The following content gives the buckling analysis of 362S162-33 (Figure D1) cold-formed steel studs at the unbraced lengths of 72 in, 144 in and 432 in.

Figure D1: 362S162-33 cold-formed steel stud

D2 Buckling Of Thin-Walled, Open Cross-Section Columns

Cold-formed, thin-walled, open cross-section steel members are widely used in construction industry, and Figure D2 [1] shows some typical cold-formed, thin-walled steel members. Cold-formed, thin-walled steel members possess the positive traits of high strength-to-weight ratio, economically viable and can be easily installed. However, due to their thin-walled and open cross-section nature, buckling analysis becomes a top priority in their structural design. Figure D3 [1] gives all the possible local (a) and global (b) buckling modes of steel studs for wall assemblies. In designing cold-formed, thin-walled steel studs, local buckling, distortional buckling and Euler buckling are the main concerns [2]. Figure D4 [3] gives the buckling analysis of a 362S162-68 (3.625 in X 1.625 in X 0.5 in X 0.0713 in) steel stud with Finite Strip Method. It can be seen that the spring stiffness provided by the gypsum boards has virtually no effect on local buckling behavior, though it does have a minor effect on distortional buckling and a major effect on global buckling. Because local buckling is independent of the unbraced length, gypusm boards are expected to have no effect on local buckling.
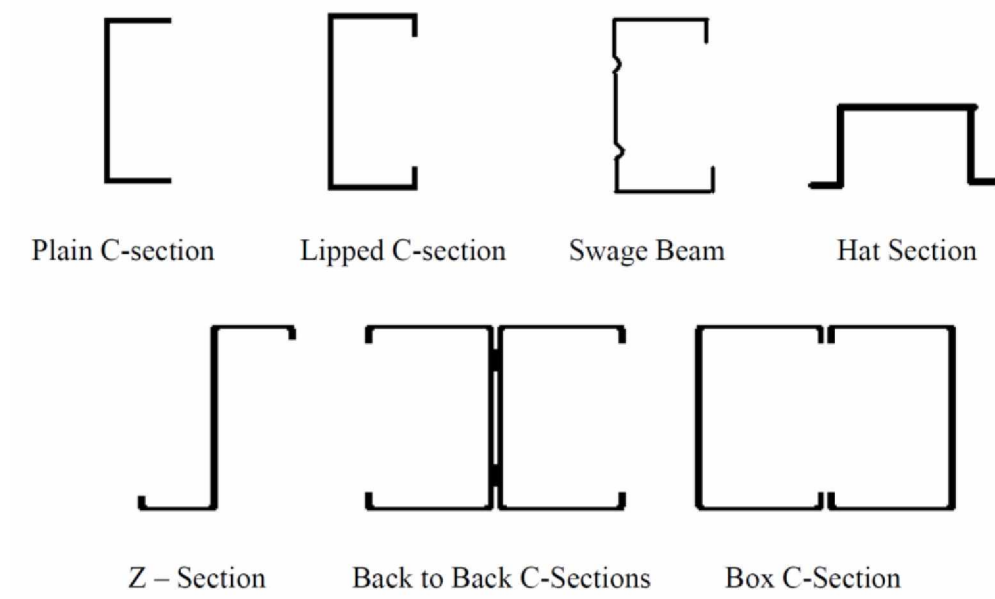
Figure D2: Typical cold-formed, thin-walled, open cross-section steel members [1]

Basic Section

Flange Buckling
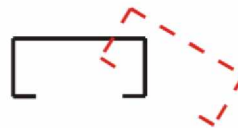
Web Buckling

Distortional Buckling

(a)

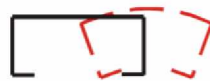Flexural Buckling about Major Axis

Flexural Buckling about Minor Axis
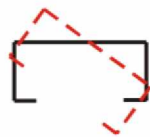
Torsional Buckling

Lateral Torsional Buckling

Lateral Distortional Buckling

(b)

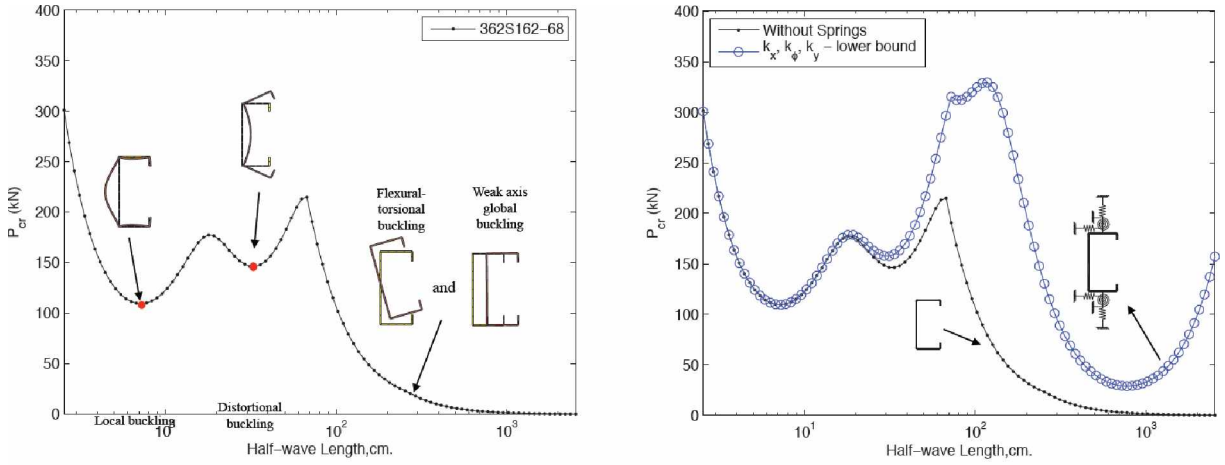Figure D3: (a) Possible local buckling modes; (b) possible global buckling modes [1]

Figure D4: Different buckling modes of a 362S162-68 steel stud with (right) and without (left) spring braces [3]

D3 Local Buckling of Plates

The local buckling phenomenon has been thoroughly experimented and studied by numerous researchers, such as Timoshenko and Gere [4]. The local buckling stress f_{cr} of a plate shown in Figure D5 [5] is given by Equation D1. The local buckling coefficient k is given in Figure D6 [5] with different boundary conditions. It can be seen that local buckling stress f_{cr} is independent of unbraced length a.
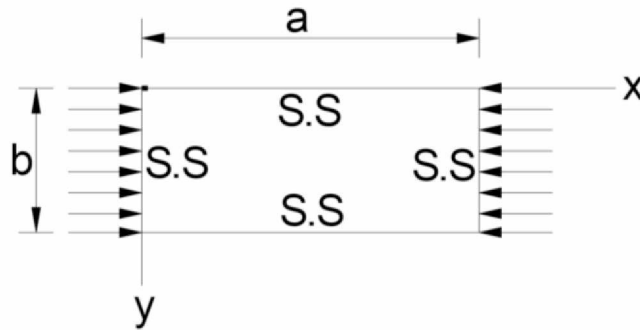
Figure D5: Plate subjected to compressive load [5]

$$f_{cr} = \frac{k\pi^2 E}{12(1-\upsilon^2)}\left(\frac{t}{b}\right)^2 \tag{1}$$

Where:

k is the local buckling coefficient and is given in Figure D5 with different boundary conditions;

E is Young's modulus of the plate;

υ is Poisson's ratio;

t is the thickness of the plate; and

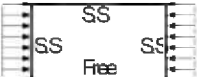b is the width of the plate under compressive load.
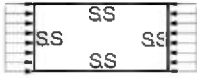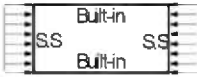
Boundary Condition	Local Buckling Coefficient, k	Half-Wavelength
SS / S.S S.S / S.S	4.0	b
Built-in / S.S S.S / Built-in	6.97	0.66b
S.S / S.S S.S / Free	0.425 0.675	∞ 2b
Built-in / S.S S.S / Free	1.247	1.636b

Figure D6: Local buckling coefficient k with different boundary conditions

Where:

"S.S" is the simply-supported boundary condition where axial deformation is allowed, and the edges are free to rotate but cannot translate out of plane;

"Free" is the non-restraint boundary condition where no restraint is imposed, and the edges are free to translate and rotate; and

"Built-in" is the rigid boundary condition where only axial deformation is allowed but no translation or rotation.

A 362S162-33 steel stud was modeled in ABAQUS, and its buckling analysis was conducted. Table D1 gives the steel properties at different temperatures. **The temperature of the steel stud was chosen to be 752 F.** Figure D7 gives two 362S162-33 steel studs in ABAQUS with 72 in and 144 in unbraced lengths. Figure D8 gives the meshing of two models. Both models used C3D20R elements with typical element size 0.5 in X 0.226 in X 0.0346 in. The stud with a 72 in unbraced length had 6,336 elements and 45,295 nodes. The stud with a 144 in unbraced length had 12,672 elements and 90,367 nodes. The boundary conditions of the two models were also identical and are given in Figure D9. The two ends of the steel stud in each model were pin-connected to the centroids with one centroid restrained in the x, y and θ_x directions and the other centroid restrained in the x, y, z and θ_x directions. The middle-line nodes of the steel stud in each model were restrained in the y direction to simulate the gypsum board bracing.

Table D1: Properties of steel used (A33) at different temperatures

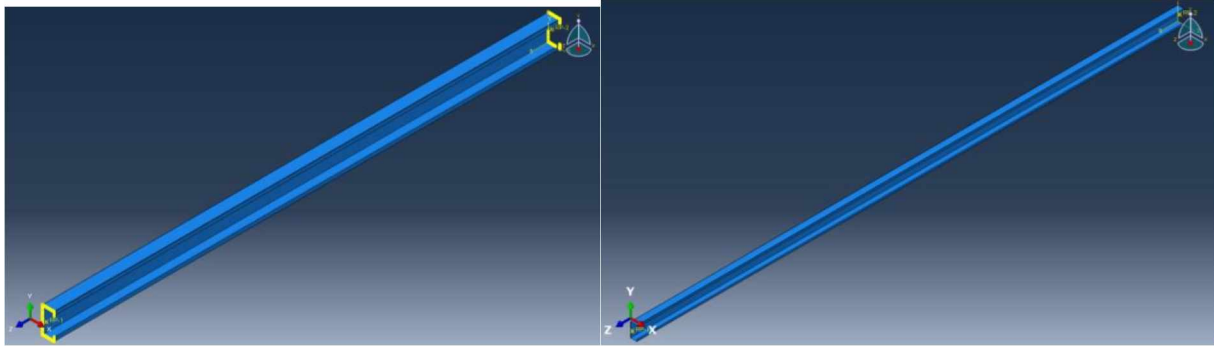| Temperature | Young's Modulus | Yield Stress | Temperature | Young's Modulus | Yield Stress |
T (F)	E (ksi)	Fy (ksi)	T (C)	E (GPa)	Fy (MPa)
68	29,000	33	20	500	227.53
200	29,000	33	93	500	227.53
400	26,100	26.4	204	450	182.02
600	22,620	19.14	316	390	131.97
750	20,300	13.86	399	350	95.56
800	19,430	13.2	427	335	91.01
1,000	14,210	9.57	538	245	65.98
1,200	6,380	4.29	649	110	29.58
1,400	3,190	1.98	760	55	13.65
1,600	2,030	1.32	871	35	9.10
1,800	1,450	0.99	982	25	6.83
2,000	580	0.33	1093	10	2.28
2,200	0	0	1204	0	0.00

Figure D7: 362S162-33 steel-stud models with 72 in (left) and 144 in (right) unbraced lengths in ABAQUS
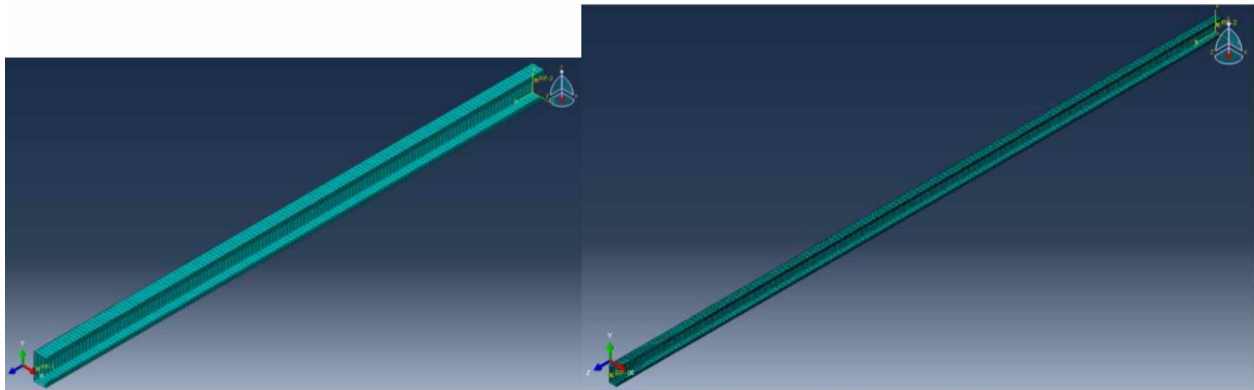

Figure D8: Meshing of two stud models with 72 in unbraced length (left) and 144 in unbraced length (right)
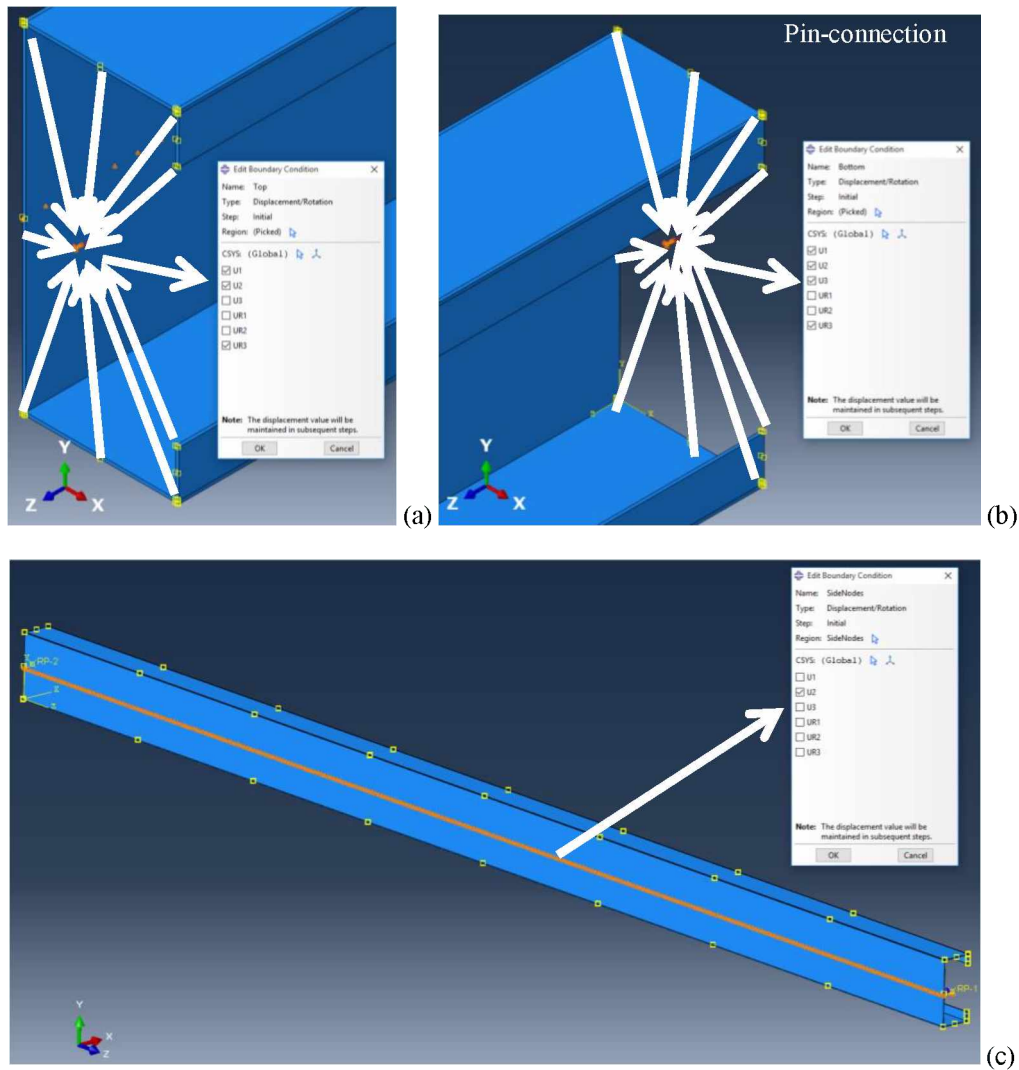
Figure D9: Boundary conditions of the steel-stud models (72 in and 144 in unbraced lengths)

The first, second and third buckling modes for both models are given in Figure D10 and Figure D11. It can be seen that the 362S162-33 model with a 72 in unbraced length never buckled globally and the first three buckling loads were almost identical. The 362S162-33 model with a 144 in unbraced length, on the other hand, buckled globally in its first buckling mode, as can be seen in Figure D11 (a). As expected, the first local buckling loads were almost identical for the 362S162-33 models with 72 in (first buckling mode) and 144 in (second buckling mode) unbraced lengths. In both models, only the first three eigenvalues were calculated. The elapsed analysis times for models with 72 in and 144 in unbraced lengths were 366.5 s and 1077 s, respectively.
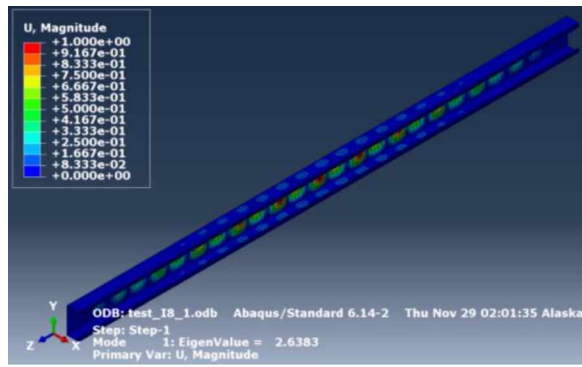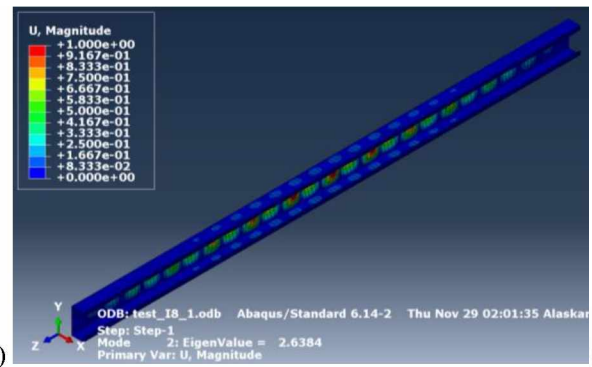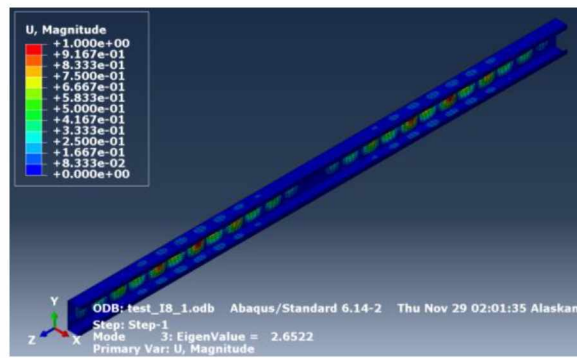
Figure D10: First three buckling modes of the steel stud with a 72 in unbraced length

(a): First buckling mode; (b): second buckling mode; (c): third buckling mode
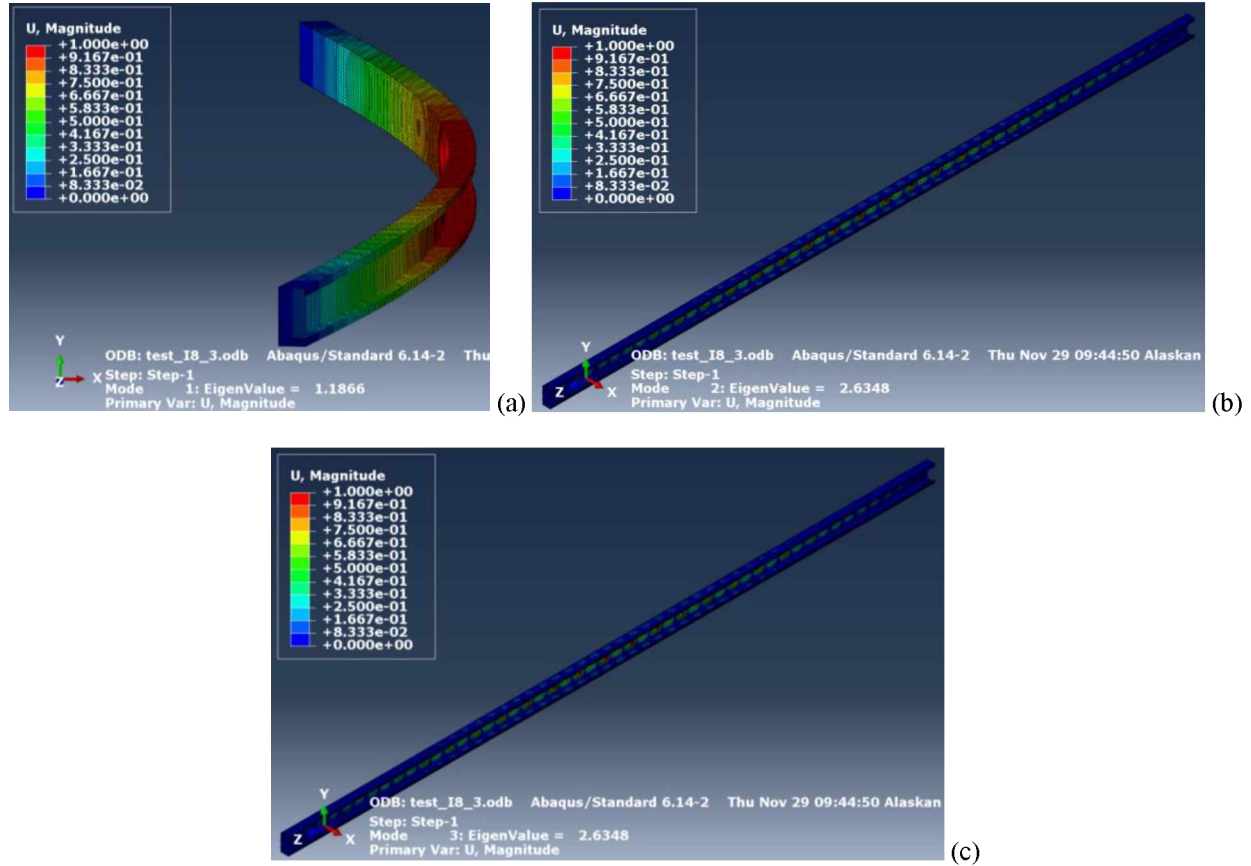
Figure D11: First three buckling modes of the steel stud with a 144 in unbraced length

(a): First buckling mode; (b): second buckling mode; (c): third buckling mode

The author also conducted buckling analysis of two 362S162-33 steel studs connected together with phenolic resin. Figure D12 shows the two connected steel studs with unbraced lengths of 144 in (a) and 432 in (b). Figure D13 shows the meshing of the two models. The temperature of the steel studs was again chosen as 752 F, and the two models used C3D20R elements with typical element size 0.5 in X 0.226 in X 0.0346 in as well. The connected-stud model with a 144 in unbraced length had 25,344 elements and 180,734 nodes. The connected-stud model with a 432 in unbraced length had 76,032 elements and 541,310 nodes. Figure D14 gives the boundary conditions of the two models of connected steel studs. The two ends of the connected steel studs in each model were pin-connected to the centroids with one centroid restrained in the x, y and θ_x directions and the other centroid restrained in the x, y, z and θ_x directions. The middle-line nodes of the steel studs in each model were restrained in the y direction to simulate the gypsum board bracing.
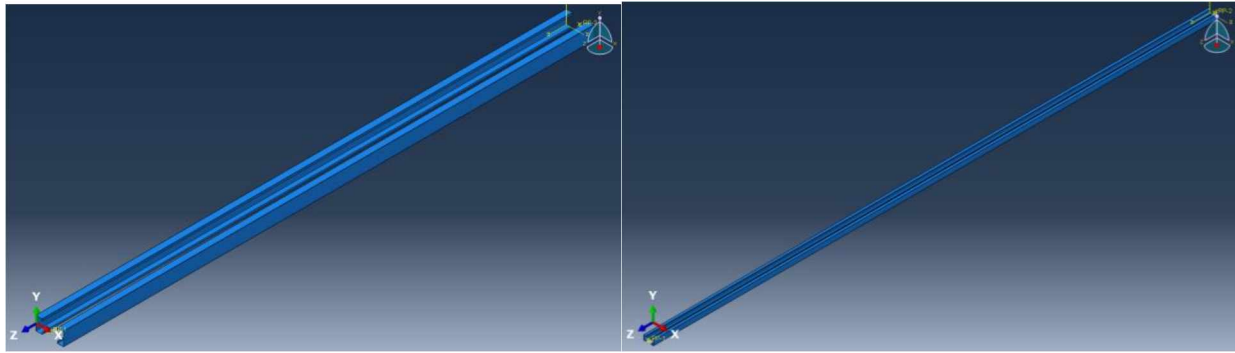
158

Figure D12: Two connected steel studs with unbraced lengths of 144 in (left) and 432 in (right)
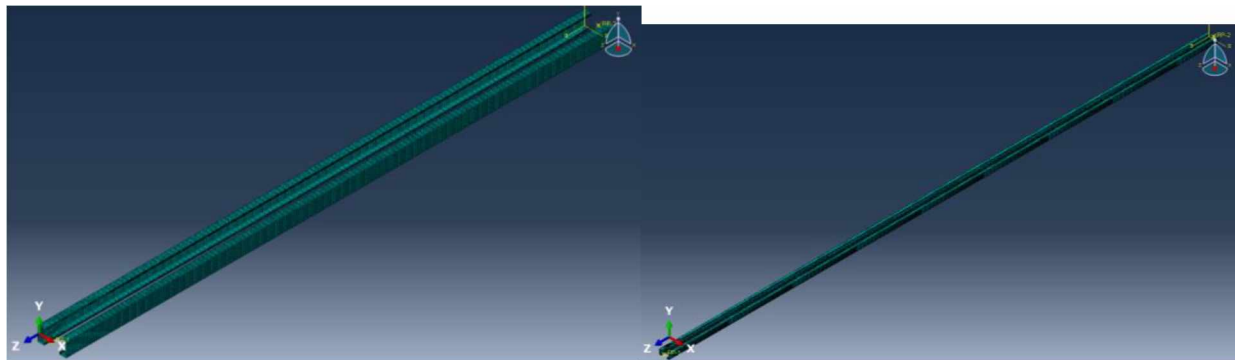

Figure D13: Meshing of the two connected-steel-stud models with unbraced lengths of 144 in (left) and 432 in (right)
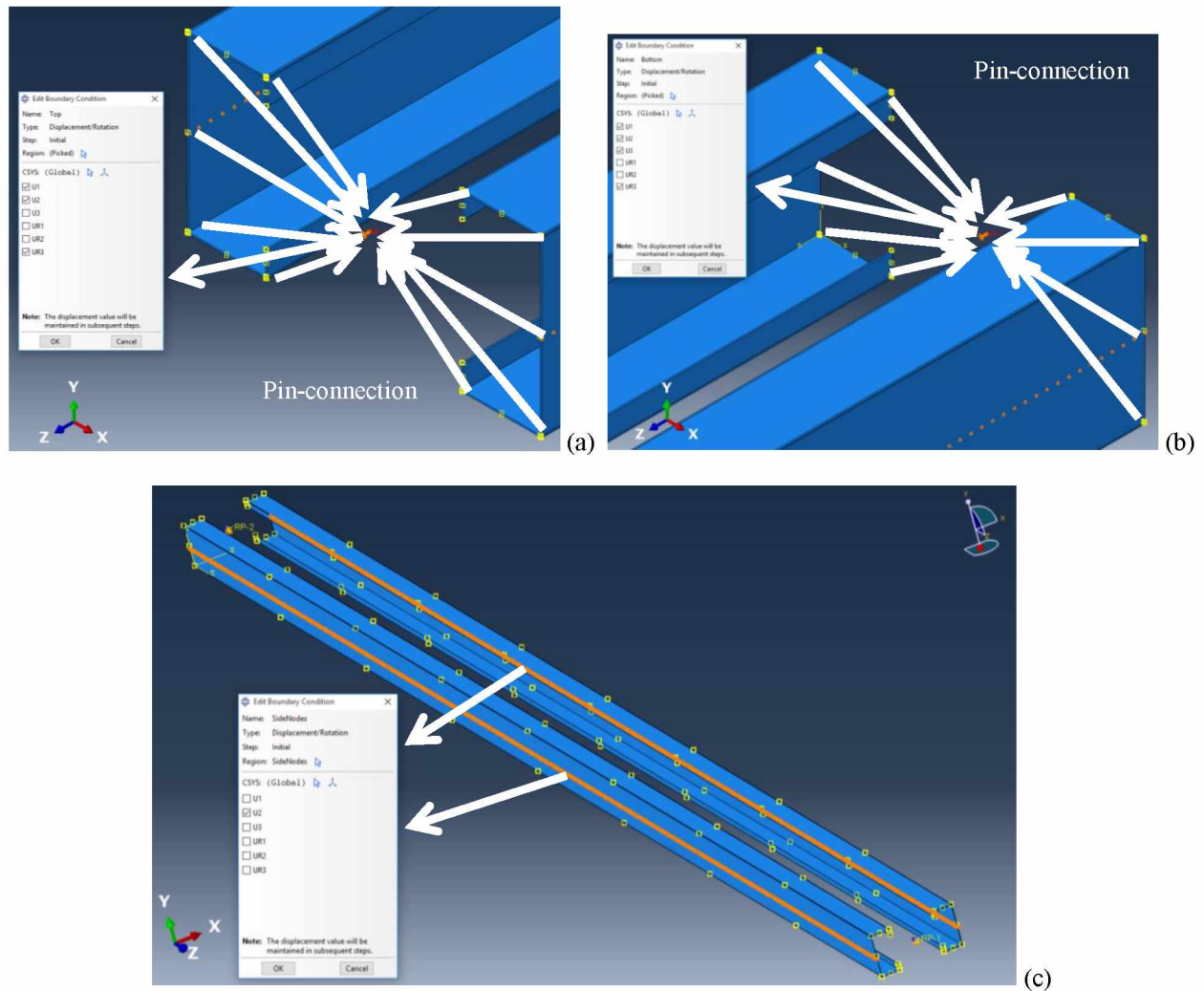
Figure D14: Boundary conditions of the connected-steel-stud models (144 in and 432 in unbraced lengths)

Figure D15 gives the results of the first and second buckling modes of the two connected steel studs with

the unbraced length of 144 in, and the buckling loads were identical. Both studs buckled locally in the first and

second buckling modes. The two modes differed only by which stud buckled due to how numerical disturbance was

assigned in ABAQUS. Figure D16 gives the first, second, third, fourth and fifth buckling modes of the connected

steel studs with the unbraced length of 432 in. It can be seen that the first five buckling modes were all global

buckling modes. Figure D17 shows the eleventh buckling mode was the first local buckling mode. The local

buckling loads were again almost identical for the two connected-steel-stud models with 144 in (first and second

buckling modes) and 432 in (eleventh buckling mode/first local buckling mode) unbraced lengths. In both models,

the first 20 eigenvalues were calculated. The elapsed analysis times for models with 144 in and 432 in unbraced

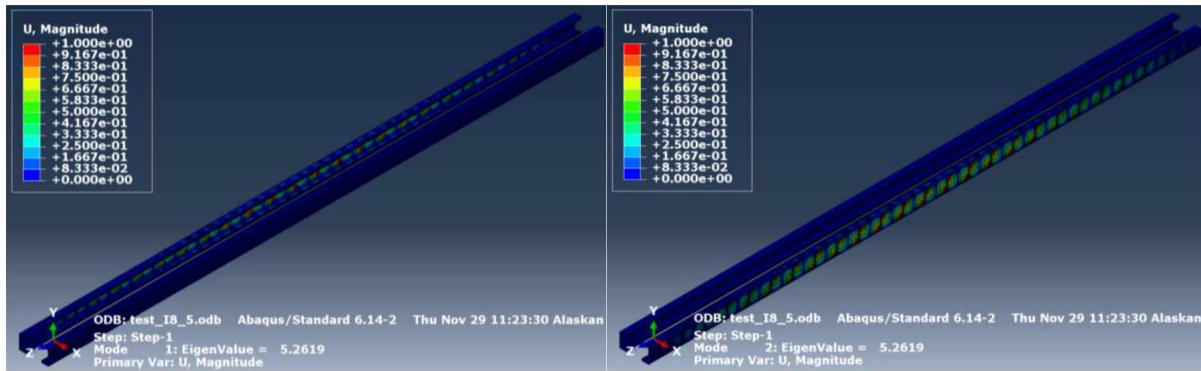lengths were 5,383.1 s and 22,380 s, respectively.

Figure D15: First (left) and second (right) buckling modes of two connected steel studs with the unbraced length of 144 in
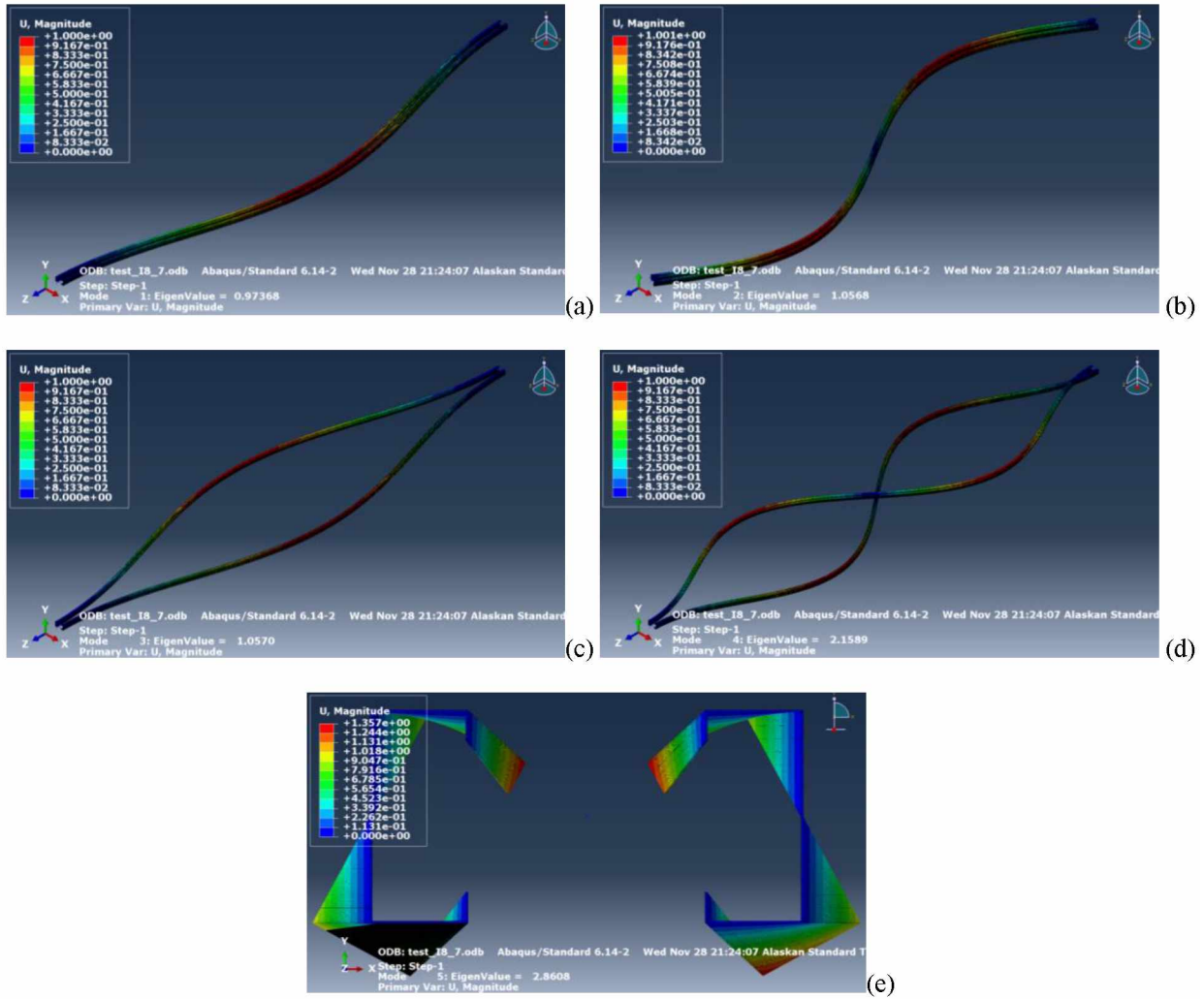
Figure D16: First five buckling modes of two connected steel studs with the unbraced length of 432 in

(a): First buckling mode; (b): second buckling mode; (c): third buckling mode; (d): fourth buckling mode; (e): fifth buckling mode
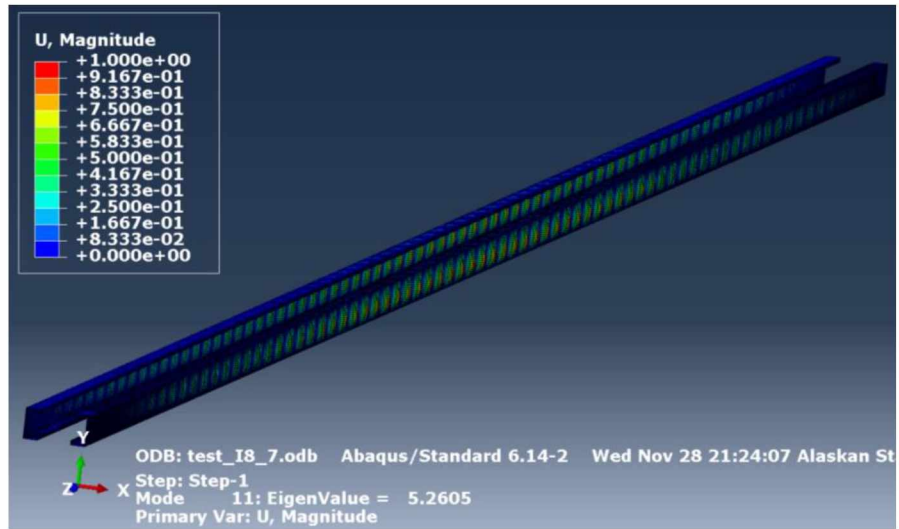
Figure D17: First local buckling mode (eleventh buckling mode overall) of two connected steel studs with the unbraced length of 432 in

D5 References

[1]. Kolarkar, P., Structural and Thermal Performance of Cold-Formed Steel Stud Wall Systems under Fire Conditions, 2010.

[2]. Schafer, B., Local, Distortional, and Euler Buckling of Thin-Walled Columns, 2002.

[3]. Vieira Jr., Luiz, Behavior and Design of Sheathed Cold-Formed Steel Stud Walls under Compression, 2011.

[4]. Timoshenko, S. and Gere, J., Theory of Elastic Stability, 1961.

[5]. Lee, Jung Hoon, Local Buckling Behavior and Design of Cold-Formed Steel Compressed Members at Elevated Temperatures, 2004.